UiT The Arctic University of Norway

Department of Chemistry

Synthesis of thiol-appended gold and rhenium corroles as potential nanoconjugants for gold nanoparticles.

Krister Engedal Johannessen

Master's thesis in synthetic chemistry, Kje-3900, Spring 2023

Table of Contents

Acknowledgements

I would like to thank my advisors – Prof. Abhik Ghosh for his generous attitude, helpfulness and support, and Dr. Abraham Alemayehu for his incredible helpfulness and brilliance.

I'm also very grateful for the positive atmosphere and great advice and help I have received from the other members of the bioinorganic research group at UiT and my fellow students, especially Dr. Simon Larsen, Stian Martinsen, Kristian Torstensen and Martin Pettersen.

Special thanks also to Truls Ingebrigtsen and Jostein Johansen for practical help with the NMR and MS machines, respectively.

Abstract

Photodynamic therapy (PDT) today is an established treatment for a variety of cancers as well as various dermatological conditions, macular degeneration and bacterial and other infections[1, 2]. Treatment involves the administration of a photosensitizer, typically a porphyrin, followed by irradiation with light[3]. The photoexcited sensitizer transfers its excess energy to oxygen in the affected tissue, thereby exciting the latter to its highly reactive singlet state. The singlet oxygen serves as the key agent that destroys the diseased tissue[1]. For PDT to work, a photosensitizer has to effectively localize in diseased tissue[1, 2]. It has long been empirically known that porphyrin-type compounds selectively localize in tumors[3]. There is much room for improvement, however, in the area of biodelivery to the tissue in question. Nanoconjugation, i.e., conjugation with nanomaterials such as gold nanoparticles can dramatically enhance drug biodelivery for a variety of target tissues[4, 5]. In this thesis, I have synthesized thiol-appended 5d metallocorroles that are potentially suitable for nanoconjugation with gold nanoparticles.

Gold and rhenium-oxo corroles synthesized in our laboratory are a new class of triplet photosensitizers that have exhibited promise in in vitro photocytotoxicity studies against multiple cancer cell lines[6, 7]. Out of a variety of strategies attempted for appending sulfur-containing substituent, the most promising has been one involving nucleophilic substitution of *meso*-pentafluorophenyl groups with dithiols. Future work will focus on the synthesis of gold nanoconjugates and testing of the conjugates for phodynamic, photothermal, and radiosensitizing activity. Multimodal activity will be an exciting and gratifying outcome for this line of research.

Abbreviations

PDT	photodynamic therapy
DCM	dichloromethane
NIR	near-infrared
THF	tetrahydrofuran
LiHMDS	lithium bis(trimethylsilyl)amide
TPFPC	tris(pentafluorophenyl)corrole

Chapter 1: Porphyrin and Porphyrinoids

General introduction

As technology advances, so does the need for new medicinal compounds and materials. While many conventional medicinal compounds and medicinal strategies work well, improvements are still sought after, as many procedures and medicines can prove to be too invasive, especially for an ageing population. Porphyrins and related compounds have been cornerstone of localized photodynamic therapy treatments for a variety of cancers[3]. This is due to their ability to generate reactive oxygen species localized in cancer cells, in a method called photodynamic therapy (PDT)[1-3, 8]. Combining PDT with other treatment modalities such as photothermal therapy and radiosensitization can greatly increase the potency of PDT. This can be very effectively achieved, at least in principle, by appending gold nanoparticles to porphyrinoids[9]. The synthetic goal for this thesis is to make thiol-appended corroles that should be able to bind to the surface of gold nanoparticles.

Porphyrin and porphyrinoids

Porphyrinioids are a class of tetrapyrrole macrocycles of which porphyrin may be viewed as the prototype. Porphyrin itself is well known for its role in hemoglobin as the heme cofactor, which is a functionalized porphyrin molecule with an iron coordinated in its center, and reduced porphyrins (chlorins and bacteriochlorins) serve as photosynthetic pigments[10, 11]. This

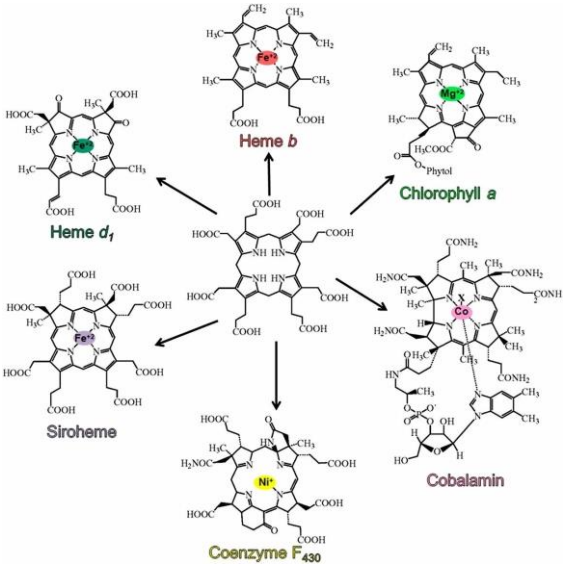

Figure 1: Biologically important porphyrin species from.

cofactor is then able to react with oxygen and transport it around the body. Porphyrins are necessary for life as we know it today[12], and these molecules have existed as long as life has, even being found in petroleum[13].

Synthetic routes to make porphyrin have been known since 1935 when Paul Rothemund first reported his synthesis of synthetic porphyrins, which he further expanded upon in 1936 and many times thereafter[14, 15]. The synthetic route has been improved since then and yields can be as good as 30-40% with reaction times of around 30 minutes[16, 17]. The reaction itself is an acid catalyzed condensation reaction of pyrrole and an aldehyde, making polymers that can ring close to give a precursor to the porphyrin. An oxidation reaction is then performed to yield the final porphyrin. This reaction is often done as a one-pot reaction, as the porphyrin is easily isolated from the byproducts. Other porphyrinoids are made from similar reactions, where some reaction conditions are changed for optimization purposes.

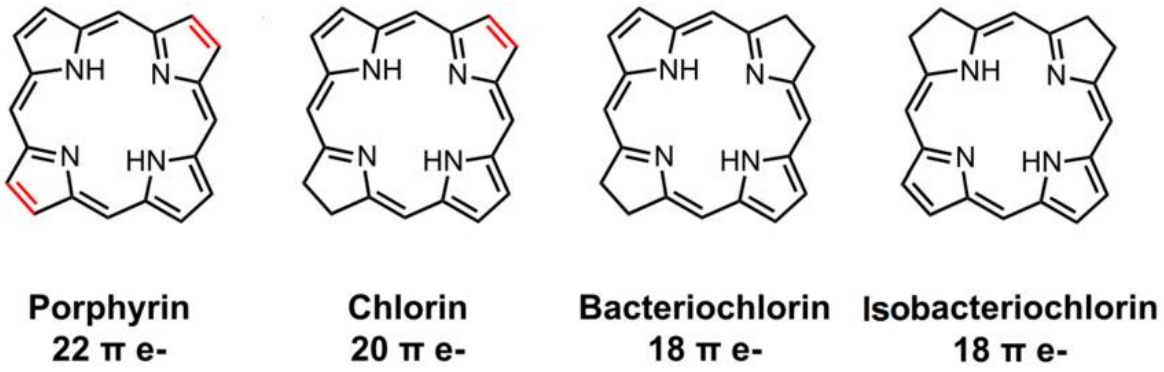

Figure 2: Porphyrin and reduced porphyrin species.

Porphyrinoids like corroles exhibit many of the properties of porphyrins, such as good absorption of visible light and good quantum properties, while enhancing some properties. One of the benefits or corroles is their ability to coordinate to high oxidation state metals such as many 5d metals[18, 19]. 5d metal-coordinated corroles usually exhibit enhanced photophysical properties that differentiate them from those of porphyrins[20]. These metal-coordinated corroles can be further designed and functionalized, for instance by using specific aldehydes in the synthesis and by other means such as halogenation[21]. Functionalization will be described in chapter 3. The structure of porphyrin, corrole and some of the many similar compounds is shown in figure 3.

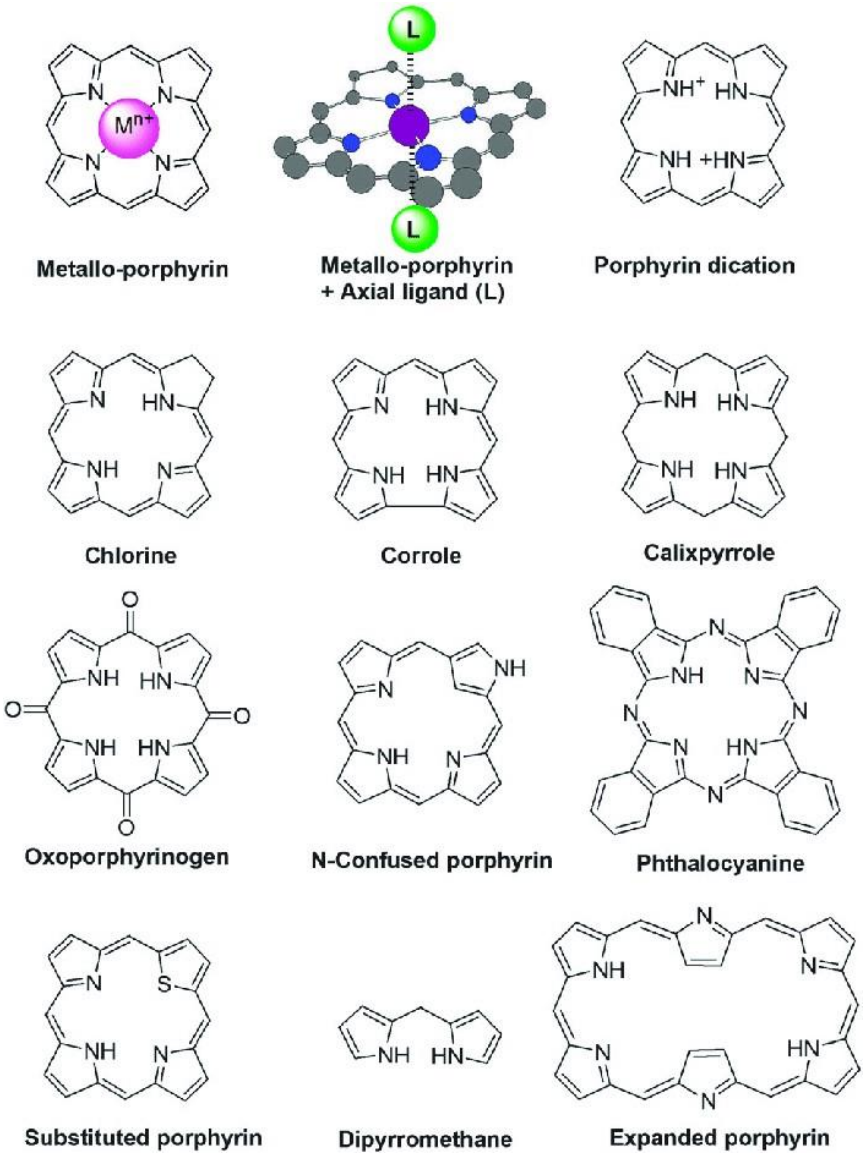

Figure 3: General structure of porphyrins, expanded porphyrins and many porphyrinioids.

Applications of porphyrins in medicine

Porphyrins and corroles are being developed and tested as photosensitizers in PDT[1, 20]. PDT works by generating reactive oxygen species (ROS) that can destroy cells through uncontrolled oxidation[2]. Cancer cells have an affinity towards porphyrinoids and they have been shown to localize in cancer cells through natural processes[22]. Metal inserted corroles can exhibit good ROS generation and are therefore good candidates for use in PDT. Increasing the absorption in the near-infrared (NIR) range of light for porphyrins and corroles is an

important method to increase the potency of PDT. Visible light is absorbed very well by the skin, making it important that compounds used as photosensitizers in PDT absorb light in regions where the skin is not as effective, such as in the NIR range. Gold and rhenium corroles exhibit absorption very close to this range, and they have proved to be good ROS generators, making them good potential candidates for usage in PDT[20].

Corroles

Corroles have been studied as a part of porphyrin chemistry since they were first synthesized in 1964 by Johnson and Kay[23, 24]. There was some time however until the field of corrole chemistry properly started up, and it is fairly recent compared to that of porphyrin chemistry. When corroles were first discovered they used a rather poor synthetic strategy to make the corrole. An important improvement in the synthetic strategy for corrole synthesis was developed in 1999 by Gross and Paolesse[25], and this was the proper starting point of corrole chemistry and the synthesis has evolved since.

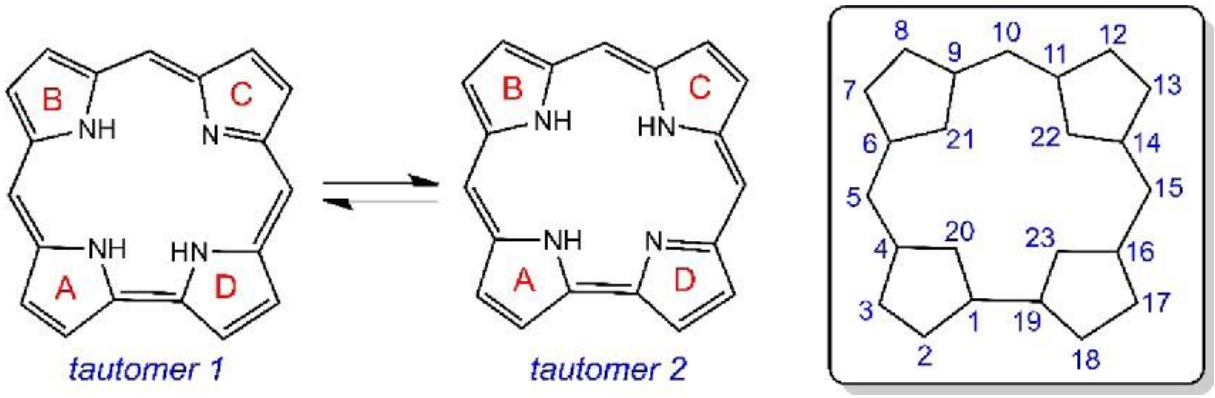

Figure 4: Different corrole tautomers and the numbering of carbons and nitrogens in corroles.

The unique properties of corroles mainly come from its highly electron rich nature and its rigid and constricted structure. Much of the work done to develop corrole chemistry has been done by the groups of Gross[26, 27], Ghosh[28], Gryko[29] and Paolesse[30] over the years. Metallocorroles have been of special interest as the metal core can heavily impact the photophysical properties of the corroles, and most transition metals have been used to successfully make metallocorroles[18].

Figure 4 shows how the carbons in corrole are numbered, where positions 2,3,7,8,12,13,17 and 18 are all referred to as β-carbons, 1,4,6,9,11,14,16,19 are referred to as α-carbons and 5,10,15 are referred to as the *meso*-carbons. Corroles and porphyrins look like planar molecules, however this is not always the case, and several different structural types occur for both[31].

Structural types

While porphyrins might be expected to be planar, this is not always the case. Due to steric hindrances and electronic configurations there are several structural types they can occur as, as shown in figure 5.

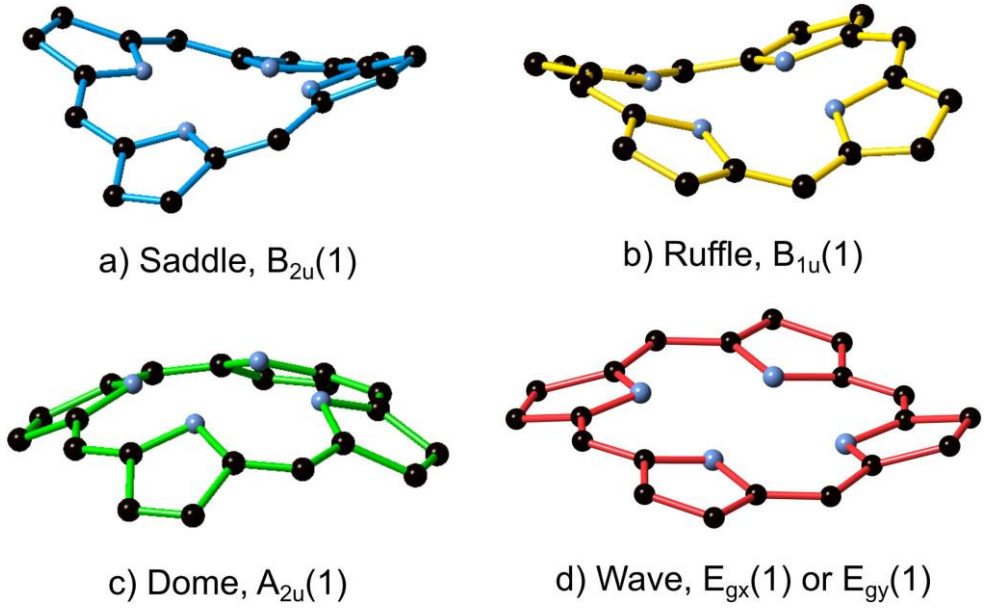

Figure 5: Different porphyrin conformations from ref 27.

The domed conformation usually occurs when the porphyrin is inserted with a metal that is too big for its center, and the metal sticks up from the plane, pushing the β-carbons under the plane[32, 33]. Ruffling usually occurs if the porphyrin has a small atom coordinated in the center, such as with phosphorus, or when the *meso*-substituents are very bulky[31].

While the domed conformation occurs in metallocorroles and saddling can occur in very specific circumstances, most metallocorroles are planar, and the waved and ruffled conformations will not occur for most metallocorroles[34]. The shape of the porphyrinoids will impact its photophysical characteristics, which will be discussed next.

Spectra and Gouterman's model

The unique photophysical properties of porphyrinoids is one of the main reasons research into such compounds occur. As such an explanation of why these properties are as they are is needed. In 1961 and 1963 Gouterman published his series of papers focused on the absorption spectra of porphyrins, where he explained the absorption spectra through a four-orbital

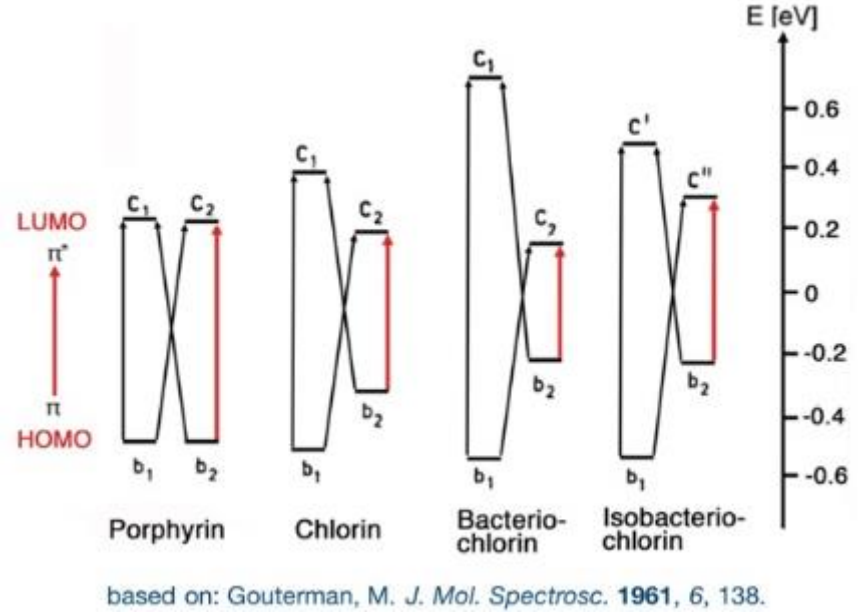

Figure 6: HOMOs and LUMOs contributing to the photophysical properties of porphyrin and different related compounds.

theory[35, 36]. His theory dictated that the photophysical properties arose from four frontier molecular orbitals in the π-system of porphyrin that were energetically well separated from the other π-system molecular orbitals. Two of these MOs are the degenerate LUMOs, while the other two are the two near-degenerate HOMOs, and the absorption of porphyrins arise from transitions among the four molecular orbitals. This is also the case for corroles as reported by Ghosh in 2000[37].

From Figure 6 we can see the four orbitals contributing to the photophysical properties of porphyrin, chlorin, bacteriochlorin and isobacteriochlorin, and Figure 7 shows the difference in the Q band and Soret bands of phenyl porphyrin, chlorin and bacteriochlorin.

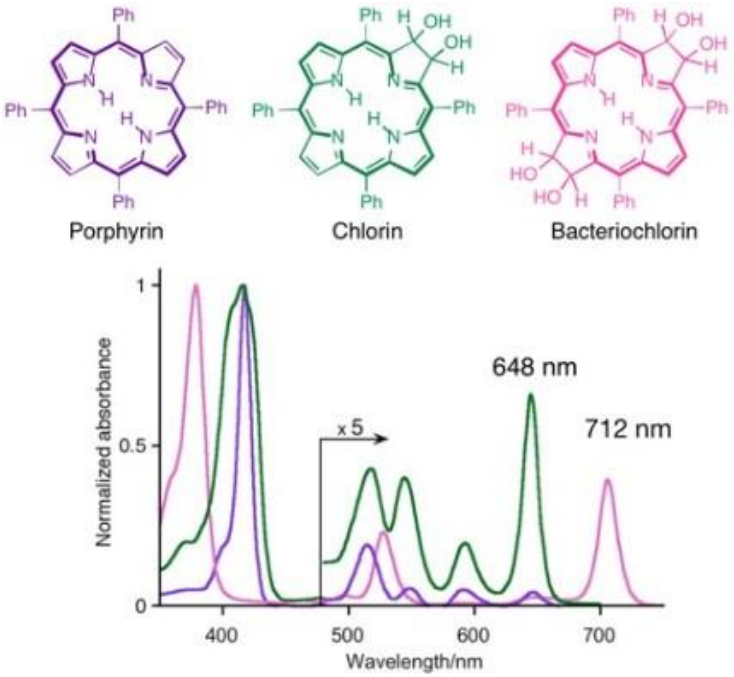

Figure 7: Absorption spectra for freebase phenyl porphyrin, chlorin and bacteriochlorin.

The addition of metal cores to porphyrins and similar compounds impacts their photophysical properties by the addition of other orbitals in the same energy range as the four Gouterman orbitals. Usually transition metals with low electronegativity is inserted into such systems it leads to red-shifting of both the Soret and Q band of the porphyrinoid, while a comparatively higher electronegativity may blue-shift the absorption[28]. While the compounds that will be discussed later in this thesis both contain such metal cores, they don't differ too much from one another, and the main differences come in the Q band. The UV-vis spectra of 5d metallocorroles have not been fully studied so the exact details of the orbital composition are still not characterized.

As mentioned earlier one of the reasons porphyrins and corroles are of great interest is due to their photophysical qualities, especially their phosphorescence. Phosphorescence is of great interest as it indicates an ability to generate singlet oxygen through triplet-triplet annihilation. As the porphyrin absorbs light it can excite electrons to a higher energy singlet state, where they can undergo intersystem crossing to generate a triplet state[38]. From there the electrons can either relax back to ground state through phosphorescence, triplet-triplet annihilation that generates singlet oxygen, or thermal deactivation. The intersystem crossing is a much slower process than fluorescence, and it is reversible, so phosphorescence usually has low quantum yields as many other processes compete with it[39]. A simplified Jablonski diagram is shown in Figure 8 that shows fluorescence, phosphorescence and intersystem crossing.

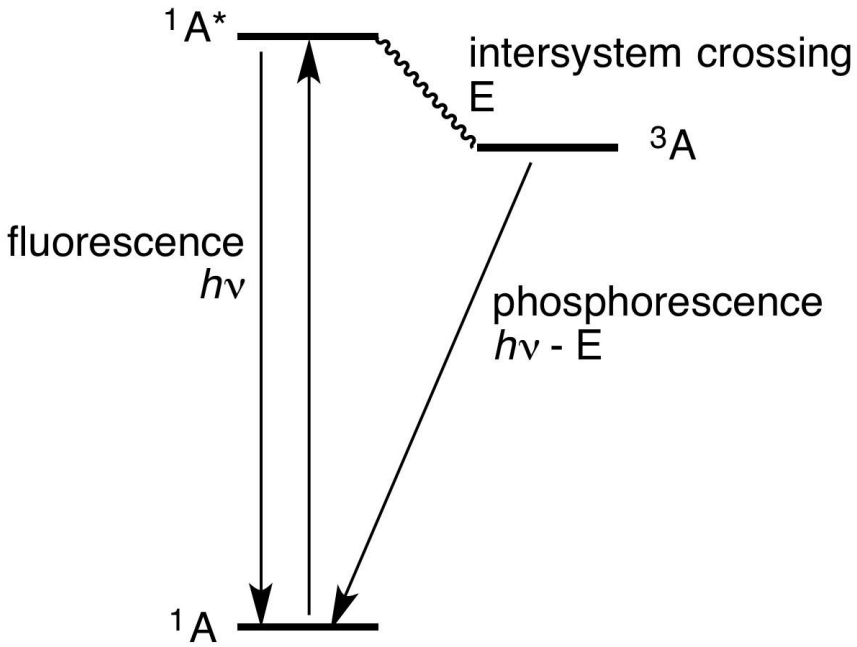

Figure 8: A simplified Jablonski diagram showing fluorescence, phosphorescence and intersystem crossing.

Chapter 2: Coordination Chemistry

Metal insertion

Corroles are excellent ligands for the great majority of transition metals[18, 40]. Because of both the 3- charge and constricted nature of corroles, metal insertion is generally slower with corroles and also requires more special conditions, relative to porphyrins. Three broad strategies are used for metal insertion into corroles, the organolithium method, organometallic method and acetate method, and these are discussed below. Metallocorroles also show distinct coordination chemistry compared with porphyrins, with a higher preference for 5-coordination over 6-coordination[18]. Also, metallocorroles are generally planar or mildly domed, with a saddled conformation largely limited to copper corroles[34]. As trianionic ligands, corroles are also more prone to ligand noninnocence, that is, to exist as partially oxidized radicals[41].

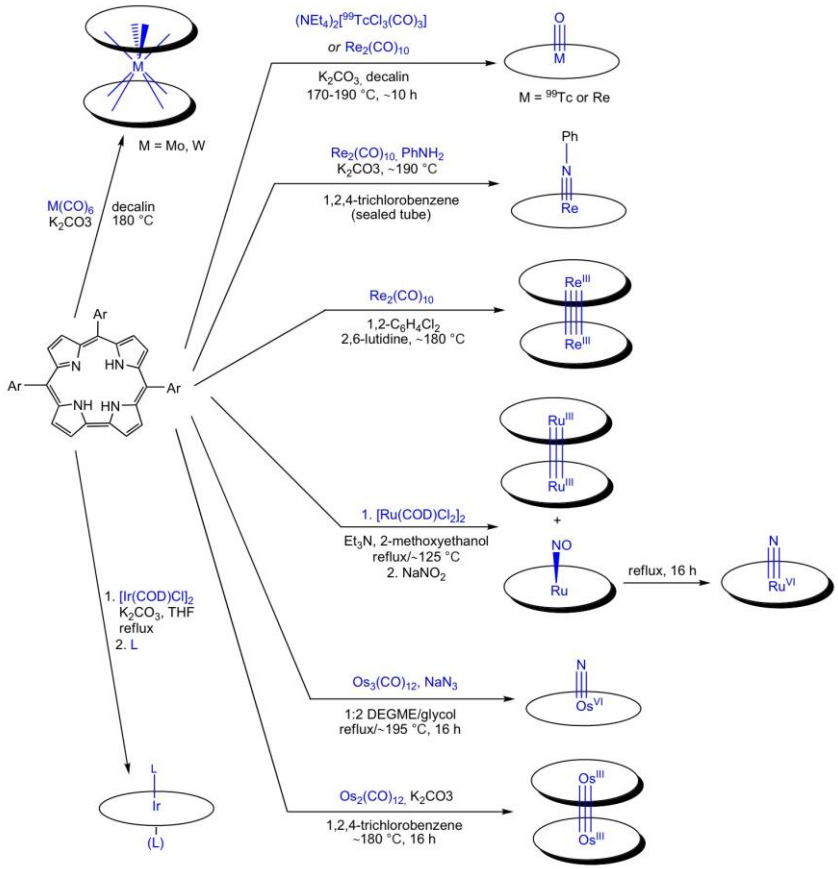

Figure 9: Different corrole metal insertion reactions from ref 7.

Organolithium method

Every group of metals is chemically distinct, and most of the metals require different reaction conditions to insert into a corrole. For the group 4 metals of titanium, zirconium and hafnium metal chlorides can react with a prepared lithium corrole reagent as shown in x.

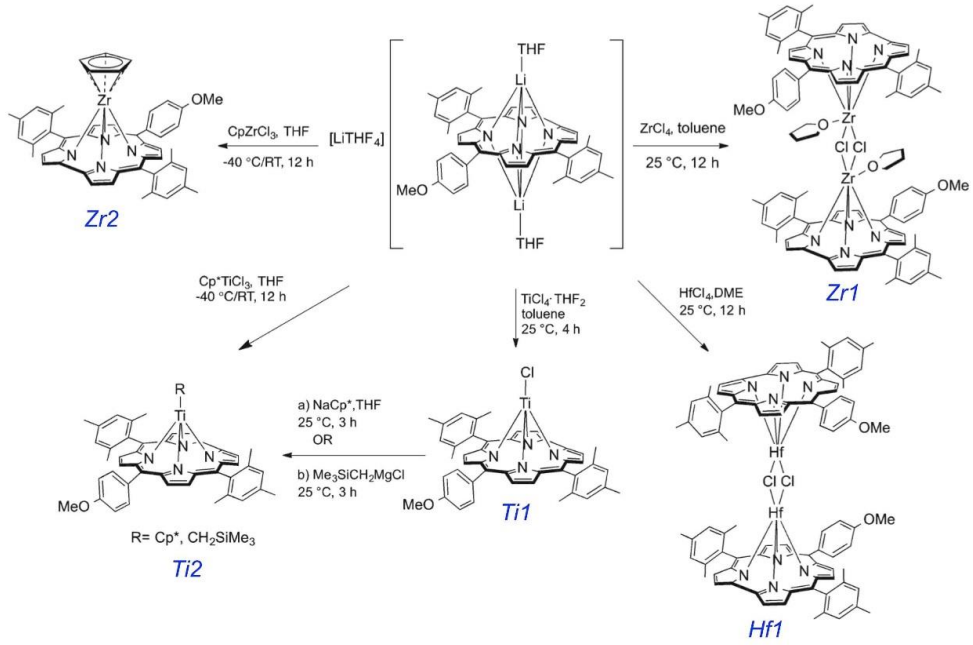

Figure 10: Metal insertions to the lithium corrole reagent from ref 40.

These lithium corrole complexes are made by reacting a free base corrole with 3eq. $LiN(SiMe_3)_2$ (LiHMDS) at -40°C in THF, then stirring at room temperature for 2 hours, as reported by Buckley and Arnold[42]. This is a fairly recent development in corrole chemistry and has proved useful as a metathesis agent to produce group 4 metal corrole complexes. All of the metal complexes made this way have a distinct out-of-plane character, yielding unique looking complexes and some unique properties[43].

Organometallic method

One of the more common methods of making metallocorrole complexes is by reacting a transition metal connected to organic molecules with a freebase corrole and a base while heating. This method is used to make Rh, Tc, Ir, Os and more metallocorrole complexes[44].

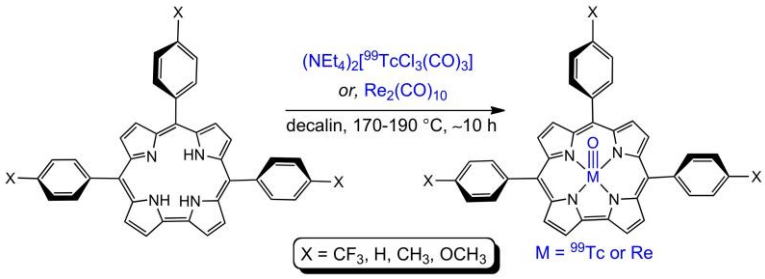

Figure 11: An example synthesis of Re and Tc-corrole complexes from ref 41.

Acetate method

Some transition metals like Au, Ag, Cu and Mn make complexes with acetate, and these acetate complexes make for good reagents in metal insertion, and generally require mild reaction conditions. Ag(I), Cu(II) and Au(III) acetates all react at room temperature using pyridine as a solvent, where the reaction with Ag and Cu will take approximately 40 minutes and the reaction with Au will take around 16 hours[20, 45-47]. The gold insertion is tricky compared to the silver and copper ones, as the corrole needs to be very pure and there can be no traces of an oxidizing agent for this reaction to work.

Innocent and non-innocent complexes

Many first-row transition metal complexes are noninnocent. That means, the metal is less oxidized than its apparent oxidation state, while the corrole is more akin to •2- than to 3-[48]. Classic examples of such systems include FeCl and MnCl corroles. These complexes are best regarded as M(III)-corrole(•2-). Noninnocent systems generally have many low-energy excited states and are not luminescent[49]. In contrast, most 5d metallocorroles including the ReO and Au systems I have studied are innocent. These are luminescent, more specifically phosphorescent, as a result of the presence of the heavy element[41].

Chapter 3: Corrole Functionalization

Functionalizing corroles, and porphyrins for that matter, is an important tool to achieve the desired photophysical properties. There are a plethora of different adjustments one can make to the corrole, and we will just focus on some of the different possibilities that exist, mainly halogenation of the β-carbons, oxidations of corrole and exploring some basic corrole post-functionalization before discussing nucleophilic aromatic substitution (NAS) with a focus on substituting *para*-F on pentafluorophenyl, as this is the main focus of the synthesis we performed.

Halogenation

It is possible to halogenate the β-positions of corroles, where synthetic methods for chlorination, bromination and iodination of the β-carbons have been developed. There is no direct method of making a corrole with fluorinated β-carbons, but they can be achieved by using fluorinated pyrrole in the corrole condensation. This method was developed by the group of Chang in 2003, where it was used to make perfluorinated corrole for the first time[50]. Later the same year Steene used a similar approach to synthesize β-octafluorinated Cu and FeCl corroles[51].

Chlorination

Chlorination, bromination and iodination are all possible through direct synthesis steps, and they can be performed on both freebase and metallocorroles. Full chlorination of the β-positions has been done either by reacting a copper corrole with N-chlorosuccinimide in dichlorobenzene at high temperatures, then using reductive demetallation to yield β-octochlorinated freebase[52], or by reacting a metallocorrole with chloride gas in benzene, then addition of pyridine and sodium borohydride to the reaction mixture[53]. The latter gave 90% yield while the former gave 46%. Chlorination has also been explored at the *meso*-positions recently by Osaka using a reagent called Palau'chlor in a 1% pydridine in chloroform mixture at room temperature[54].

Bromination

Full bromination of the β-positions has been achieved through several methods, mainly through reacting freebase corrole with NBS in chloroform at room temperature, yielding 18-58% depending on *meso*-substituents as reported by Paolesse[55]. Gross has also achieved full

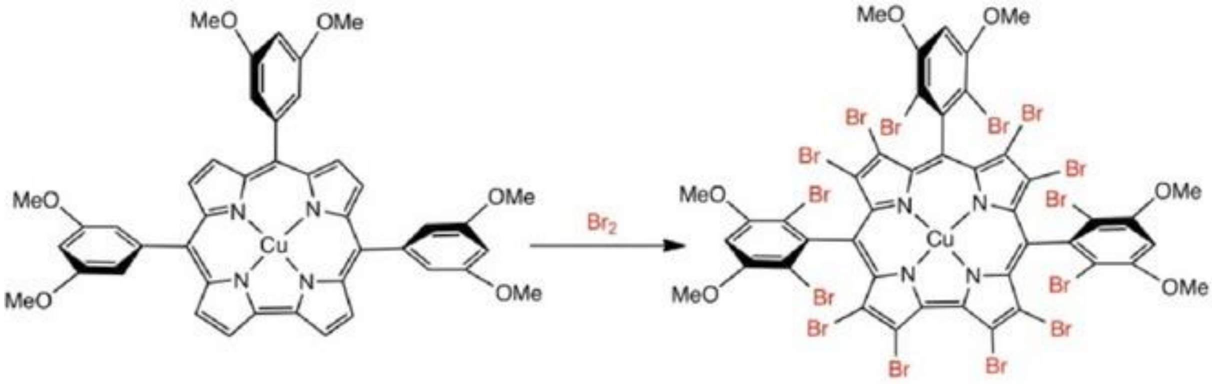

Figure 12: Full bromination of Cu[Tm,m'MeOPC] using elemental bromine perfomed by H. K. Norheim from ref 54.

bromination of Ga[TPFPC](py) and Al[TPFPC](py_2) in benzene by adding bromine at room temperature to yield 90% and 78% yield respectively[56, 57]. Partial bromination has been achieved by Paolesse and Chen through a variety of methods[21]. A 14-fold bromination of a corrole was performed by Norheim in 2017, shown in figure 12[58].

Iodination

Iodination of the β-positions of corroles has been achieved by Gross and coworkers, only achieving iodination of the 2,3,17 and 18 positions of Al[TPFPC](py$_2$) using NIS in MeOH at room temperature, and the 2,3,17 positions of Ga[TPFPC](py) by using excess iodine in a toluene and pyridine solution, refluxing for 1 hour[59, 60]. Thomassen synthesized an β-octaiodinated corrole in 2018 by dissolving a copper-corrole in DCM then adding 80eq. NIS dissolved in toluene with a few drops of TFA added. After refluxing overnight and some work up the desired product was isolated at 22% yield[47]. β-octaiodinated porphyrin was synthesized by Ghosh et. al. in 2015 through an indirect method[61].

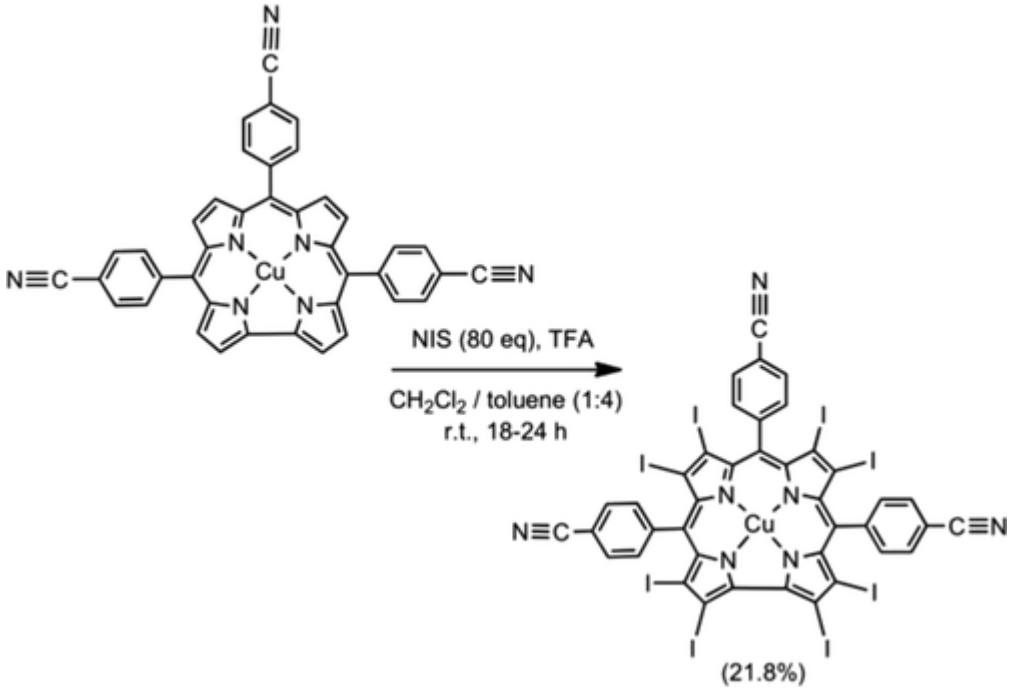

Figure 13: Reaction scheme of iodination performed by Thomassen from ref 44.

Oxidation

In 1998 Guilard et. al. reported the oxidation and subsequent ring opening of freebase corroles when dissolved in DCM and exposed to ambient light and air[62], and soon after Paolesse et. al. reported the photodegradation of a corrole-porphyrin dyad[63]. While corroles are stable compounds for the most part, freebase corroles are prone to photodegradation, while freebase porphyrins are much more stable. The oxidation reported by Guilard occurred at carbons 1 and 19, cleaving the pyrrole-pyrrole bond and yielding an open chain biliverdin compound. Many other ring-opening photooxidations have been reported over time for freebase corroles, where they usually occur between the 9 and 10 carbons or the 15 and 16 carbons of the corrole.

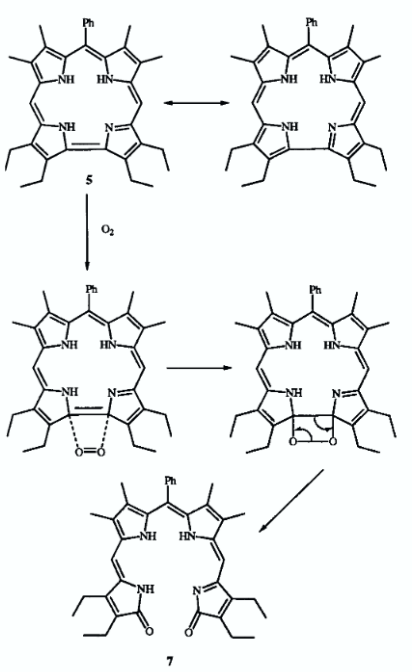

Figure 14: Cleaving experienced by Guilard from ref 58.

Corrole post-functionalization

There are many different ways of functionalizing corrole peripheral carbons through ordinary organic transformations, such as reducing β-nitro groups to amines, and reacting those with carboxylic acids to generated amides[21]. Among the different methods, nucleophilic aromatic substitution of *para*-fluorine on a pentafluorophenyl group at the *meso* position with a good

nucleophile is a particularly popular method. In chapter 4 we perform such a substitution using a dithiol to make thiol-appended gold and rhenium corroles.

Nucleophilic aromatic substitution

For porphyrins and corroles the use of pentafluorophenyl as a *meso*-substituent is common. Corroles with *meso*-pentafluorophenyl usually exhibit enhanced photophysical properties, while also making ^{1}H NMR easier to resolve due to the lack of C-H bonds[64]. Pentafluorophenyl groups can undergo nucleophilic aromatic substitution (NAS), where the *para* fluorine group is displaced by a nucleophile. Fluorine is a good leaving group compared to other halogens for this reaction, where the opposite is usually true.

S_N1 and benzyne mechanisms

There are many different mechanisms for NAS. The most widely known mechanisms are the S_NAr, $S_N1$through diazonium salt and benzyne mechanism. The S_N1 mechanism occurs whit the very good leaving group dinitrogen (N_2), leading to the creation of a cation by dissociation upon heating. A nucleophile will then attack the cationic carbon to give the desired product. The rate determining step for this reaction will be the dissociation of the nitrogen gas to create the cation[65].

The benzyne reaction mechanism works very differently. Instead of making an arene cation, we make a benzyne as the name suggests. This is done by using a very strong base to deprotonate the arene *ortho* to the leaving group, eliminating the leaving group to give the benzyne. The nucleophile then attacks the least hindered benzyne carbon, which then protonates the other benzyne carbon to yield the final product. The rate limiting step in this reaction will be the formation of benzyne[65].

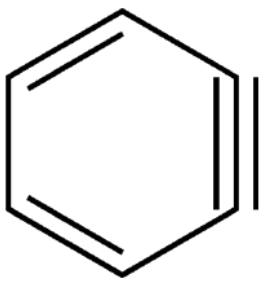

Figure 15: Structure of a benzyne

S_NAr mechanism

S_NAr works by having electron withdrawing groups capable of stabilizing a negative charge *ortho* or *para* to the species we want to substitute. The mechanism occurs in 2 steps, addition then elimination. First the nucleophile attacks the aryl, where the resulting negative charge is stabilized through resonance. Then the aromaticity is restored by elimination of the leaving group[66]. The reaction rate is impacted by the leaving group through inductive effects, where a stronger electron withdrawing leaving groups, such as fluoride reacts faster than iodide. This is opposite to the reactivity expected by S_N1 and S_N2 substitution reactions. The fluoride will draw more of the electron density towards it making the aryl carbon electrophilic, leading to

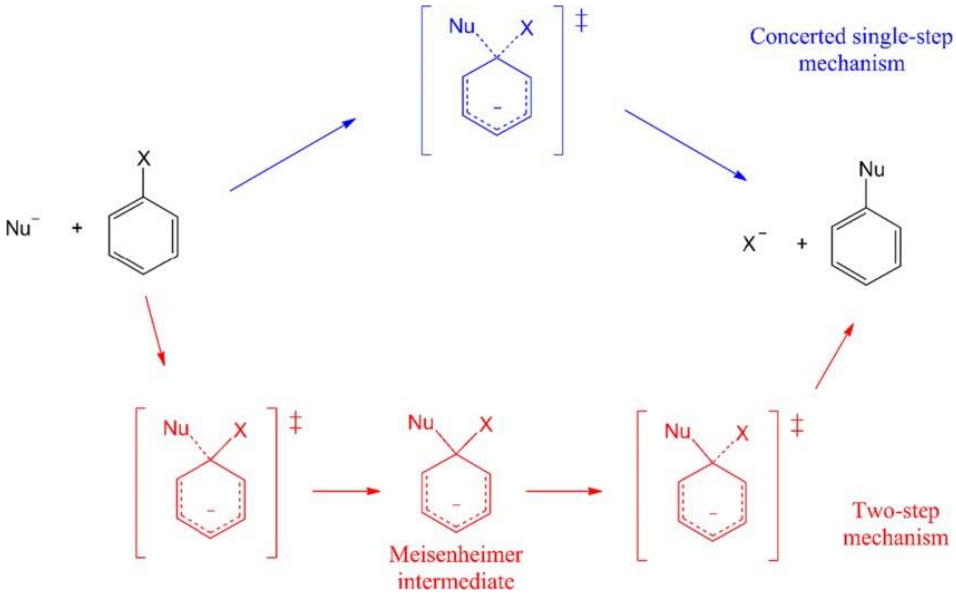

Figure 16: S_NAr and cS_NAr reaction mechanisms from ref 62.

its reactivity towards nucleophiles. As the attack of the nucleophile disturbs the aromaticity of the system, this step will be rate limiting, whereas the elimination is much faster as it restores aromaticity[65].

The evidence for an addition-elimination mechanism has been known since intermediates of the S_NAr were isolated by Meisenheimer in 1902[67]. Further studies have established this mechanism as the norm, so long as the electron withdrawing groups on the arene can help with stabilizing the reaction through resonance[68]. This is not always the case however, and

having F or CF_3 as substituents yields similar reactivity as NO_2 or Ac would. This has led to the exploration of a concerted mechanism of S_NAr to explain the discrepancies.

cS_NAr mechanism

In recent times the evidence for a concerted nucleophilic aromatic mechanism (cS_NAr) has grown. In the 1980s studies that proposed a potential concerted mechanism as opposed to the normal mechanism started popping up[69, 70]. These proposed mechanisms were difficult to study however, and the computational models as well as computing power of the time was not good enough to study these systems. Over time computational models have improved, and now many computer models predict cS_NAr where S_NAr was seen as the norm. cS_NAr closely resembles S_N2 and the reactivity of certain systems show a preference for better leaving groups such as a leaving bromide over fluoride, which is opposite to what we expect in a S_NAr reaction[71].

Chapter 4: Synthesis of thiol-appended ReO and Au corroles

Synthetic strategy

My goal was to find a one-step synthesis for making thiol-appended metallocorroles. I originally thought this challenge would be straightforward, however complications arose that would limit the useability of our preferred synthesis. I discovered that Schoefberger had succeeded in making similar compounds to those I was after, but when I tried a similar synthesis I could not get it to work properly, and therefore had to simplify the system to figure out what was happening.

Results

I managed to synthesize and isolate thiol-appended gold- and rhenium-corroles, using 1,3-propanedithiol, 1,5-pentanedithiol and 1,8-octanedithiol. I tried to synthesize rhenium-corrole using both 1,2-ethanedithiol and 1,3-benzenedithiol, but the reactions were not fruitful and more work is required for these reactions.

I aimed to use a similar approach to Schoefberger[72] for our synthesis. By using M[TPFPC] with a dithiol and a base we should get the desired product, hopefully with minimal sidereactions. There were however safety concerns around using NaH in DMSO as reported by Yang et. al.[73] As our group has had success using K_2CO_3 as a base, I decided to use that instead. I also decided to use THF as a solvent, as it is non-protic and easy to remove due to its low boiling point compared to DMF or DMSO. For trial reactions pentane dithiol was mainly used, as this was the dithiol used in the synthesis by Schoefberger. These experiments failed, as the desired product could not be found using MS, and when removing the solvent, the product of the reactions formed a polymer that was no longer soluble in anything. I then tried loading directly onto a column, but this did not yield any results either. That said, TPFPC complexes were found to exhibit superior phosphorescence relative to nonfluorinated corroles, as described in the appendix. I synthesized the ReO and Au[TPFPC] as described in

the manuscript in the appendix, as we hoped these compounds could be used for this thesis as well.

From the MS it seemed like two different things were happening that made the results more complex than anticipated. Firstly, the reaction did not necessarily stop after one fluorine was substituted at any one phenyl. This led to self-cyclisation as well as polymerization between different species. Secondly there were issues with oxidation of the free thiol. Any free thiol group will oxidize in contact with oxygen and peroxides, and I tried to reduce oxidation by degassing with argon, which slightly helped. I also tried using chloroform as a solvent to remove any issues of oxidation from THF peroxides, but the reaction didn't work with chloroform as a solvent.

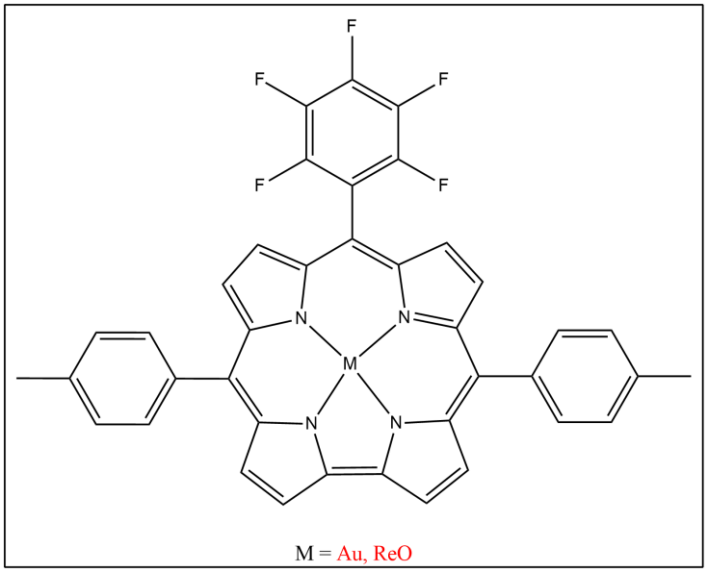

Figure 17: M[5,15-Tol-10-C_6F_5-Corrole]

After many failures, I decided to work on a simpler system with only one pentafluorophenyl group, instead of three. I decided on tolyl as the other *meso*-substituent, but any group that cannot easily undergo S_NAr should work. This simpler system should not be able to polymerize much, leading to a more manageable procedure. This simpler system still did not work as expected though, and some self-cyclisation still occurred for certain reactions, where I ended up with the dithiol substituting one more fluorine leaving no open thiol. This was not ideal, as generating a free thiol connected to a corrole in one-step was the main goal of the project. I thought the self-cyclisation might be temperature dependent, and as I was using K_2CO_3 as the base, I needed to heat the reaction to reflux for it to progress.

The base was changed from K_2CO_3 to LiHMDS after trials using LiHMDS, triethylamine and NaH, and it allowed us to use a slight excess (2eq.) of both dithiol and base, compared to before where we needed to use a large excess base (approx. 30eq.). Some of the reactions I performed were at very small scales, and when using less than 5mg metallocorrole I used higher equivalents of the dithiol and base as the low volumes required became difficult to work with.

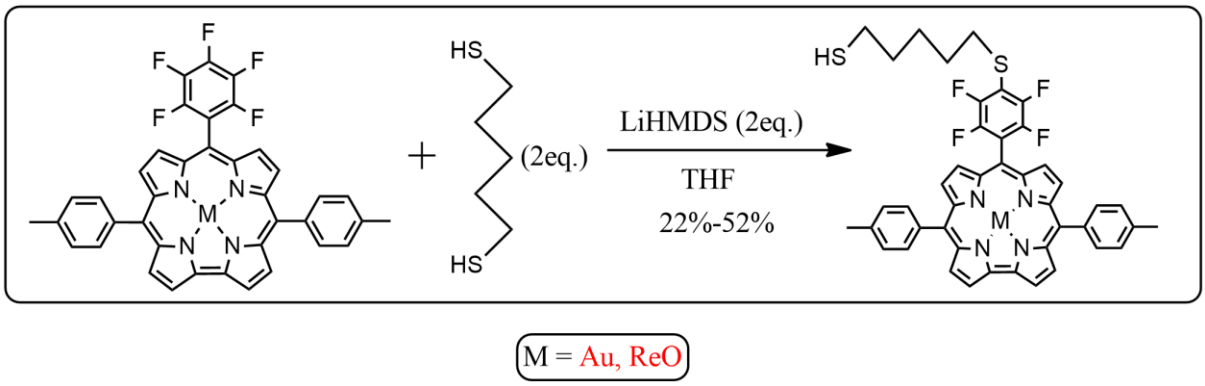

Figure 18: The synthetic strategy I employed with 1,5-pentanedithiol as an example.

Purifying our products was more difficult than expected. I tried to isolate the product by using column chromatography, which seemed to work well to remove any byproducts like any oxidized species. Removing any excess dithiol however became a hassle, and I did not have time to optimize the isolation of the compounds, so I never managed to fully isolate and clean the very small-scale reactions. The compounds also interacted in some way to both silica and neutral alumina TLC plates, which reduced the yield through each step in the isolation making it impossible to do more than 2 or 3 steps before I had less than 1mg product.

Data analysis

The majority of my syntheses were successful. Some however failed, like Re[5,15-Tol-10-C_6F_4-SC_6H_4SH-Corrole](O) and Re[5,15-Tol-10-C_6F_4-SC_2H_4SH-Corrole](O). Both Re[5,15-Tol-10-C_6F_5-Corrole](O) and Au[5,15-Tol-10-C_6F_5-Corrole] were made without any issues, and we got very good NMR spectra from these compounds.

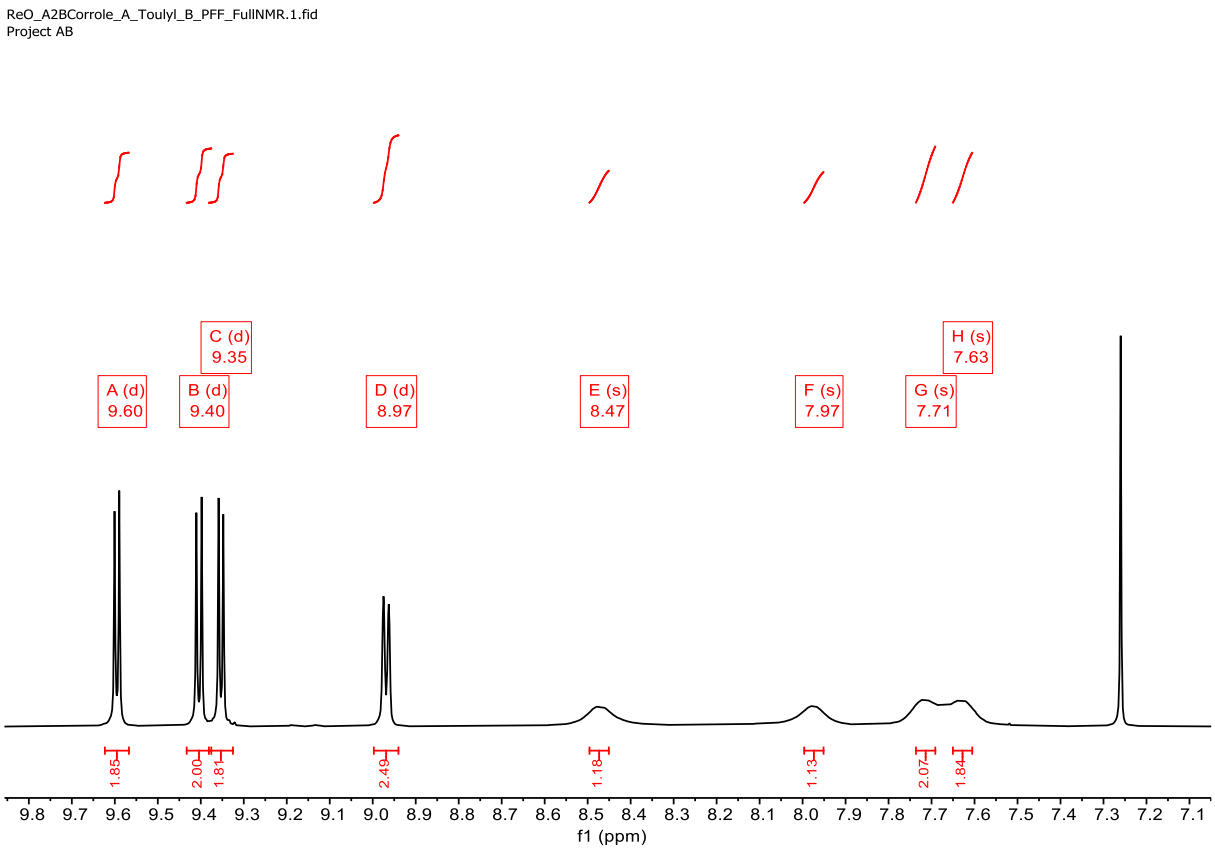

Figure 19: Aromatic ^{1}H NMR region of Re[5,15-Tol-10-C_6F_5-Corrole](O)

From Figure 18 we can clearly see the 8 β-hydrogens between 9.6 and 8.9 ppm as peaks A to D, where all show up as doublets as expected. The aromatic hydrogens from the tolyl group can be found as peaks E to H, where they show up as singlets, which is different between the gold and rhenium oxo complexes as seen in figure 2. The reason for the difference is the geometry of the two compounds. The *meso*-aryl groups have hindered rotation and the chemical shift of the *ortho* hydrogens, and the *meta* hydrogens to a lesser extent, will depend on which side of the ReO corrole they are on, as it is not flat but domed. At higher

temperatures the rotation becomes faster which leads to less distinguished peaks for each hydrogen environment, and the peaks will look like the gold-complex peaks.

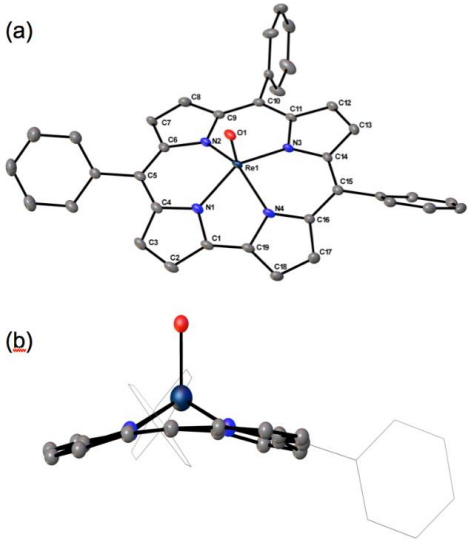

Figure 20: Geometry of ReO corrole complexes from ref 7.

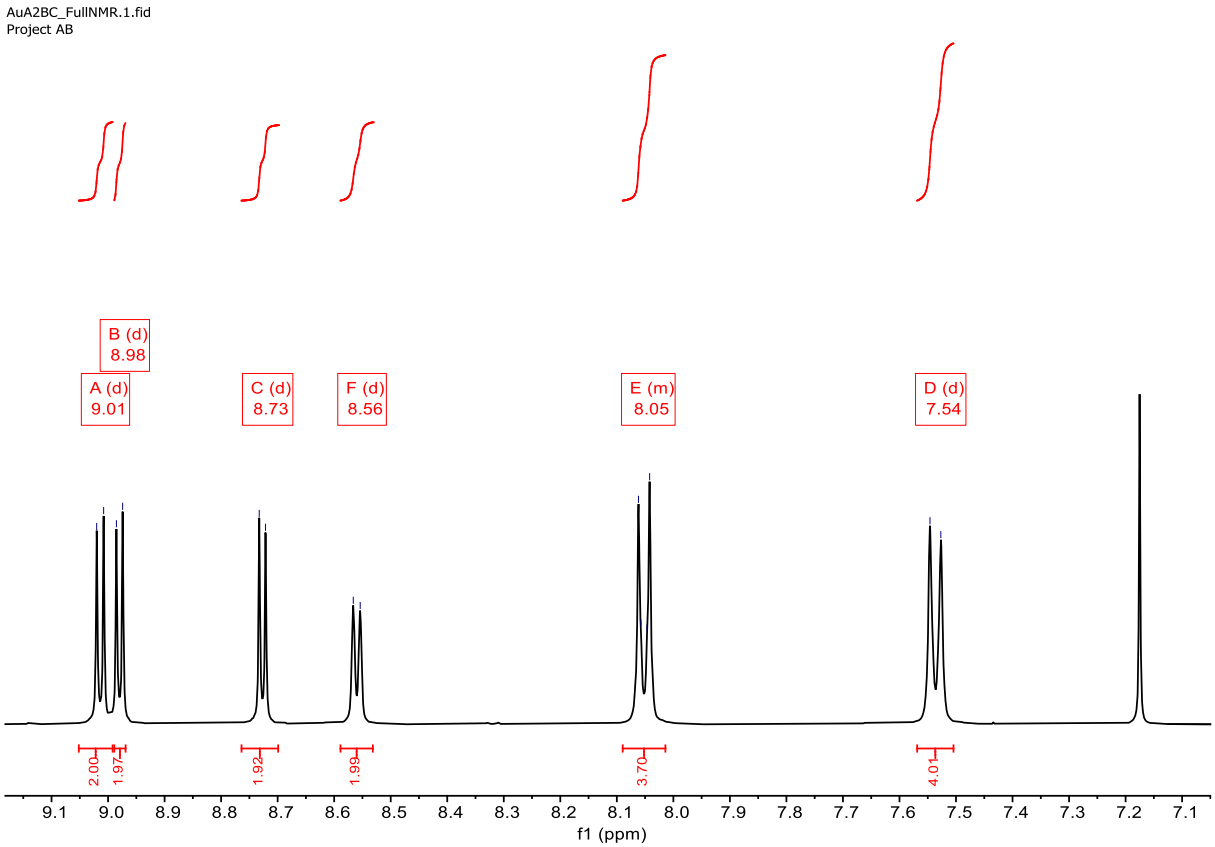

Figure 21: Aromatic 1H NMR region of Au[5,15-Tol-10-C6F5-Corrole]

The aliphatic region of both Re[5,15-Tol-10-C_6F_5-Corrole](O) and Au[5,15-Tol-10-C_6F_5-Corrole] are similar and show small impurities and a peak around 2.7 ppm which is the CH_3 group of the tolyl as seen in figure 3.

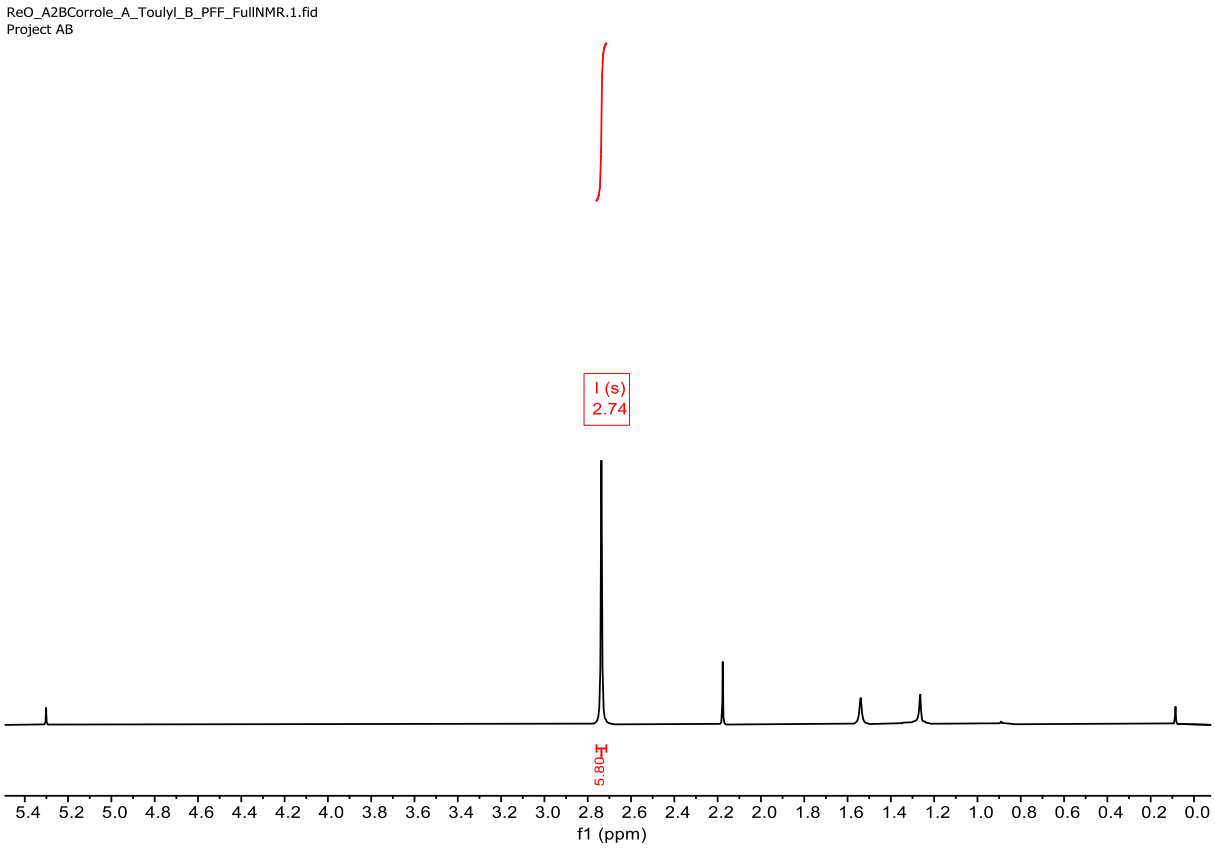

Figure 22: Aliphatic ^{1}H NMR region of Re[5,15-Tol-10-C_6F_5-Corrole](O)

These motifs are expected to be the same for the substituted species, and the only difference should come in the aliphatic region as the functional groups added will not have any aromatic characteristics.

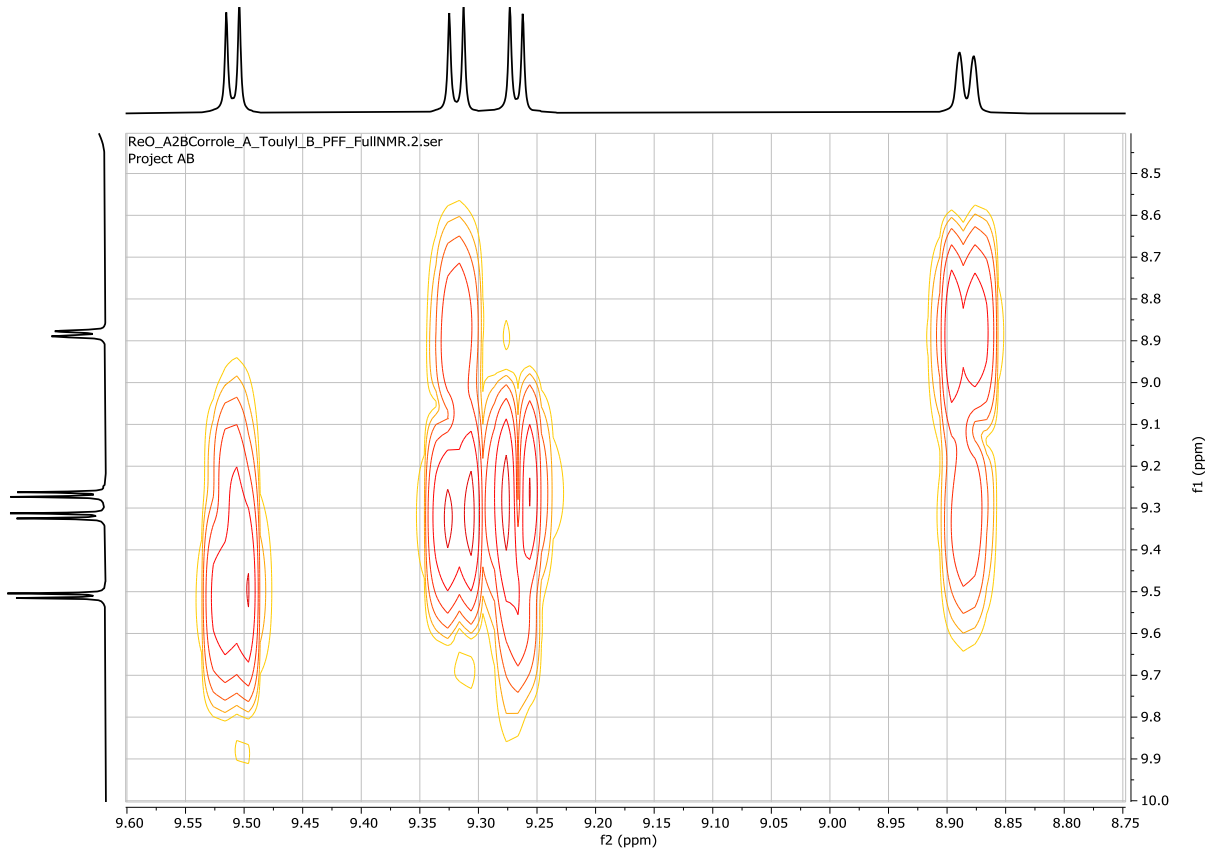

Figure 23: COSY of the β-carbons of Re[5,15-Tol-10-C_6F_5-Corrole](O)

From figure 22 we can assign each of the β-hydrogen pairs. The lowest ppm β-hydrogen peak is around 8.88 ppm as seen in figure 22, and this peak will come from hydrogens 1 and 8 shown in Figure 23. This peak is paired with the peak around 9.32 ppm which will be

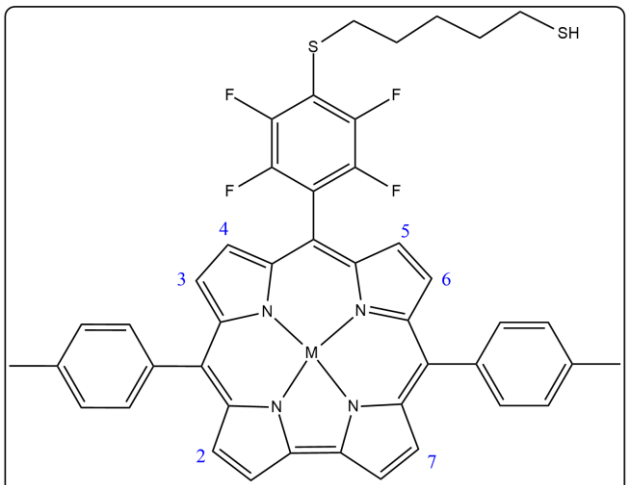

Figure 24: M[5,15-Tol-10-C_6F_4-$SC_5H_{10}SH$-Corrole] with labelled β-hydrogens

hydrogens 2 and 7. As hydrogens 4 and 5 are closest to the pentafluoro group, these will be the highest ppm peak at around 9.5 ppm. The peak around 9.28 is then hydrogens 3 and 6.

The same phenomenon that occurs with the aromatic tolyl hydrogens is also expected for the fluorines at the pentafluorophenyl groups, where the gold complex should have three peaks while the rhenium-oxo complex should have 5. We can clearly see that this is the case from figures 25 and 26.

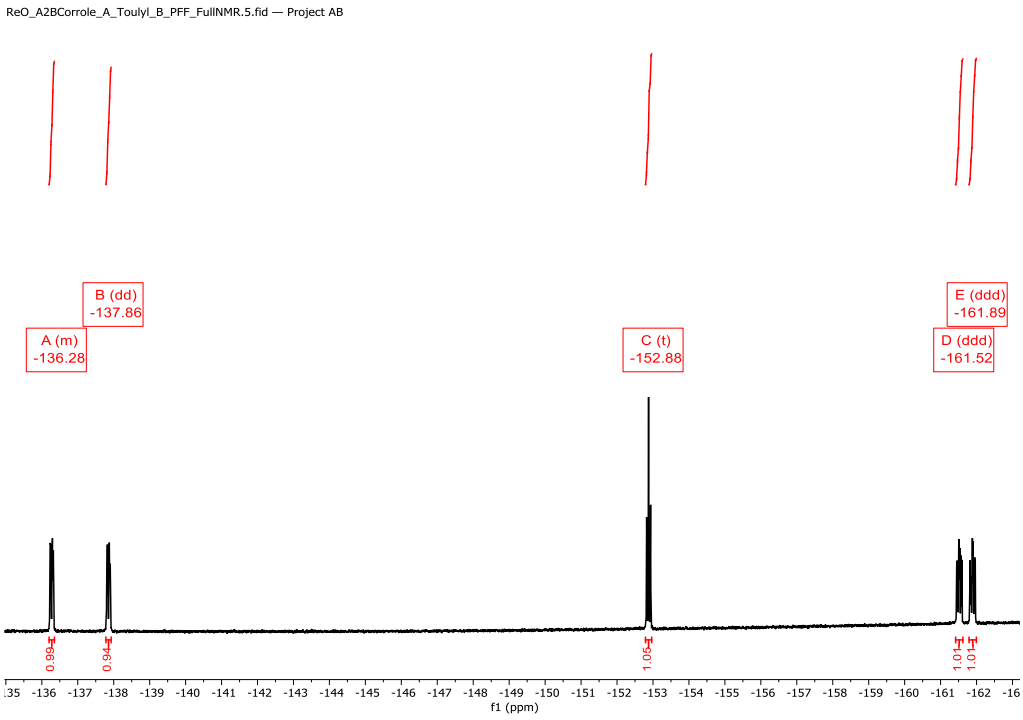

Figure 25: ^{19}F NMR for Re[5,15-Tol-10-C_6F_5-Corrole](O)

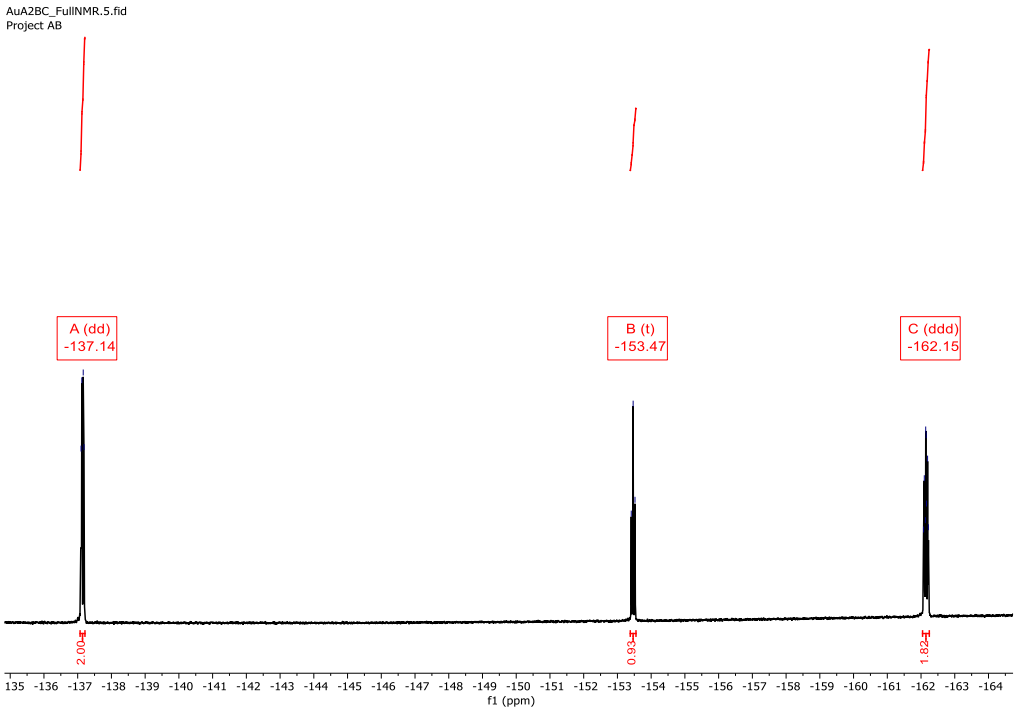

Figure 26: ^{19}F NMR for Au[5,15-Tol-10-C_6F_5-Corrole]

We can also assign each fluorine from figures 26 and 27. The fluorine pair at -137 ppm are the *ortho* fluorines, which can be gathered from figure 25, as the splitting of the peaks is more pronounced compared to the *meta* fluorines as expected. The -153ppm peak is the *para* fluorine while the – 162ppm peaks comes from the *meta* fluorines.

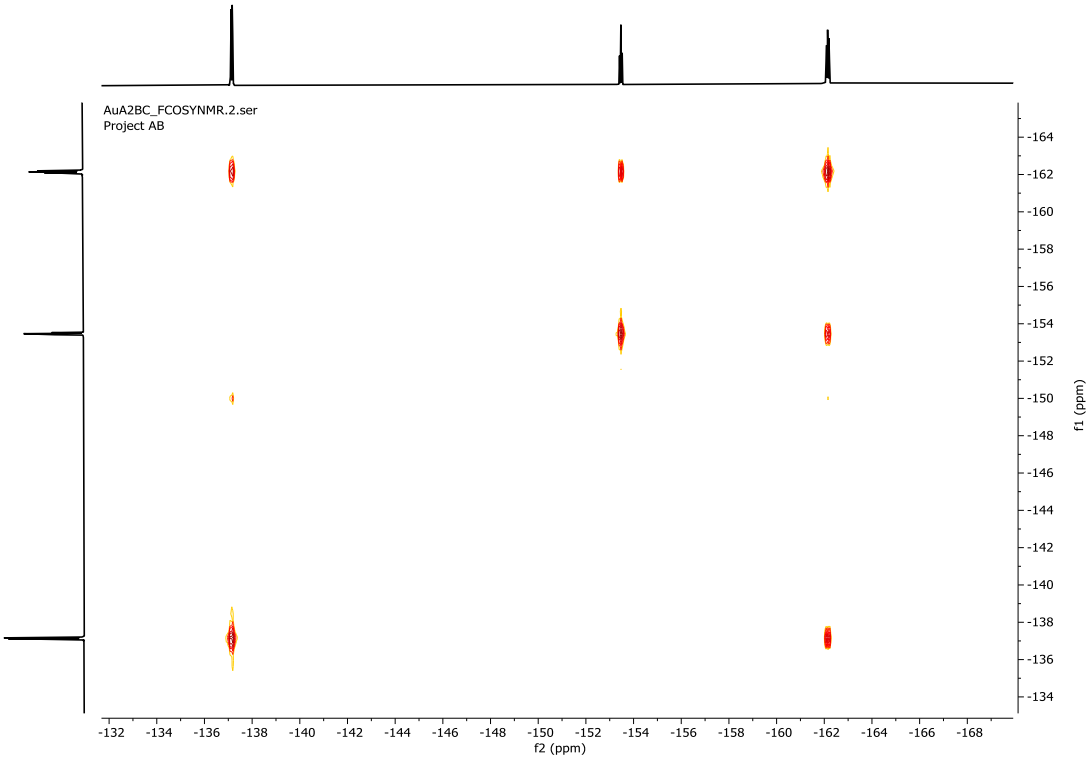

Figure 27: ^{19}F-COSY for Au[5,15-Tol-10-C_6F_5-Corrole]

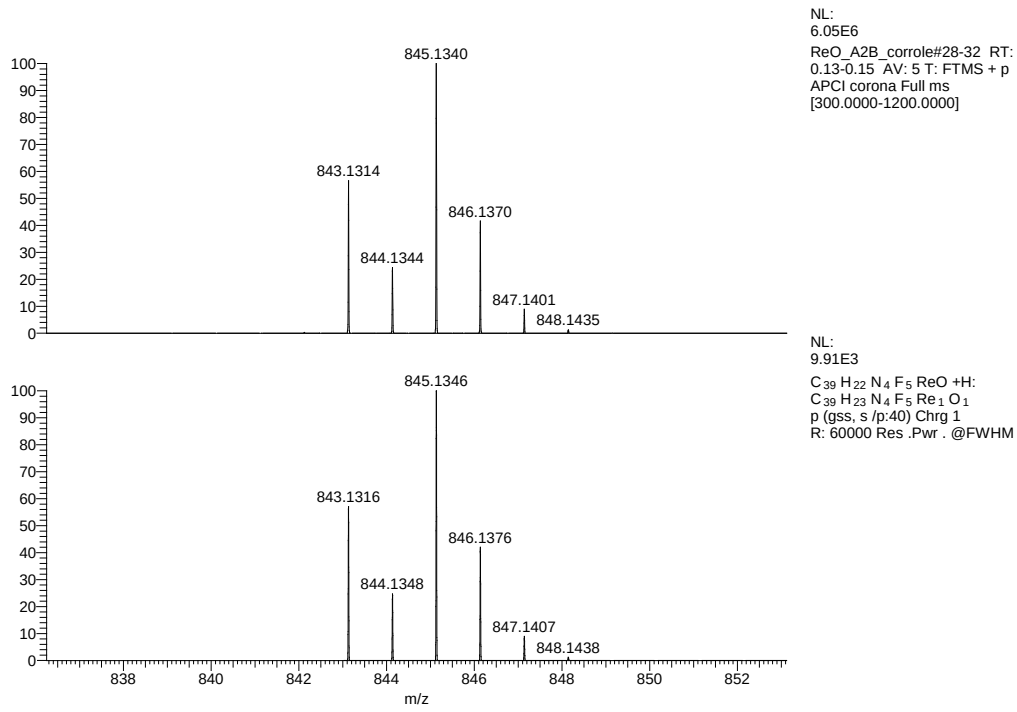

Figure 28: FTMS APCI of Re[5,15-Tol-10-C_6F_5-Corrole](O)

All the NMR information is as expected for ReO and Au[5,15-Tol-10-C_6F_5-Corrole], and the MS as shown in figure 28 also agrees with expected values, which gives us great confidence that the compounds we targeted were made.

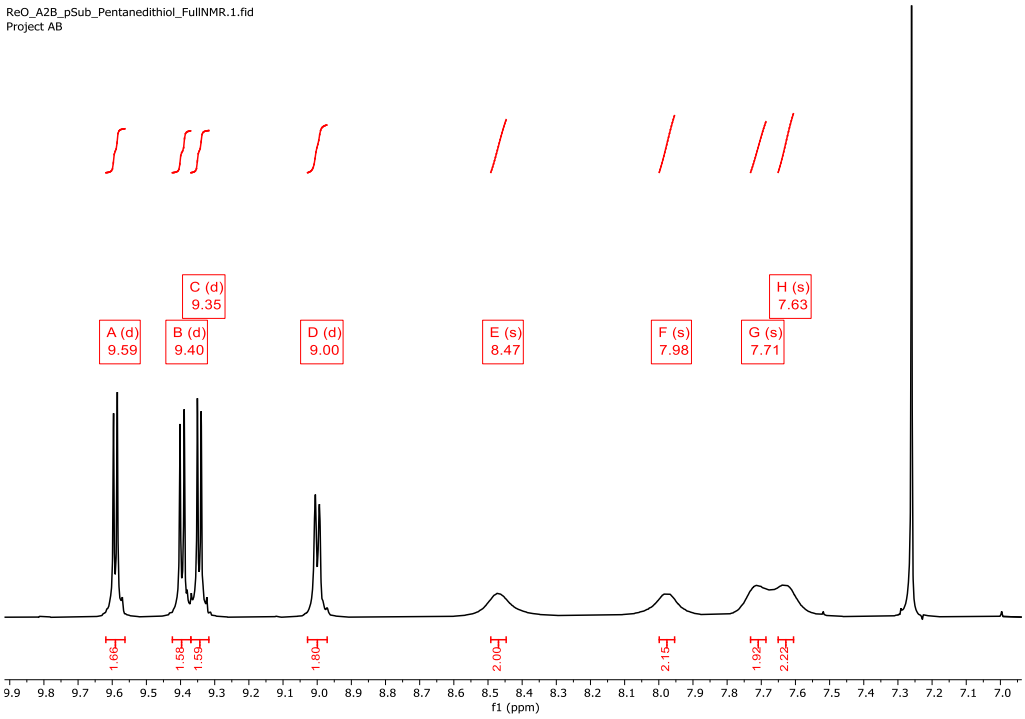

Figure 29: ^{1}H NMR of the aromatic region for Re[5,15-Tol-10-C_6F_4-$SC_5H_{10}SH$-Corrole](O)

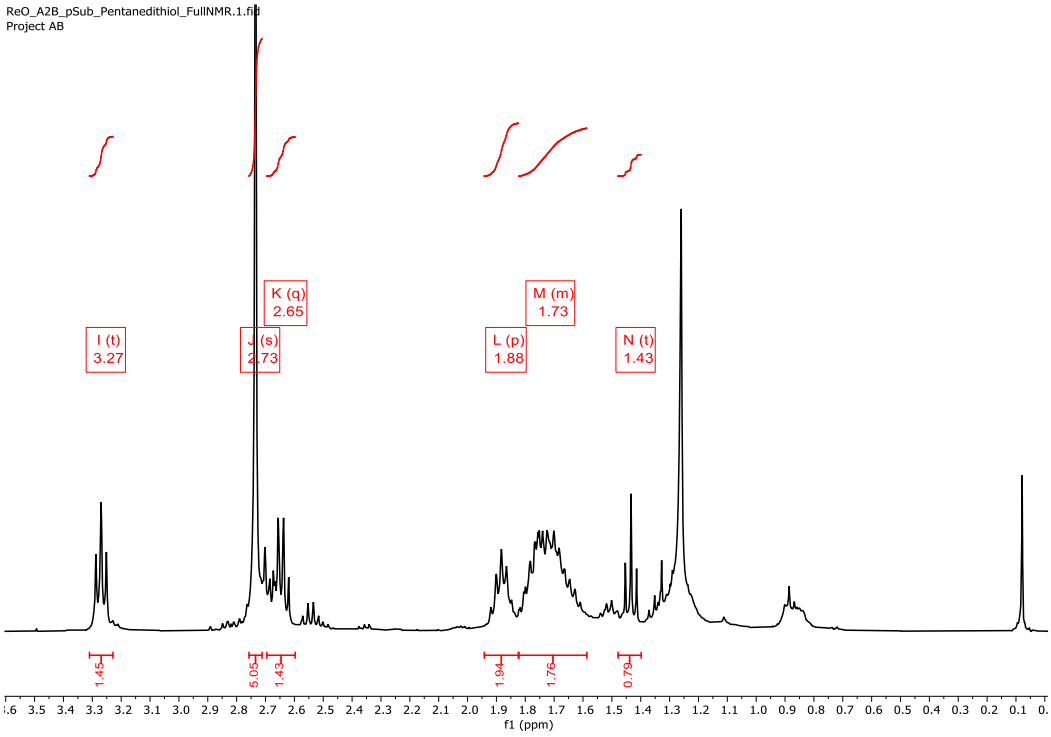

Figure 30: ^{1}H NMR of the aliphatic region of Re[5,15-Tol-10-C6F4-SC5H10SH-Corrole](O)

From the ^{1}H NMR of Re[5,15-Tol-10-C_6F_4-SC_5H_{10}SH-Corrole](O) shown in figures 29 and 30 we can see that the aromatic region is unchanged from the precursor, while the aliphatic region is changed by the addition of the pentanedithiol. This can also be seen in the ^{13}C NMR of both compounds shown in figures 31 and 32. It is clear that the aliphatic region has been altered which is a good sign that our synthesis was a success.

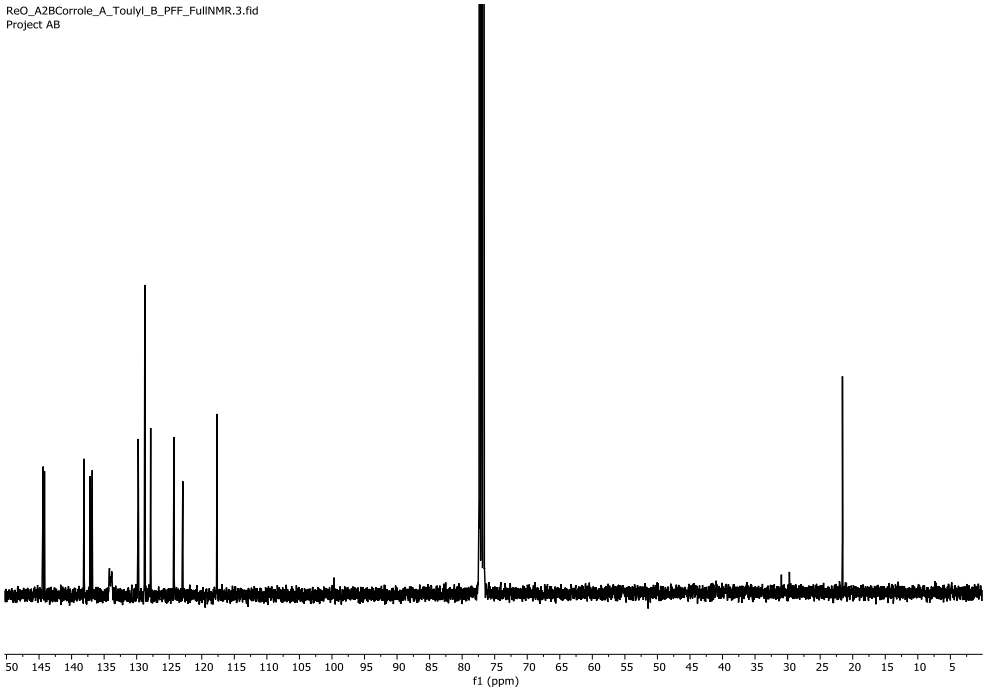

Figure 31: ^{13}C NMR of Re[5,15-Tol-10-C_6F_5-Corrole](O)

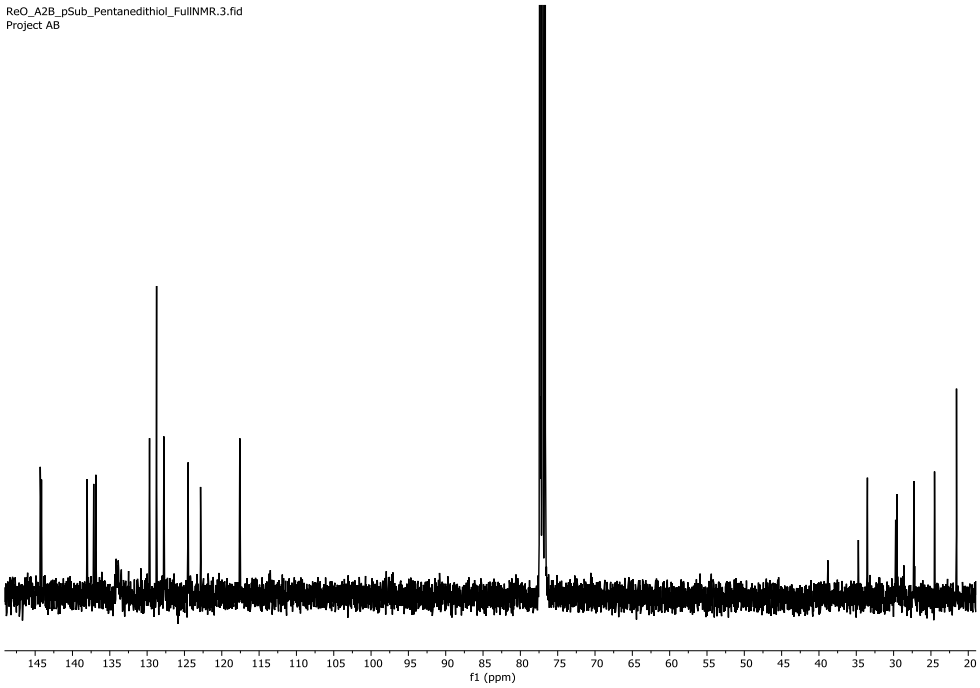

Figure 32: ^{13}C NMR of Re[5,15-Tol-10-C_6F_4-$SC_5H_{10}SH$-Corrole](O)

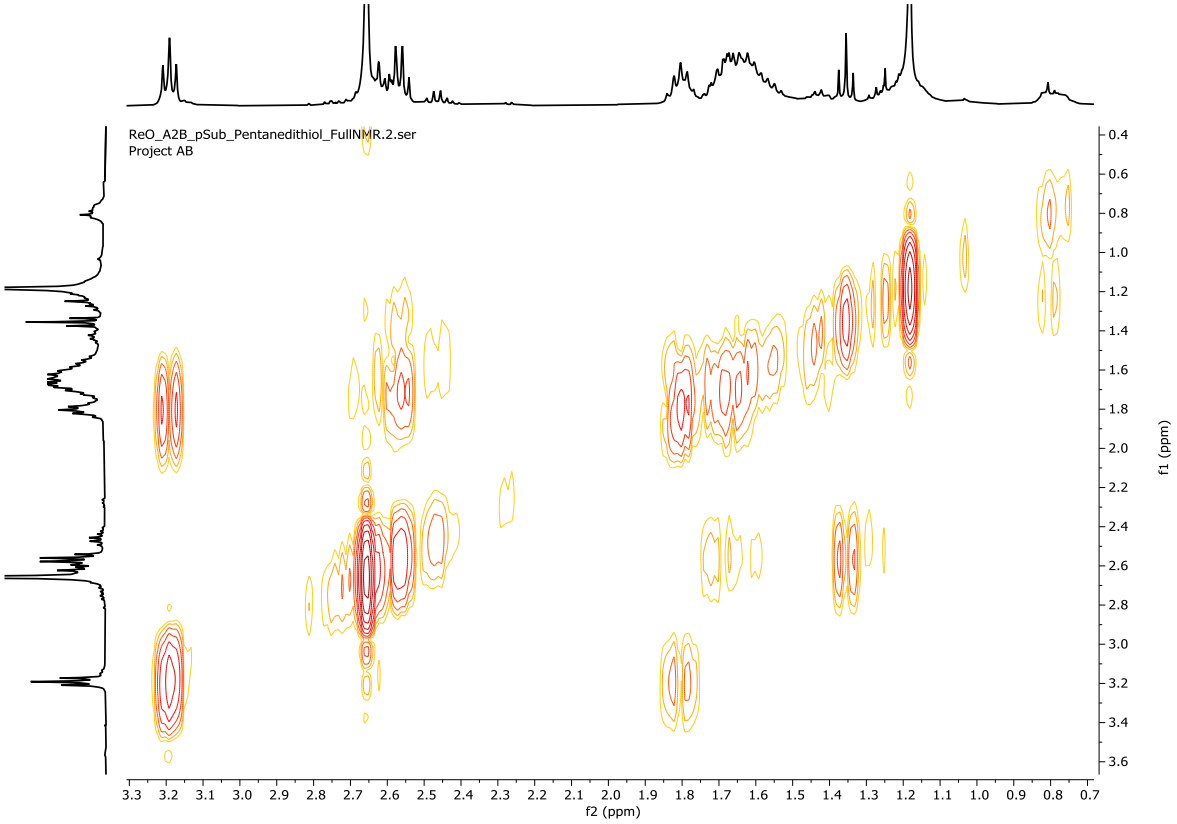

Figure 33: ^{1}H COSY of aliphatic region of Re[5,15-Tol-10-C_6F_4-SC_5H_{10}SH-Corrole](O)

Being able to fully assign each hydrogen pair of the pentane chain would increase the confidence of our results, it is however also very difficult due to some slight impurities and stacking of peaks to form unintelligible multiplets as seen in figure 33.

We can still have good confidence that we made our target compound in the case of Re[5,15-Tol-10-C_6F_4-SC_5H_{10}SH-Corrole](O), and this is mostly due to both the ^{19}F NMR and FTMS shown in figures 34 and 35. Our compound was very similar to the expected values and also had the same splitting pattern in MS, and the ^{19}F-NMR was also as expected, with 4 peaks that show the *meta* and *ortho* fluorines.

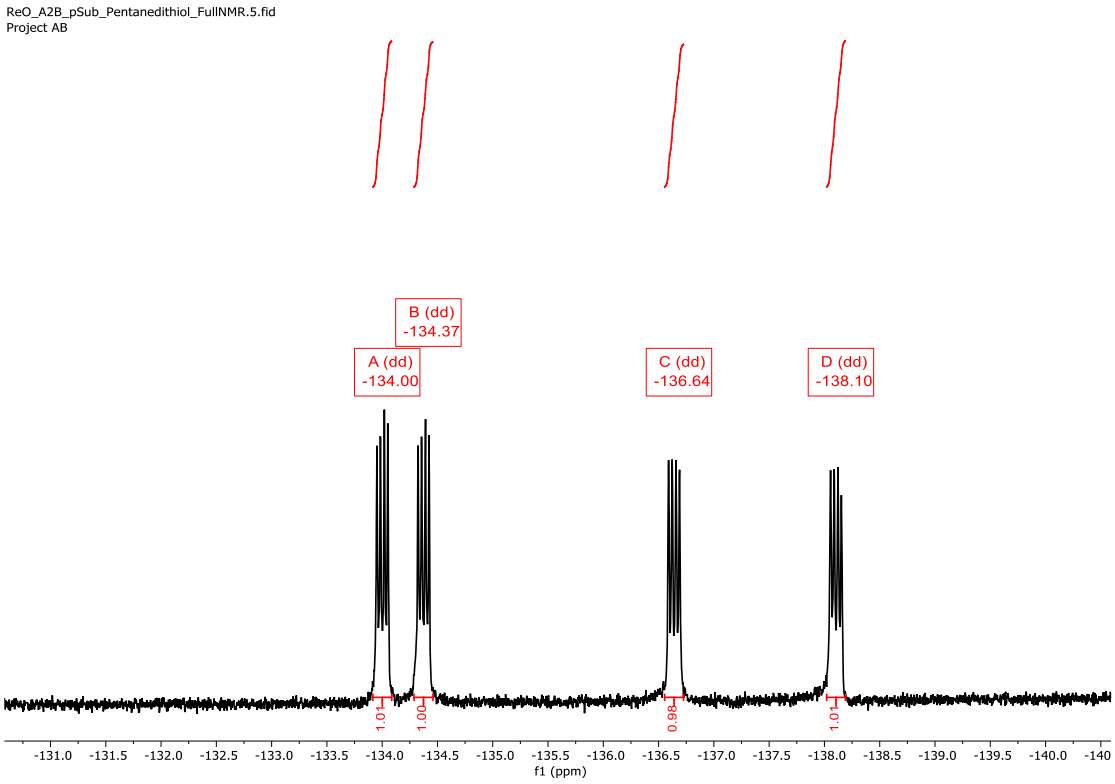

Figure 34: ^{19}F NMR of Re[5,15-Tol-10-C_6F_4-$SC_5H_{10}SH$-Corrole](O)

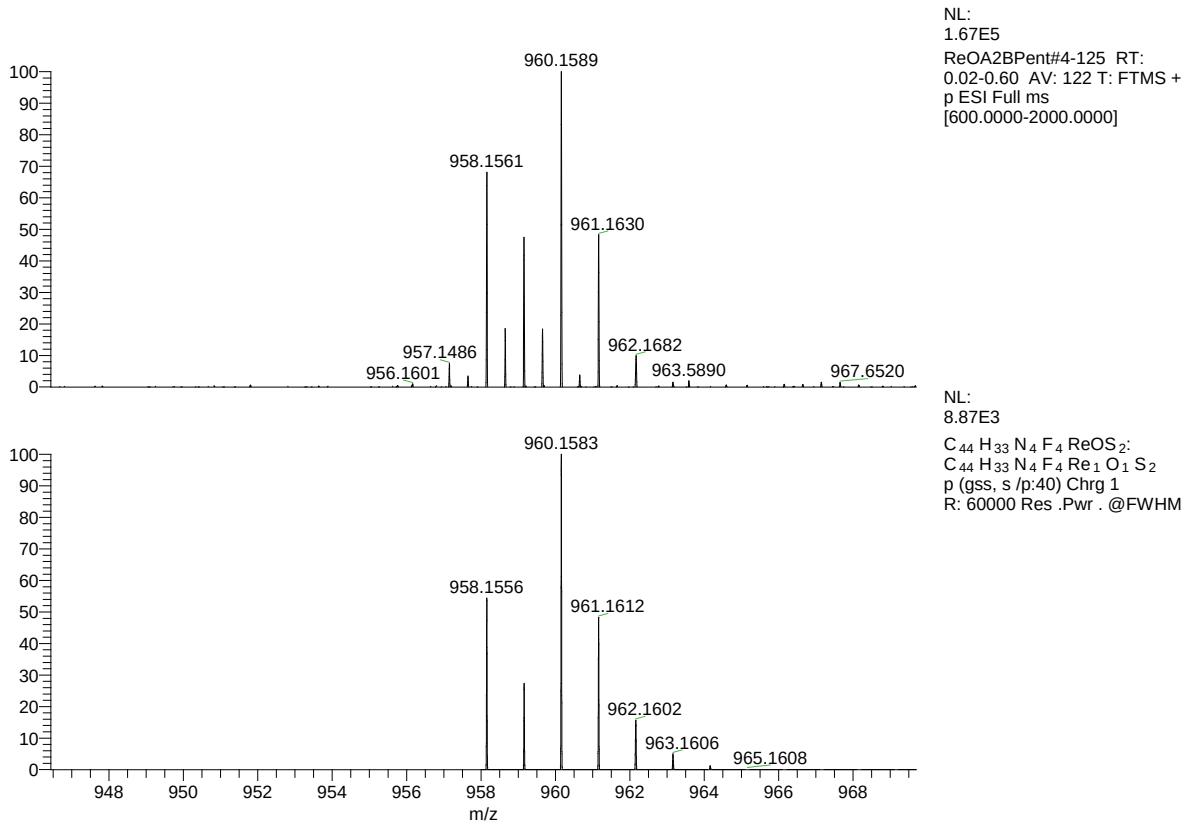

Figure 35: FTMS ESI of Re[5,15-Tol-10-C_6F_4-SC_5H_{10}SH-Corrole](O)

The characterisation of the products was not so simple for the gold-complexes, and it is difficult to fully know what was made in some of the cases. Most of the NMR data was poor as seen in figures 36 to 39. It looks like we may have more than one complex as we have overlap of peaks in the aromatic region, where we don't expect any change from the precursors. We can also see that the aliphatic region is unintelligible due to impurities. These compounds were difficult to isolate and purify as explained earlier, and the issues were exacerbated for the gold complexes as the reactions were done in much smaller scales due to the difficulty in making gold complexes compared to rhenium ones.

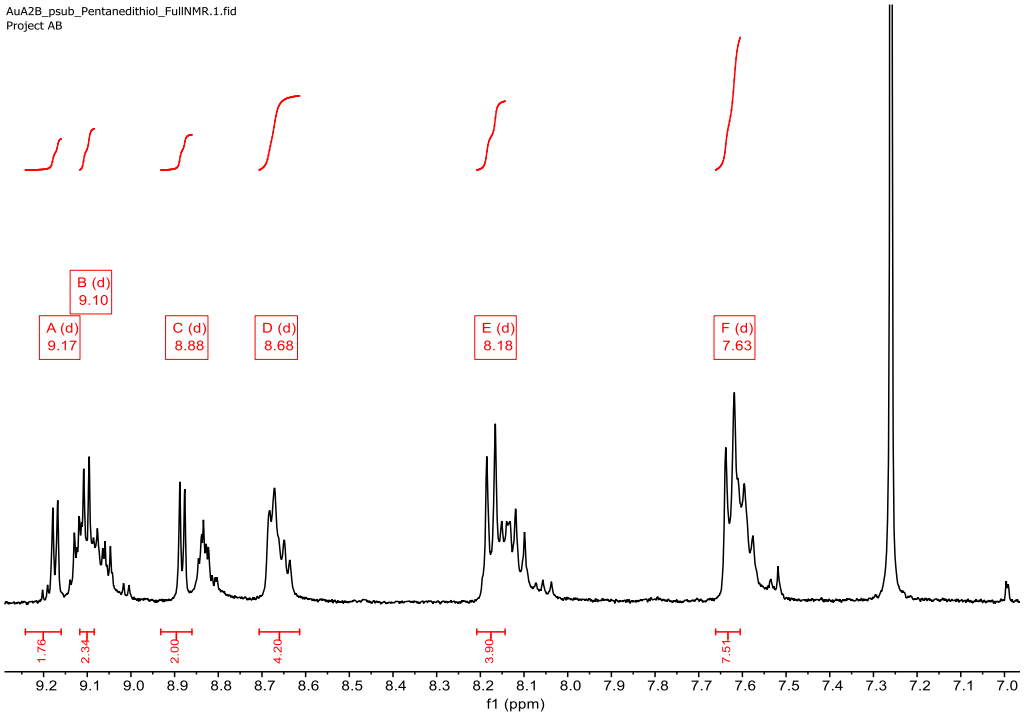

Figure 36: ^{1}H NMR of aromatic region of Au[5,15-Tol-10-C_6F_4-SC_5H_{10}SH-Corrole]

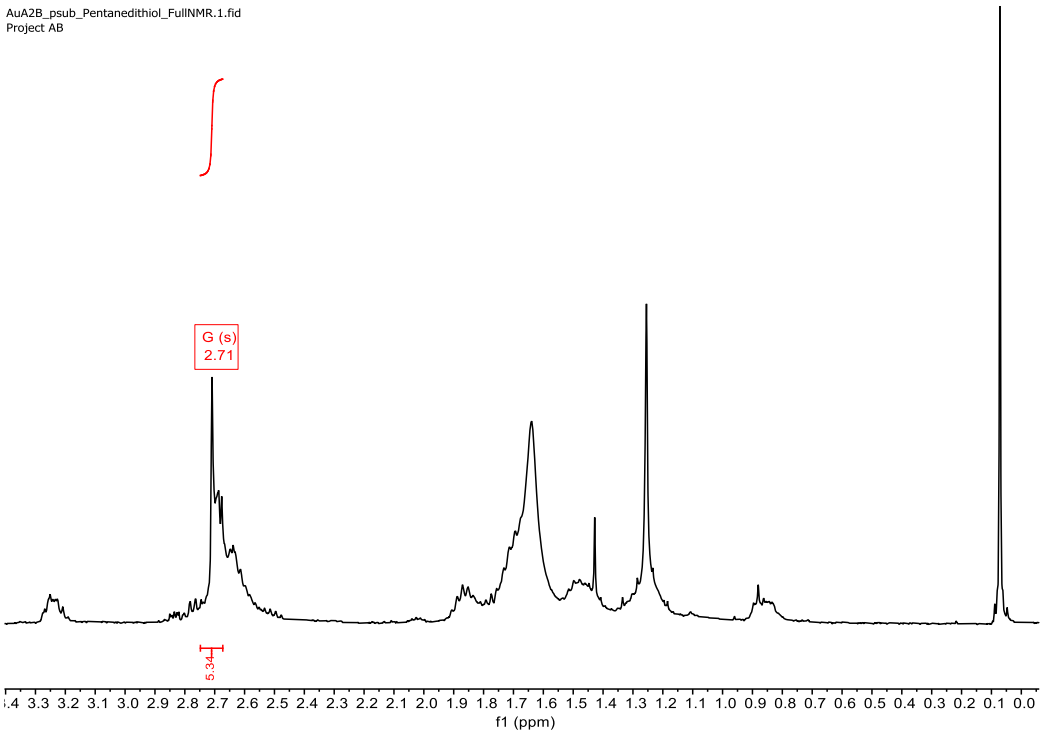

Figure 37: ^{1}H NMR of aliphatic region of Au[5,15-Tol-10-C_6F_4-SC_5H_{10}SH-Corrole]

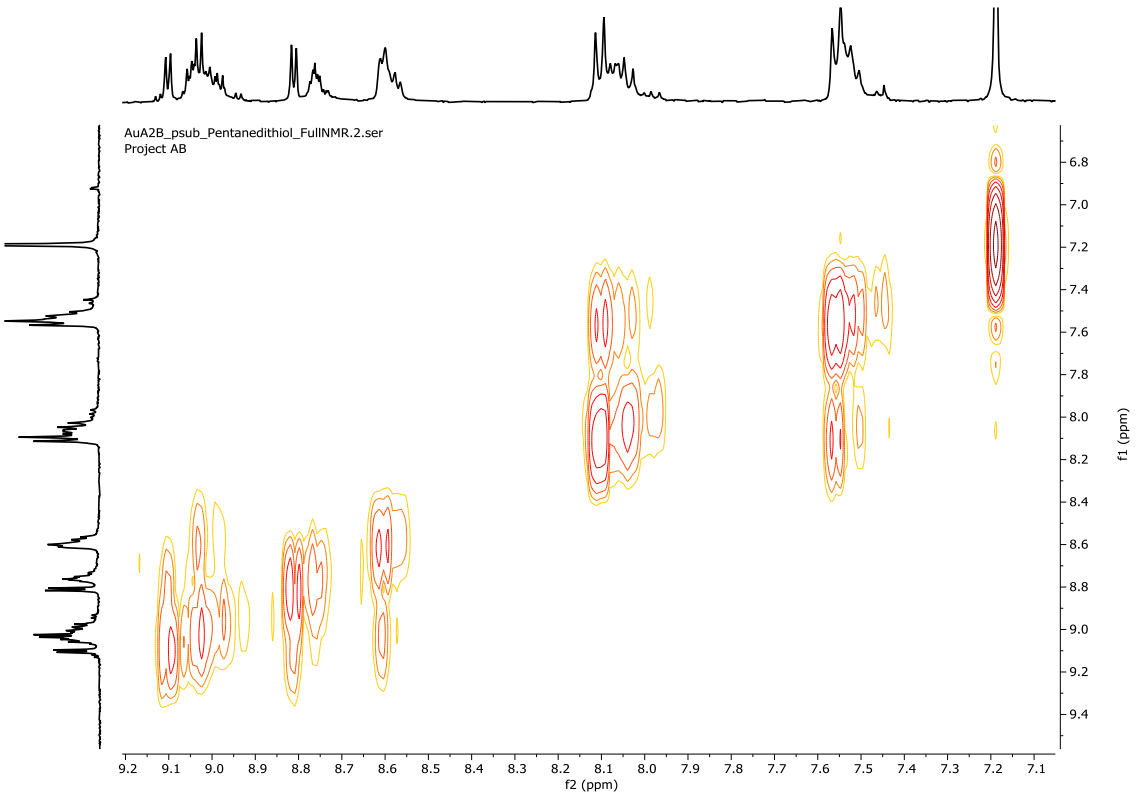

Figure 38: COSY of aromatic region of Au[5,15-Tol-10-C_6F_4-SC_5H_{10}SH-Corrole]

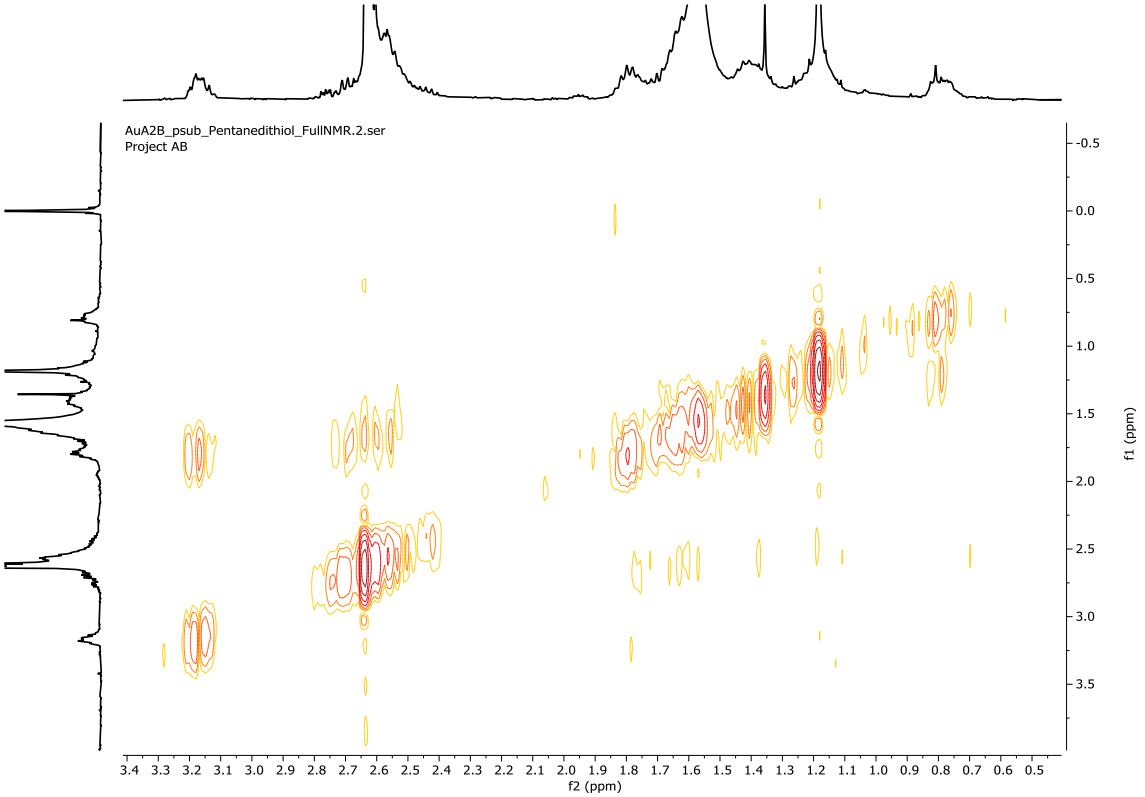

Figure 39: COSY of aliphatic region of Au[5,15-Tol-10-C_6F_4-$SC_5H_{10}SH$-Corrole]

While the ^{1}H NMR based spectra are poor for the compound, the ^{19}F spectra are rather decent, and clearly show two peaks of the same intensity. From the COSY shown in figure 39 we can see that we only have *meta* and *para* fluorines, and no *para*, meaning our substitution was a success. Our MS result however was unexpected, and the main peak we could identify that could come from our compound had one fluorine atom and one hydrogen less than expected. This would then indicate that we would have cyclisation of the dithiol to the phenyl by substituting one more fluorine, which seems highly unlikely, as that would mean that we need to have a completely racemic mix between *ortho* and *meta* substitution. The MS also shows a mixture between two compounds where the only difference is 2 hydrogens. We don't know why this is the case, and it is unexpected.

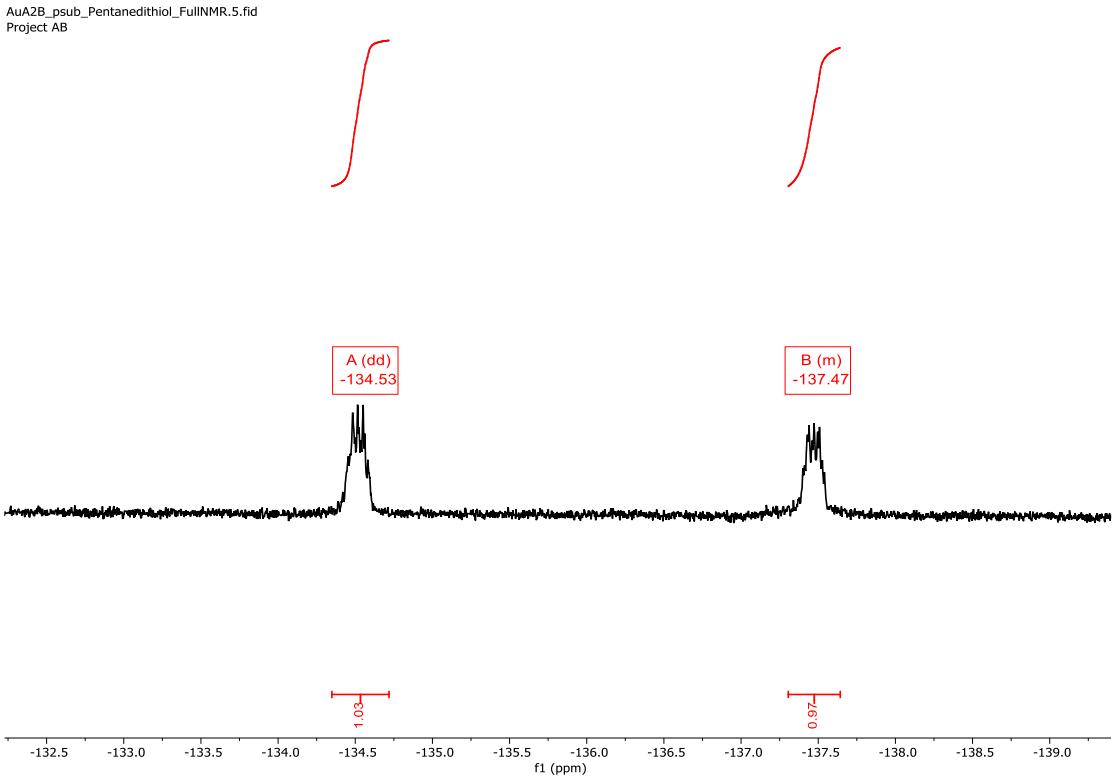

Figure 40: ^{19}F NMR of Au[5,15-Tol-10-C_6F_4-$SC_5H_{10}SH$-Corrole]

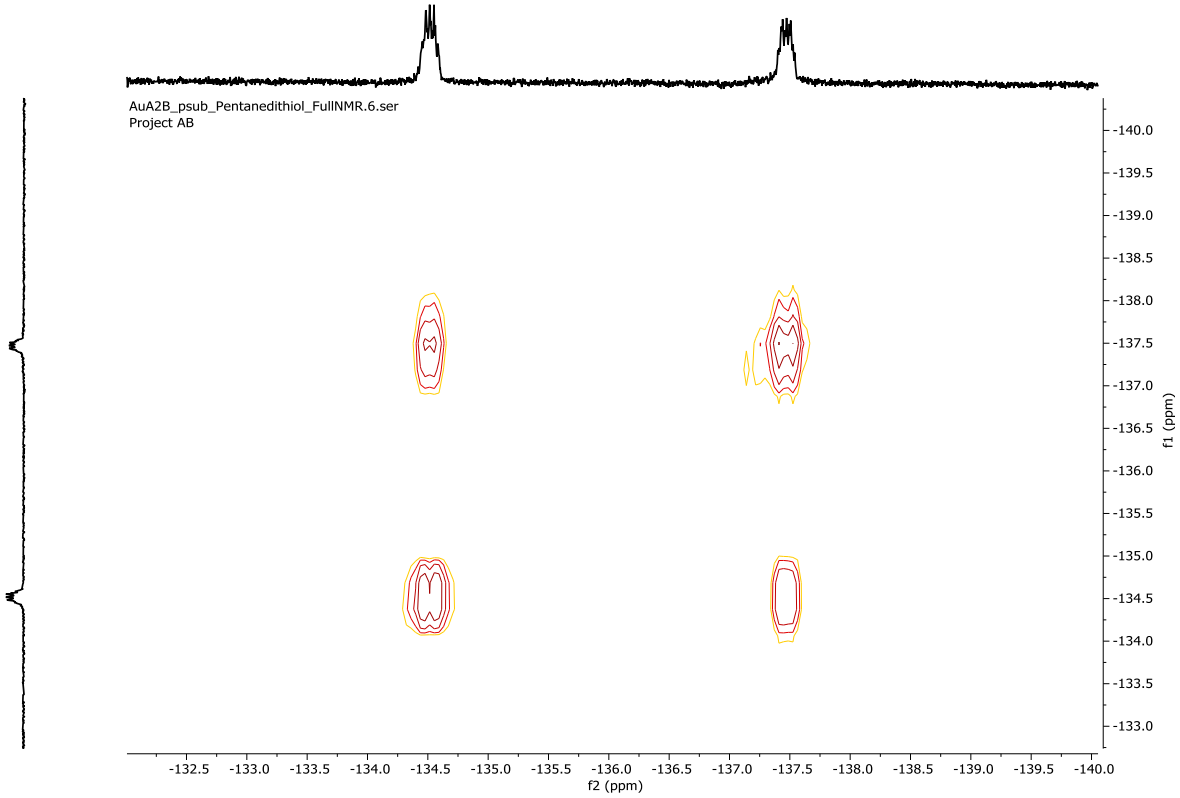

Figure 41: ^{19}F COSY of Au[5,15-Tol-10-C_6F_4-$SC_5H_{10}SH$-Corrole]

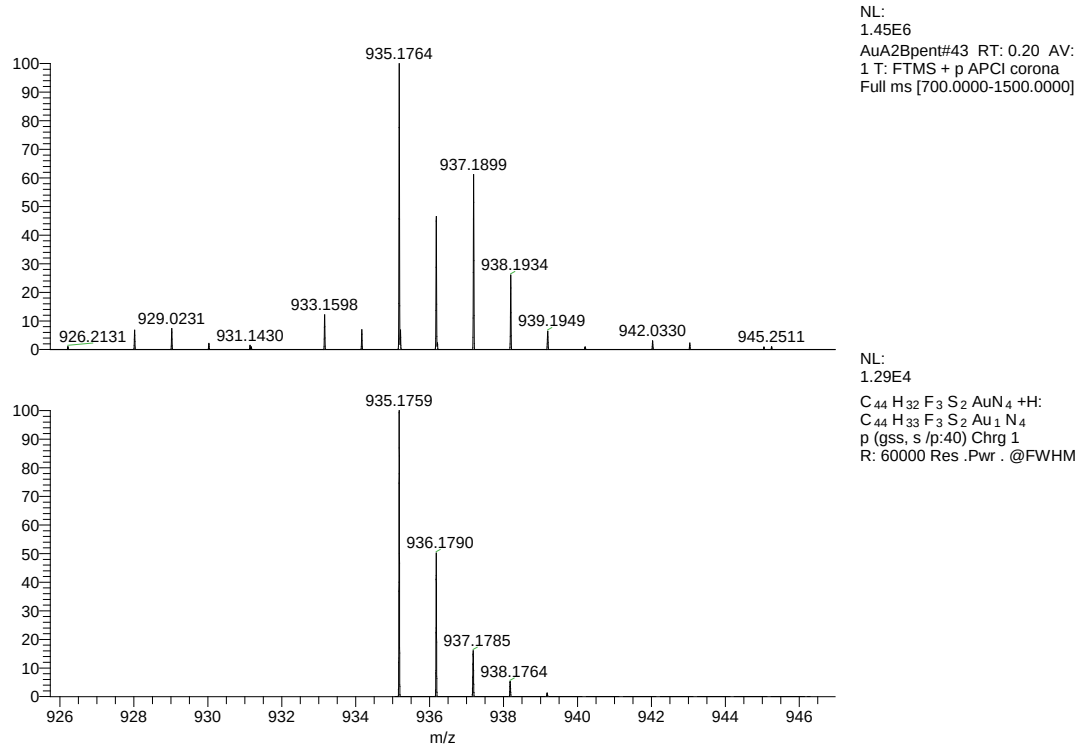

Figure 42: FTMS APCI of Au[5,15-Tol-10-C_6F_4-SC_5H_{10}SH-Corrole]

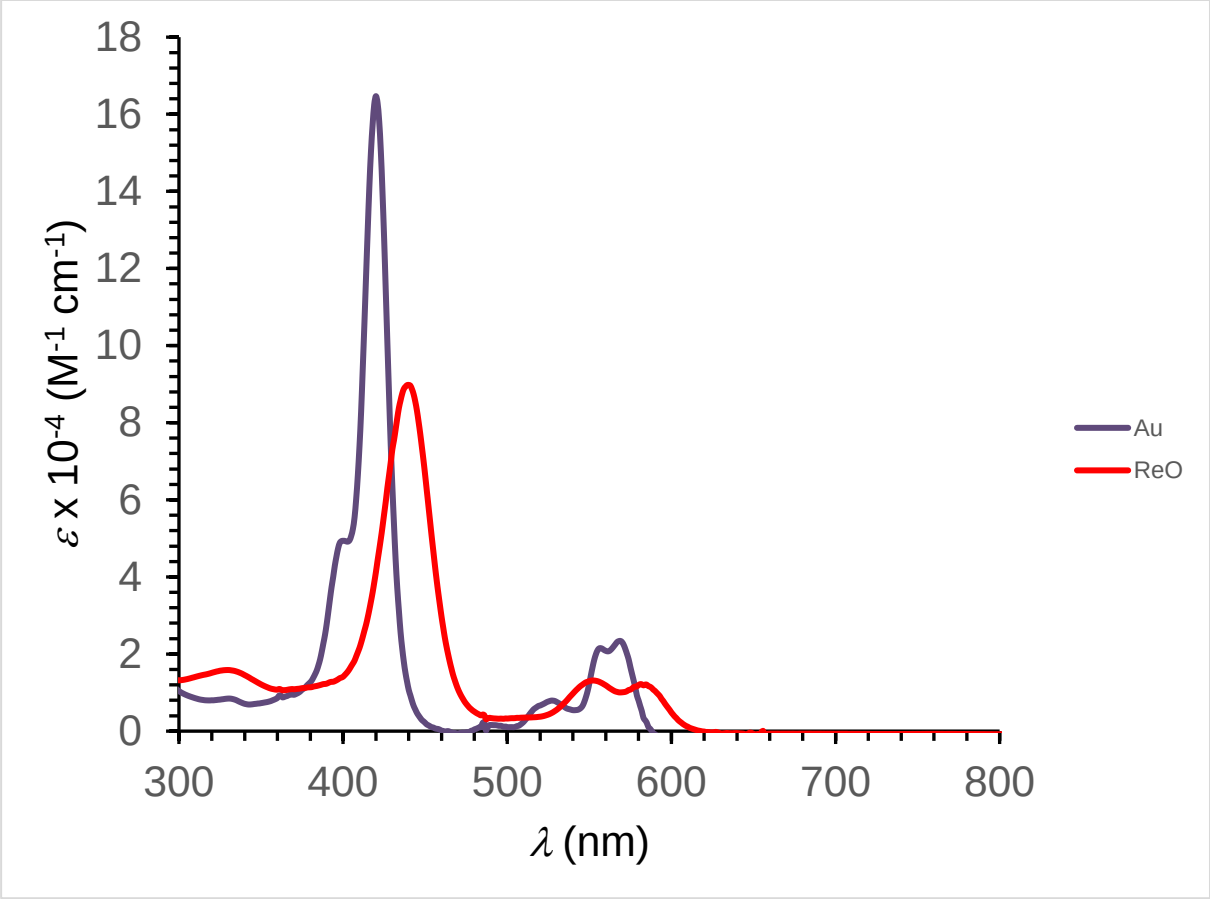

Figure 43: UV-vis spectra of Au[5,15-Tol-10-C_6F_5-Corrole] and Re[5,15-Tol-10-C_6F_5-Corrole](O)

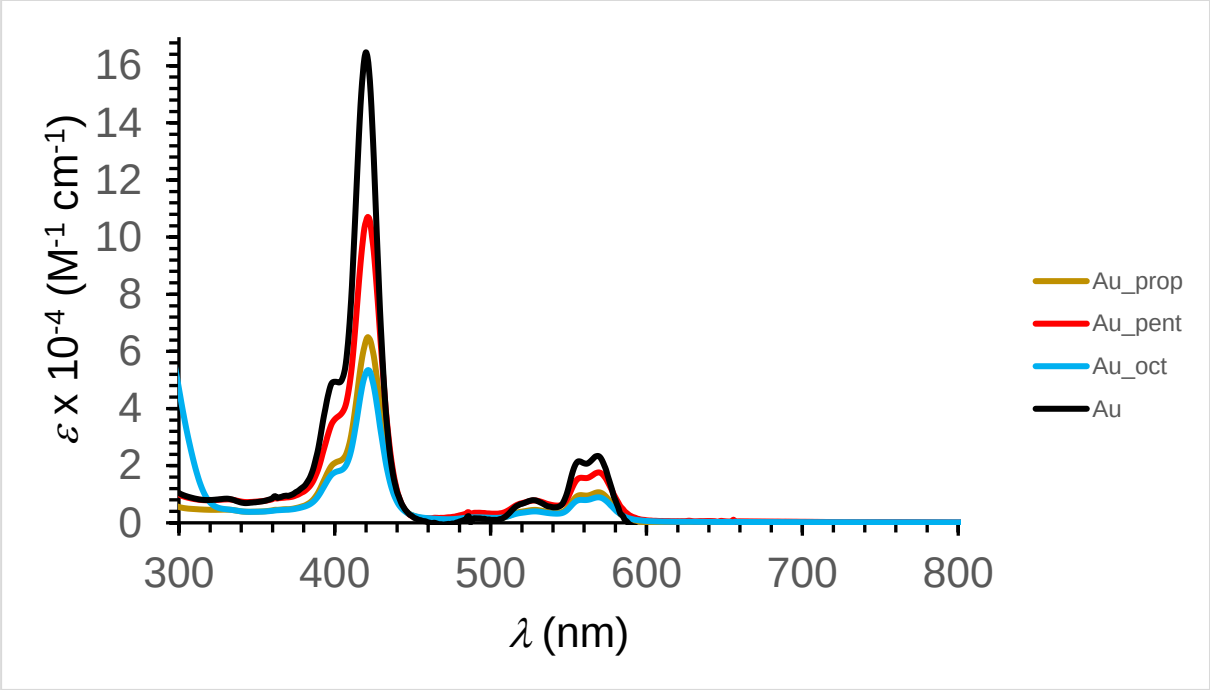

Figure 44: UV-vis of all Au-complexes

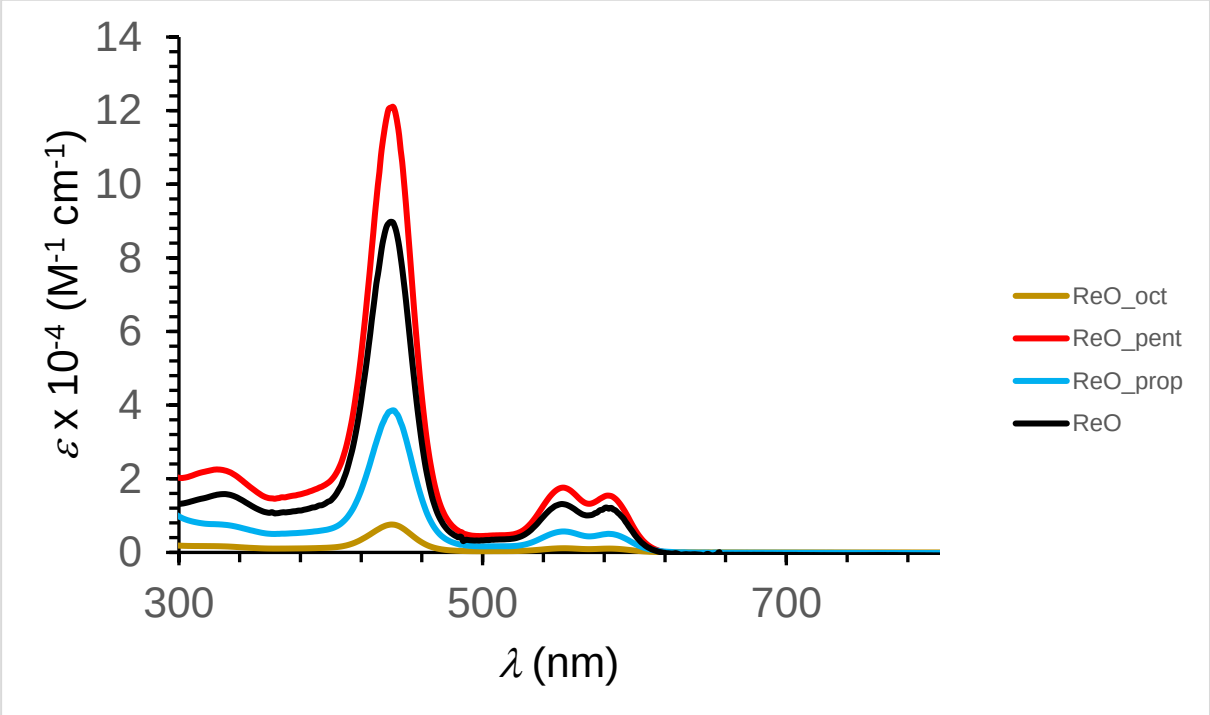

Figure 45:UV-vis of all ReO-complexes

The UV-vis spectra of the products are as expected, and clearly show the characteristics of gold and rhenium-oxo inserted corroles. We don't expect any change in UV-vis from the precursors to the products because our substitution doesn't impact the pi system in any way. The difference in excitation coefficients between the compounds arise from a difference in purity, where we can assume that the precursor compounds were purer than the product compounds, and are a better representation of the xxx efficiency of these types of compounds.

To further our research a better method for isolating and purifying the products is needed, and it would be of great interest to use dithiols which could interact with the pi system of the products.

Method

Materials

All reagents were purchased from Sigma-Aldrich and used as received, except pyrrole which was distilled and stored in the freezer. Silica gel 60 (0.04-0.063 mm particle size, 230-400 mesh, Merck) was employed for flash chromatography. Silica gel 60 preparative thin-layer chromatographic plates (20 cm x 20 cm x 0.5 mm, Merck) were used for final purification of all compounds.

General instrumental methods

UV-visible spectra were recorded on an HP 8454 spectrophotometer. 1H NMR spectra were recorded on a 400 MHz Bruker Avance III HD spectrometer equipped with a 5 mm BB/1H SmartProbe and referenced to either residual CH2Cl2 at 5.32 ppm or residual CHCl3 at 7.26 ppm. High-resolution electrospray-ionization mass spectra were recorded on an Orbitrap Exploris 120 spectrometer using methanolic solutions.

H_3[TPFPC]

1 eq. (1.5708g) pentafluorobenzaldehyde and 80µl of a TFA/DCM solution was mixed and stirred at 40°C. To this mixture 1.5 eq. (840µl) pyrrole and 2 ml DCM was added. The

solution was stirred for 30 minutes, and a solution of 1 eq. (2.0112g) DDQ in 12ml THF/Toluene (1:1) was added. 20 ml DCM was added, and the reaction was stirred for 15 minutes. The product was then isolated using column chromatography once using 1:3 DCM/n-hexane as eluent then using 1:5 DCM/n-hexane as eluent, where the purple fraction matching the expected UV-vis was collected. The solvent was evaporated yielding 0.1656g (8%)

H_3[5,15-Tol-10-C_6F_5-Corrole]

6 eq. (7ml) pyrrole and 1 eq. (2ml) p-tolualdehyde was dissolved in 300ml distilled water and 1 ml HCl was added to the solution. The solution was stirred at room temperature (r.t.) for 2 hours and then filtered and washed with dist. H_2O. The compound was then purified using column chromatography with silica gel and an eluent of 1:9 diethyl ether/pentane. The solvent was removed yielding 0.9846g (25%) of dipyrromethane. The dipyrromethane (2eq.) was then dissolved along with 1eq. (0.4818g) pentafluorobenzaldehyde in 200ml MeOH. A solution of 2ml HCl in 200ml dist. H_2O was added to the solution, and the mixture was stirred for 1 hour and 20 minutes at r.t. An extraction was then performed using 200ml $CHCl_3$, washing twice with dist. H_2O. 1 eq. (0.6230g) p-chloranil was added, and the solution was refluxed with stirring for 1 hour. The product was then isolated using column chromatography with 1:4 DCM/n-heptane as the eluent, collecting the first purple fraction. The solvent was then removed yielding 0.1004g (6%) H_3[5,15-Tol-10-C_6F_5-Corrole].

General procedure for rhenium insertion

1 eq. freebase corrole, 1.5 eq. of dirhenium decacarbonyl and 10 eq. potassium carbonate was dissolved in 10 ml dichlorobenzene. This mixture was then refluxed with stirring for 18-24 hours. The solution was purified using column chromatography, where it was flushed with n-heptane to remove the dichlorobenzene, then an eluent of 1:2 DCM/n-heptane was used, and the red frontrunning band was collected.

General procedure for gold insertion

1 eq. freebase and 3 eq. gold(III) acetate was dissolved in 10 ml pyridine and stirred at r.t. overnight. The solvent was then removed, and column chromatography was used to purify the

compound using 1:3 DCM/n-heptane as eluent, collecting the front running red band. The solvent was removed.

Nucleophilic substitution of F with dithiol

1 eq. M[5,15-TOL-10-C_6F_5-Corrole] and 2 eq. dithiol was dissolved in 10 ml THF. The solution was degassed with argon and 2 eq. 1 M LiHMDS in THF was added to the solution. The solution was stirred for 2 hours at r.t. and mass spec was used to confirm that there no longer were any M[5,15-TOL-10-C_6F_5-Corrole] in the solution. The solvent was removed, and the product was purified using column chromatography, first flushing with n-heptane then using 1:5 DCM/n-heptane as eluent and increasing polarity until the first red band was collected. Any red band left only moved on column with the addition of methanol to the eluent system, indicating it was oxidized species.

Re[TPFPC](O)

Yield 52.6mg (45%). UV-vis (CH_2Cl_2) λ_{max} [nm, ε x 10^{-4} ($M^{-1}cm^{-1}$)]: 326 (1.52), 434 (8.71), 550 (1.18), 583 (1.31). ^{1}H NMR (400 MHz, CDCl3, 25 °C) δ 9.75 (d, J = 4.5 Hz, 2H, β-H), 9.32 (d, J = 4.6 Hz, 2H, β-H), 9.25 (d, J = 5.0 Hz, 2H, β-H), 9.14 (d, J = 4.9 Hz, 2H, β-H); ^{19}F NMR -136.03 (dddd, J = 43.4, 23.8, 8.9., 3.7 Hz, 3F, 5,10,15-o1-PF), -137.29-137.93 (m, 3F, 5,10,15-o2-PF), -151.99 (dt, J = 27.7, 21.1 Hz, 3F, 5,10,15-p-PF), -160.89 (tdd, J = 21.5, 12.5, 8.5 Hz, 3F, 5,10,15-m1-PF), -161.17 (dddd, J = 44.9, 23.7, 20.9, 8.6Hz, 3F, 5,10,15-m2-PF. MS (ESI): M^+ = 996.0014 (expt), 996.0012 (calcd for C37H8F15N4ORe). Spectral data will be published in manuscript submitted to ACS Organic & Inorganic under the name “Influence of Fluorinated Substituents on the Near-Infrared Phosphorescence of 5d Metallocorroles”

Au[5,15-Tol-10-C_6F_5-Corrole]

Yield 11mg (34%). UV-vis (CH_2Cl_2) λ_{max} (nm), [ε x 10^{-4} (M^{-1} cm^{-1})]: 400 (4.94), 420 (16.47), 527 (0.79), 557 (2.15), 569 (2.34) ^{1}H NMR (400 MHz, $CDCl_3$) δ 9.10 (d, *J* = 4.9 Hz, 2H), 9.06 (d, *J* = 4.4 Hz, 2H), 8.81 (d, *J* = 4.4 Hz, 2H), 8.64 (d, *J* = 4.9 Hz, 2H), 8.14 (d, *J* = 7.9 Hz, 4H), 7.62 (d, *J* = 7.7 Hz, 4H), 2.71 (s, 6H). ^{19}F NMR (377 MHz, $CDCl_3$) δ -137.14 (dd, *J* = 24.2, 8.3 Hz), -153.47 (t, *J* = 20.9 Hz), -162.15 (ddd, *J* = 24.1, 20.5, 8.3 Hz). FTMS (APCI): M+ = 839.1503 (expt), 839.1502 (calcd for $C_{39}H_{22}N_4F_5Au$ +H)

Au[5,15-Tol-10-C_6F_4-SC_3H_6SH-Corrole]

Yield 3.3mg (69%). UV-vis (CH_2Cl_2) λ_{max} (nm), [ε x 10^{-4} (M^{-1} cm^{-1})]: 421 (6.49), 528 (0.45), 558 (0.97), 569 (1.07). ^{19}F NMR (377 MHz, $CDCl_3$) δ -134.06 – -134.25 (m), -136.86 (dd, *J* = 25.7, 12.2 Hz), -137.09 – -137.24 (m). FTMS (APCI): M+ = 907.1446 (expt), 907.1446 (calcd for $C_{42}H_{28}N_4F_3AuS_2$ +H)

Au[5,15-Tol-10-C_6F_4-$SC_5H_{10}SH$-Corrole]

Yield 3.3mg (52%). UV-vis (CH_2Cl_2) λ_{max} (nm), [ε x 10^{-4} (M^{-1} cm^{-1})]: 421 (10.70), 528 (0.78), 558 (1.58), 569 (1.76) ^{19}F NMR (377 MHz, $CDCl_3$) δ -134.53 (dd, *J* = 25.8, 12.4 Hz), -137.31 – -137.64 (m). FTMS (APCI): M+ = 935.1759 (expt), 935.1764 (calcd for $C_{44}H_{33}N_4F_3AuS_2$ +H)

Au[5,15-Tol-10-C_6F_4-$SC_8H_{16}SH$-Corrole]

Yield 2.5mg (48%). UV-vis (CH_2Cl_2) λ_{max} (nm), [ε x 10^{-4} (M^{-1} cm^{-1})]: 421 (5.34), 528 (0.40), 558 (0.80), 569 (0.89) ^{19}F NMR (377 MHz, $CDCl_3$) δ -134.27 – -134.88 (m), -137.60. FTMS (APCI): M+ = 979.2385 (expt), 979.2370 (calcd for $C_{47}H_{40}N_4F_3AuS_2$ +H)

Re[5,15-Tol-10-C_6F_5-Corrole](O)

Yield 75.3mg (27%). UV-vis (CH_2Cl_2) λ_{max} (nm), [ε x 10^{-4} (M^{-1} cm^{-1})]: 440 (8.98), 552 (1.32), 584 (1.21) ^{1}H NMR (400 MHz, $CDCl_3$) δ 9.60 (d, *J* = 4.4 Hz, 2H), 9.40 (d, *J* = 4.9 Hz, 2H), 9.35 (d, *J* = 4.4 Hz, 2H), 8.97 (d, *J* = 4.9 Hz, 2H), 8.47 (s, 2H), 7.97 (s, 2H), 7.71 (s, 2H), 7.63 (s, 2H), 2.74 (s, 6H). ^{19}F NMR (377 MHz, $CDCl_3$) δ -136.27 (ddd, *J* = 24.3, 8.6, 3.2 Hz), -137.85 (dt, *J* = 24.4, 5.5 Hz), -152.88 (t, *J* = 20.9 Hz), -161.52 (ddd, *J* = 23.9, 20.7, 8.4 Hz), -161.89 (ddd, *J* = 23.8, 20.8, 8.5 Hz). FTMS (APCI): M+ = 845.1346 (expt), 845.1340 (calcd for $C_{39}H_{22}N_4F_5ReO$ +H)

Re[5,15-Tol-10-C_6F_4-SC_3H_6SH](O)

Yield 4.3mg (22%). UV-vis (CH_2Cl_2) λ_{max} (nm), [ε x 10^{-4} (M^{-1} cm^{-1})]: 441 (3.86), 553 (0.57), 583 (0.51) ^{1}H NMR (400 MHz, $CDCl_3$) δ 9.59 (t, *J* = 4.5 Hz, 1H), 9.44 – 9.36 (m, 1H), 9.37 – 9.25 (m, 1H), 9.00 (d, *J* = 4.0 Hz, 1H), 8.45 (s, 2H), 7.96 (s, 2H), 7.63 (s, 4H), 2.76 – 2.67 (m,

5H). ^{19}F NMR (377 MHz, $CDCl_3$) δ -133.58, -133.76 – -134.13 (m), -136.22 – -136.52 (m), -137.79. FTMS (APCI): M+ = 913.1286 (expt), 913.1288 (calcd for $C_{42}H_{28}N_4F_3ReOS_2$ +H)

Re[5,15-Tol-10-C_6F_4-SC_5H_{10}SH-Corrole](O)

Yield 9.6mg (50%). UV-vis (CH_2Cl_2) λ_{max} (nm), [ε x 10^{-4} (M^{-1} cm^{-1})]: 440 (12.08), 553 (1.76), 582 (1.54) ^{1}H NMR (400 MHz, $CDCl_3$) δ 9.51 (d, *J* = 4.4 Hz, 2H), 9.32 (d, *J* = 4.9 Hz, 2H), 9.27 (d, *J* = 4.4 Hz, 2H), 8.92 (d, *J* = 5.0 Hz, 2H), 8.39 (s, 2H), 7.90 (s, 2H), 7.63 (s, 2H), 7.55 (s, 2H), 3.19 (t, *J* = 7.2 Hz, 2H), 2.66 (s, 6H), 2.57 (q, *J* = 7.1 Hz, 2H), 1.80 (p, *J* = 7.4 Hz, 2H), 1.74 – 1.51 (m, 2H), 1.36 (t, *J* = 7.8 Hz, 1H). ^{19}F NMR (377 MHz, $CDCl_3$) δ -134.00 (dd, *J* = 25.3, 12.2 Hz), -134.37 (dd, *J* = 25.3, 12.2 Hz), -136.64 (dd, *J* = 25.2, 11.7 Hz), -138.11 (dd, *J* = 25.2, 12.2 Hz). FTMS (ESI): M+ = 960.1583 (expt), 960.1589 (calcd for $C_{44}H_{33}N_4F_4ReOS_2$)

Re[5,15-Tol-10-C_6F_4-SC_8H_{16}SH-Corrole](O)

Yield 4.8mg (27%). UV-vis (CH_2Cl_2) λ_{max} (nm), [ε x 10^{-4} (M^{-1} cm^{-1})]: 440 (0.76), 554 (0.11), 583 (0.10) ^{1}H NMR (400 MHz, $CDCl_3$) δ 9.51 (d, *J* = 4.4 Hz, 2H), 9.32 (d, *J* = 4.9 Hz, 2H), 9.26 (d, *J* = 4.4 Hz, 2H), 8.92 (d, *J* = 5.0 Hz, 2H), 8.39 (s, 1H), 7.90 (s, 2H), 7.63 (s, 2H), 7.55 (s, 2H), 3.18 (t, *J* = 7.4 Hz, 2H), 2.65 (s, 5H), 2.63 – 2.57 (m, 6H), 2.46 (dq, *J* = 14.5, 7.3 Hz, 6H), 1.78 (t, *J* = 7.5 Hz, 2H). ^{19}F NMR (377 MHz, $CDCl_3$) δ -134.05 (dd, *J* = 25.2, 12.2 Hz), -134.42 (dd, *J* = 25.3, 12.2 Hz), -136.78 (dd, *J* = 25.3, 12.1 Hz), -138.25 (dd, *J* = 25.1, 12.0 Hz). FTMS (APCI): M+ = 1003.2131 (expt), 1003.2133 (calcd for $C_{47}H_{39}N_4F_4ReOS_2$ +H)

Conclusion

I succeeded in synthesizing and isolating thiol-appended gold- and rhenium-corroles, using 1,3-propanedithiol, 1,5-pentanedithiol and 1,8-octanedithiol. While the current synthesis is promising, the final purification needs some refinement. Further work should focus on synthesizing a 1,3-benzenedithiol-appended corrole, as the enhanced electronic communication it could yield between the corrole, and a gold nanoparticle would be of great interest. The next priority is to use the corroles synthesized in this thesis as gold nanoparticle ligands to ensure the approach discussed herein is of any practical use. If nano-conjugation of the thiol-appended corroles proves fruitful, then testing the nanoconjugates for photodynamic, photothermal and radio-sensitizing activity should be the next step.

Works cited

(1) Agostinis, P.; Berg, K.; Cengel, K. A.; Foster, T. H.; Girotti, A. W.; Gollnick, S. O.; Hahn, S. M.; Hamblin, M. R.; Juzeniene, A.; Kessel, D.; et al. Photodynamic therapy of cancer: An update. *CA: A Cancer Journal for Clinicians* **2011**, *61* (4), 250-281. DOI: 10.3322/caac.20114.
(2) Dougherty, T. J.; Gomer, C. J.; Henderson, B. W.; Jori, G.; Kessel, D.; Korbelik, M.; Moan, J.; Peng, Q. Photodynamic Therapy. *JNCI: Journal of the National Cancer Institute* **1998**, *90* (12), 889-905. DOI: 10.1093/jnci/90.12.889 (acccessed 5/29/2023).
(3) Ethirajan, M.; Chen, Y.; Joshi, P.; Pandey, R. K. The role of porphyrin chemistry in tumor imaging and photodynamic therapy. *Chem. Soc. Rev.* **2011**, *40* (1), 340-362. DOI: 10.1039/b915149b.
(4) Sztandera, K.; Gorzkiewicz, M.; Klajnert-Maculewicz, B. Gold Nanoparticles in Cancer Treatment. *Molecular Pharmaceutics* **2019**, *16* (1), 1-23. DOI: 10.1021/acs.molpharmaceut.8b00810.
(5) Fan, M.; Han, Y.; Gao, S.; Yan, H.; Cao, L.; Li, Z.; Liang, X.-J.; Zhang, J. Ultrasmall gold nanoparticles in cancer diagnosis and therapy. *Theranostics* **2020**, *10* (11), 4944.
(6) Teo, R. D.; Gray, H. B.; Lim, P.; Termini, J.; Domeshek, E.; Gross, Z. A cytotoxic and cytostatic gold (III) corrole. *Chem. Commun.* **2014**, *50* (89), 13789-13792.
(7) Einrem, R. F.; Alemayehu, A. B.; Borisov, S. M.; Ghosh, A.; Gederaas, O. A. Amphiphilic Rhenium-Oxo Corroles as a New Class of Sensitizers for Photodynamic Therapy. *ACS Omega* **2020**, *5* (18), 10596-10601. DOI: 10.1021/acsomega.0c01090.
(8) Lemon, C. M. Corrole photochemistry. **2020**, *92* (12), 1901-1919. DOI: doi:10.1515/pac-2020-0703 (acccessed 2023-05-29).
(9) Barata, J. F. B.; Serra, V. V.; Daniel-da-Silva, A. L.; Neves, M. G. P. M. S.; Costa, S. M. B.; Cavaleiro, J. A. S.; Trindade, T. Corrole-gold nanoparticles: Synthesis, ground and excited state solvation. *Dyes and Pigments* **2022**, *201*, 110108. DOI: https://doi.org/10.1016/j.dyepig.2022.110108.
(10) Antonini, E.; Brunori, M. Hemoglobin. *Annu. Rev. Biochem* **1970**, *39* (1), 977-1042.
(11) Björn, L. O.; Papageorgiou, G. C.; Blankenship, R. E.; Govindjee. A viewpoint: Why chlorophyll a? *Photosynth. Res.* **2009**, *99* (2), 85-98. DOI: 10.1007/s11120-008-9395-x.
(12) Auwärter, W.; Écija, D.; Klappenberger, F.; Barth, J. V. Porphyrins at interfaces. *Nature Chemistry* **2015**, *7* (2), 105-120. DOI: 10.1038/nchem.2159.
(13) Baker, E. W. Porphyrins. In *Organic Geochemistry: Methods and Results*, Eglinton, G., Murphy, M. T. J. Eds.; Springer Berlin Heidelberg, 1969; pp 464-497.
(14) Rothemund, P. Formation of porphyrins from pyrrole and aldehydes. *Journal of the American Chemical Society* **1935**, *57* (10), 2010-2011.
(15) Rothemund, P. A new porphyrin synthesis. The synthesis of porphin1. *Journal of the American Chemical Society* **1936**, *58* (4), 625-627.
(16) Lindsey, J. S.; Schreiman, I. C.; Hsu, H. C.; Kearney, P. C.; Marguerettaz, A. M. Rothemund and Adler-Longo reactions revisited: synthesis of tetraphenylporphyrins under equilibrium conditions. *The Journal of Organic Chemistry* **1987**, *52* (5), 827-836.
(17) Adler, A. D.; Longo, F. R.; Finarelli, J. D.; Goldmacher, J.; Assour, J.; Korsakoff, L. A simplified synthesis for meso-tetraphenylporphine. *The Journal of Organic Chemistry* **1967**, *32* (2), 476-476.

(18) Nardis, S.; Mandoj, F.; Stefanelli, M.; Paolesse, R. Metal complexes of corrole. *Coord. Chem. Rev.* **2019**, *388*, 360-405. DOI: https://doi.org/10.1016/j.ccr.2019.02.034.
(19) Aviv, I.; Gross, Z. Corrole-based applications. *Chem. Commun.* **2007**, (20), 1987. DOI: 10.1039/b618482k.
(20) Alemayehu, A. B.; Thomas, K. E.; Einrem, R. F.; Ghosh, A. The Story of 5d Metallocorroles: From Metal–Ligand Misfits to New Building Blocks for Cancer Phototherapeutics. *Acc. Chem. Res.* **2021**, *54* (15), 3095-3107. DOI: 10.1021/acs.accounts.1c00290.
(21) Barata, J. F.; Neves, M. G.; Faustino, M. A.; Tome, A. C.; Cavaleiro, J. A. Strategies for Corrole Functionalization. *Chem Rev* **2017**, *117* (4), 3192-3253. DOI: 10.1021/acs.chemrev.6b00476 From NLM PubMed-not-MEDLINE.
(22) Nishida, K.; Tojo, T.; Kondo, T.; Yuasa, M. Evaluation of the correlation between porphyrin accumulation in cancer cells and functional positions for application as a drug carrier. *Scientific Reports* **2021**, *11* (1). DOI: 10.1038/s41598-021-81725-3.
(23) Johnson, A.; Kay, I. 306. Corroles. Part I. Synthesis. *Journal of the Chemical Society (Resumed)* **1965**, 1620-1629.
(24) Johnson, A. W.; Kay, I. Synthesis of corroles and related ring systems. *Proceedings of the Royal Society of London. Series A. Mathematical and Physical Sciences* **1965**, *288* (1414), 334-341.
(25) Gross, Z.; Galili, N.; Saltsman, I. The first direct synthesis of corroles from pyrrole. *Angew. Chem. Int. Ed.* **1999**, *38* (10), 1427-1429.
(26) Kumar, A.; Kim, D.; Kumar, S.; Mahammed, A.; Churchill, D. G.; Gross, Z. Milestones in corrole chemistry: historical ligand syntheses and post-functionalization. *Chem. Soc. Rev.* **2023**.
(27) Teo, R. D.; Hwang, J. Y.; Termini, J.; Gross, Z.; Gray, H. B. Fighting cancer with corroles. *Chem. Rev.* **2017**, *117* (4), 2711-2729.
(28) Ghosh, A. Electronic Structure of Corrole Derivatives: Insights from Molecular Structures, Spectroscopy, Electrochemistry, and Quantum Chemical Calculations. *Chem. Rev.* **2017**, *117* (4), 3798-3881. DOI: 10.1021/acs.chemrev.6b00590.
(29) Orłowski, R.; Gryko, D.; Gryko, D. T. Synthesis of corroles and their heteroanalogs. *Chem. Rev.* **2017**, *117* (4), 3102-3137.
(30) Di Natale, C.; Gros, C. P.; Paolesse, R. Corroles at work: A small macrocycle for great applications. *Chem. Soc. Rev.* **2022**, *51* (4), 1277-1335.
(31) Kingsbury, C. J.; Senge, M. O. The shape of porphyrins. *Coord. Chem. Rev.* **2021**, *431*, 213760. DOI: https://doi.org/10.1016/j.ccr.2020.213760.
(32) Foley, T. J.; Abboud, K. A.; Boncella, J. M. Synthesis of Ln (III) chloride tetraphenylporphyrin complexes. *Inorg. Chem.* **2002**, *41* (7), 1704-1706.
(33) Zhu, X.; Wong, W. K.; Guo, J.; Wong, W. Y.; Zhang, J. P. Reactivity of Cationic Lanthanide (III) Monoporphyrinates towards Anionic Cyanometallates‐Preparation, Crystal Structure, and Luminescence Properties of Cyanido ‐ Bridged Di ‐ and Trinuclear d‐f Complexes. Wiley Online Library: 2008.
(34) Thomas, K. E.; Alemayehu, A. B.; Conradie, J.; Beavers, C. M.; Ghosh, A. The Structural Chemistry of Metallocorroles: Combined X-ray Crystallography and Quantum Chemistry Studies Afford Unique Insights. *Acc. Chem. Res.* **2012**, *45* (8), 1203-1214. DOI: 10.1021/ar200292d.

(35) Gouterman, M. Spectra of porphyrins. *J. Mol. Spectrosc.* **1961**, *6*, 138-163. DOI: https://doi.org/10.1016/0022-2852(61)90236-3.
(36) Gouterman, M.; Wagnière, G. H.; Snyder, L. C. Spectra of porphyrins: Part II. Four orbital model. *J. Mol. Spectrosc.* **1963**, *11* (1), 108-127. DOI: https://doi.org/10.1016/0022-2852(63)90011-0.
(37) Ghosh, A.; Wondimagegn, T.; Parusel, A. B. J. Electronic Structure of Gallium, Copper, and Nickel Complexes of Corrole. High-Valent Transition Metal Centers versus Noninnocent Ligands. *Journal of the American Chemical Society* **2000**, *122* (21), 5100-5104. DOI: 10.1021/ja9943243.
(38) Sternberg, E. D.; Dolphin, D.; Brückner, C. Porphyrin-based photosensitizers for use in photodynamic therapy. *Tetrahedron* **1998**, *54* (17), 4151-4202.
(39) Feng, G.; Zhang, G.-Q.; Ding, D. Design of superior phototheranostic agents guided by Jablonski diagrams. *Chem. Soc. Rev.* **2020**, *49* (22), 8179-8234.
(40) Paolesse, R. Corrole: The Little Big Porphyrinoid. *Synlett* **2008**, *2008* (15), 2215-2230. DOI: 10.1055/s-2008-1078687.
(41) Wamser, C. C.; Ghosh, A. The Hyperporphyrin Concept: A Contemporary Perspective. *JACS Au* **2022**, *2* (7), 1543-1560. DOI: 10.1021/jacsau.2c00255 From NLM PubMed-not-MEDLINE.
(42) Buckley, H. L.; Chomitz, W. A.; Koszarna, B.; Tasior, M.; Gryko, D. T.; Brothers, P. J.; Arnold, J. Synthesis of lithium corrole and its use as a reagent for the preparation of cyclopentadienyl zirconium and titanium corrole complexes. *Chem Commun (Camb)* **2012**, *48* (87), 10766-10768. DOI: 10.1039/c2cc35984g From NLM Medline.
(43) Buckley, H. L.; Arnold, J. Recent developments in out-of-plane metallocorrole chemistry across the periodic table. *Dalton Trans* **2015**, *44* (1), 30-36. DOI: 10.1039/c4dt02277g From NLM PubMed-not-MEDLINE.
(44) Einrem, R. F.; Gagnon, K. J.; Alemayehu, A. B.; Ghosh, A. Metal–Ligand Misfits: Facile Access to Rhenium–Oxo Corroles by Oxidative Metalation. *Chemistry – A European Journal* **2016**, *22* (2), 517-520. DOI: 10.1002/chem.201504307.
(45) Lemon, C. M.; Huynh, M.; Maher, A. G.; Anderson, B. L.; Bloch, E. D.; Powers, D. C.; Nocera, D. G. Electronic Structure of Copper Corroles. *Angew. Chem. Int. Ed. Engl.* **2016**, *55* (6), 2176-2180. DOI: 10.1002/anie.201509099 From NLM PubMed-not-MEDLINE.
(46) Luobeznova, I.; Simkhovich, L.; Goldberg, I.; Gross, Z. Electronic Structures and Reactivities of Corrole−Copper Complexes. *Eur. J. Inorg. Chem.* **2004**, *2004* (8), 1724-1732. DOI: 10.1002/ejic.200300806.
(47) Thomassen, I. K.; McOrmick, L. J.; Ghosh, A. Synthesis and Molecular Structure of a Copper Octaiodocorrole. *ACS Omega* **2018**, *3* (5), 5106-5110. DOI: 10.1021/acsomega.8b00616.
(48) Ghosh, A.; Steene, E. High-valent transition metal centers and noninnocent ligands in metalloporphyrins and related molecules: a broad overview based on quantum chemical calculations. *JBIC Journal of Biological Inorganic Chemistry* **2001**, *6* (7), 739-752. DOI: 10.1007/s007750100275.
(49) Lee, W.; Zhan, X.; Palma, J.; Vestfrid, J.; Gross, Z.; Churchill, D. G. Minding our P-block and Q-bands: paving inroads into main group corrole research to help instil broader potential. *Chem. Commun.* **2021**, *57* (38), 4605-4641. DOI: 10.1039/d1cc00105a.
(50) Liu, H.-Y.; Lai, T.-S.; Yeung, L.-L.; Chang, C. K. First Synthesis of Perfluorinated Corrole and Its MnO Complex. *Org. Lett.* **2003**, *5* (5), 617-620. DOI: 10.1021/ol027111i.

(51) Steene, E.; Dey, A.; Ghosh, A. β-Octafluorocorroles. *Journal of the American Chemical Society* **2003**, *125* (52), 16300-16309. DOI: 10.1021/ja021158h.
(52) Ngo, T. H.; Van Rossom, W.; Dehaen, W.; Maes, W. Reductive demetallation of Cu-corroles—a new protective strategy towards functional free-base corroles. *Org. Biomol. Chem.* **2009**, *7* (3), 439-443. DOI: 10.1039/b819185a.
(53) Mahammed, A.; Botoshansky, M.; Gross, Z. Chlorinated corroles. *Dalton Transactions* **2012**, *41* (36), 10938-10940.
(54) Ooi, S.; Yoneda, T.; Tanaka, T.; Osuka, A. meso‐Free Corroles: Syntheses, Structures, Properties, and Chemical Reactivities. *Chemistry‐A European Journal* **2015**, *21* (21), 7772-7779.
(55) Paolesse, R.; Nardis, S.; Sagone, F.; Khoury, R. G. Synthesis and Functionalization of m eso-Aryl-Substituted Corroles. *The Journal of organic chemistry* **2001**, *66* (2), 550-556.
(56) Wagnert, L.; Berg, A.; Stavitski, E.; Berthold, T.; Kothe, G.; Goldberg, I.; Mahammed, A.; Simkhovich, L.; Gross, Z.; Levanon, H. Exploring the photoexcited triplet states of aluminum and tin corroles by time-resolved Q-band EPR. *Appl. Magn. Reson.* **2006**, *30*, 591-604.
(57) Wagnert, L.; Rubin, R.; Berg, A.; Mahammed, A.; Gross, Z.; Levanon, H. Photoexcited triplet state properties of brominated and nonbrominated Ga (III)-corroles as studied by time-resolved electron paramagnetic resonance. *The Journal of Physical Chemistry B* **2010**, *114* (45), 14303-14308.
(58) Norheim, H.-K.; Schneider, C.; Gagnon, K. J.; Ghosh, A. One-Pot Synthesis of a bis-Pocket Corrole through a 14-fold Bromination Reaction. *ChemistryOpen* **2017**, *6* (2), 221-225. DOI: 10.1002/open.201600168.
(59) Vestfrid, J.; Botoshansky, M.; Palmer, J. H.; Durrell, A. C.; Gray, H. B.; Gross, Z. Iodinated aluminum (III) corroles with long-lived triplet excited states. *Journal of the American Chemical Society* **2011**, *133* (33), 12899-12901.
(60) Vestfrid, J.; Goldberg, I.; Gross, Z. Tuning the photophysical and redox properties of metallocorroles by iodination. *Inorg. Chem.* **2014**, *53* (19), 10536-10542.
(61) Thomassen, I. K.; Vazquez-Lima, H.; Gagnon, K. J.; Ghosh, A. Octaiodoporphyrin. *Inorg. Chem.* **2015**, *54* (23), 11493-11497. DOI: 10.1021/acs.inorgchem.5b02127.
(62) Tardieux, C.; Gros, C. P.; Guilard, R. On corrole chemistry. An isomerization study and oxidative cleavage of the corrole macroring to a biliverdin structure. *J. Heterocycl. Chem.* **1998**, *35* (4), 965-970. DOI: 10.1002/jhet.5570350430.
(63) Kadish, K. M.; Guo, N.; Caemelbecke, E. V.; Froiio, A.; Paolesse, R.; Monti, D.; Tagliatesta, P.; Boschi, T.; Prodi, L.; Bolletta, F. Synthesis, electrochemical, and photophysical study of covalently linked porphyrin dimers with two different macrocycles. *Inorg. Chem.* **1998**, *37* (10), 2358-2365.
(64) Aviv‐Harel, I.; Gross, Z. Aura of corroles. *Chemistry‐A European Journal* **2009**, *15* (34), 8382-8394.
(65) Clayden, J.; Greeves, N.; Warren, S. *Organic chemistry*; Oxford university press, 2012.
(66) Silva, D. R.; Pliego, J. R. How difficult are anion-molecule SNAr reactions of unactivated arenes in the gas phase, dimethyl sulfoxide, and methanol solvents? *Struct. Chem.* **2019**, *30* (1), 75-83. DOI: 10.1007/s11224-018-1172-7.
(67) Meisenheimer, J. Ueber Reactionen aromatischer Nitrokörper. *Justus Liebig's Annalen der Chemie* **1902**, *323* (2), 205-246. DOI: 10.1002/jlac.19023230205.

(68) Artamkina, G. A.; Egorov, M. P.; Beletskaya, I. P. Some aspects of anionic .sigma.-complexes. *Chem. Rev.* **1982**, *82* (4), 427-459. DOI: 10.1021/cr00050a004.
(69) Fry, S. E.; Pienta, N. J. Effects of molten salts on reactions. Nucleophilic aromatic substitution by halide ions in molten dodecyltributylphosphonium salts. *Journal of the American Chemical Society* **1985**, *107* (22), 6399-6400. DOI: 10.1021/ja00308a045.
(70) Handel, H.; Pasquini, M. A.; Pierre, J. L. Effets de cryptands et activation de bases—VII11Partie précédente Réf. 1.: Réduction des halogénures de phényle par l'hydrure de potassium. *Tetrahedron* **1980**, *36* (22), 3205-3208. DOI: https://doi.org/10.1016/0040-4020(80)80166-9.
(71) Rohrbach, S.; Smith, A. J.; Pang, J. H.; Poole, D. L.; Tuttle, T.; Chiba, S.; Murphy, J. A. Concerted Nucleophilic Aromatic Substitution Reactions. *Angew. Chem. Int. Ed.* **2019**, *58* (46), 16368-16388. DOI: 10.1002/anie.201902216.
(72) Schoefberger, W.; Faschinger, F.; Aichhorn, S.; Himmelsbach, M. Bismuth A3-Corroles: Useful Precursors for the Development of meso-Substituted Free-Base Corroles. *Synthesis* **2014**, *46* (22), 3085-3096. DOI: 10.1055/s-0034-1379012.
(73) Yang, Q.; Sheng, M.; Henkelis, J. J.; Tu, S.; Wiensch, E.; Zhang, H.; Zhang, Y.; Tucker, C.; Ejeh, D. E. Explosion Hazards of Sodium Hydride in Dimethyl Sulfoxide, N,N-Dimethylformamide, and N,N-Dimethylacetamide. *Organic Process Research & Development* **2019**, *23* (10), 2210-2217. DOI: 10.1021/acs.oprd.9b00276.

Appendix

Au[5,15-Tol-10-C6F4-SC8H16SH-Corrole]

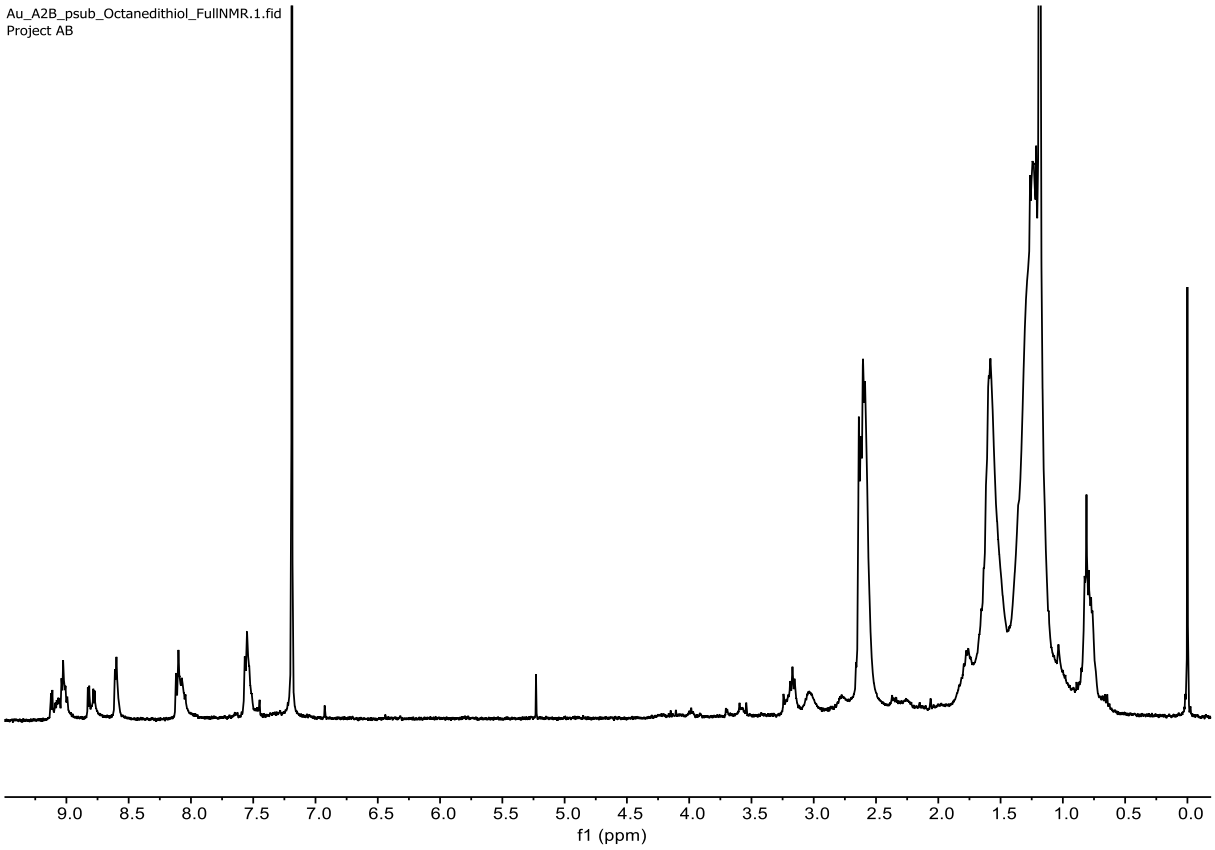

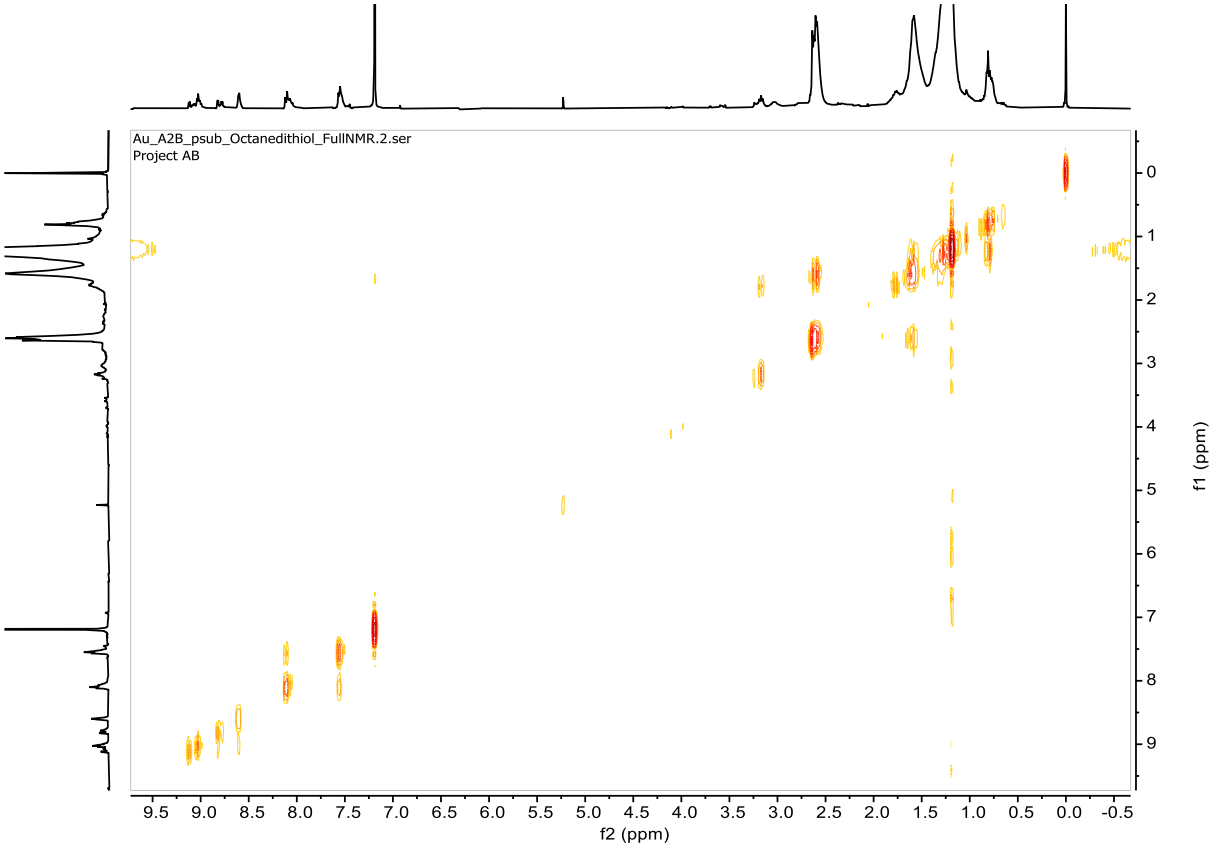
Au_A2B_psub_Octanedithiol_FullNMR.2.ser
Project AB
f2 (ppm)
f1 (ppm)

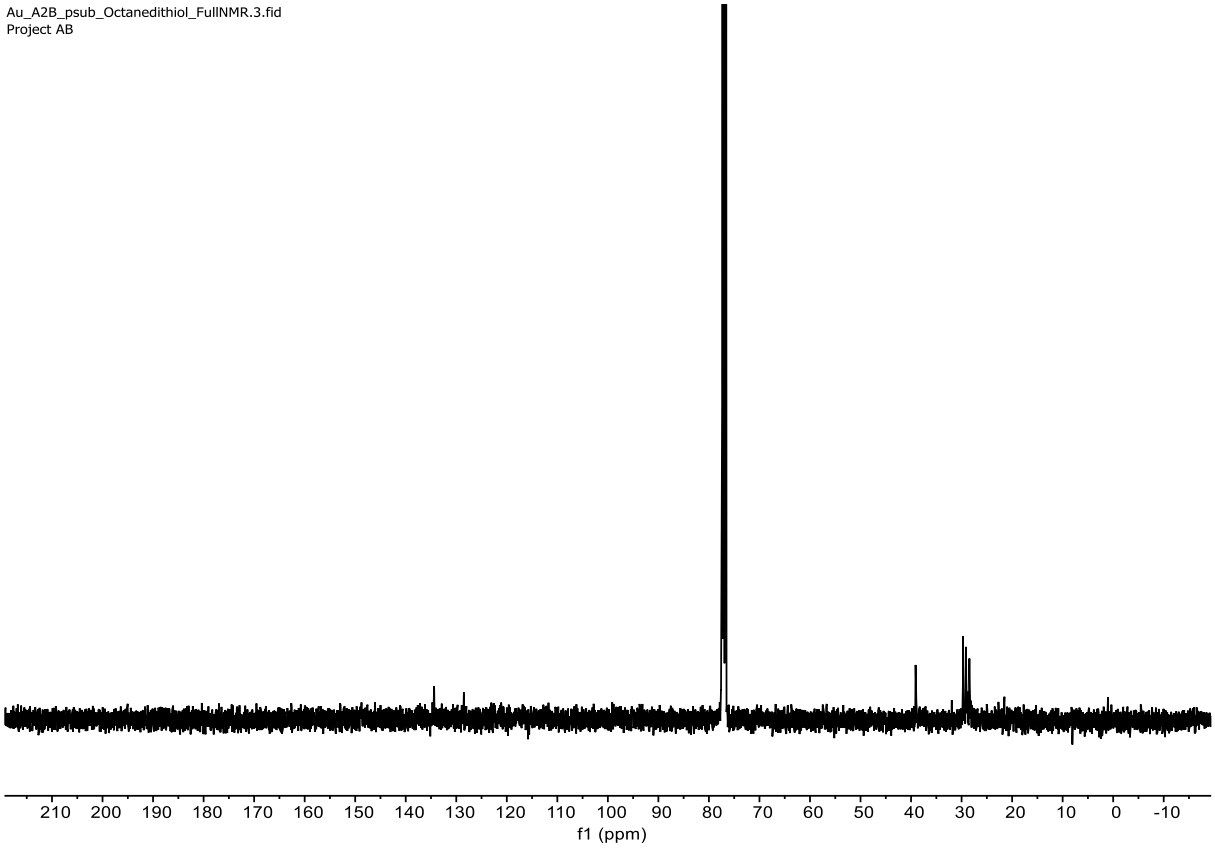
Au_A2B_psub_Octanedithiol_FullNMR.3.fid
Project AB
210 200 190 180 170 160 150 140 130 120 110 100 90 80 70 60 50 40 30 20 10 0 -10
f1 (ppm)

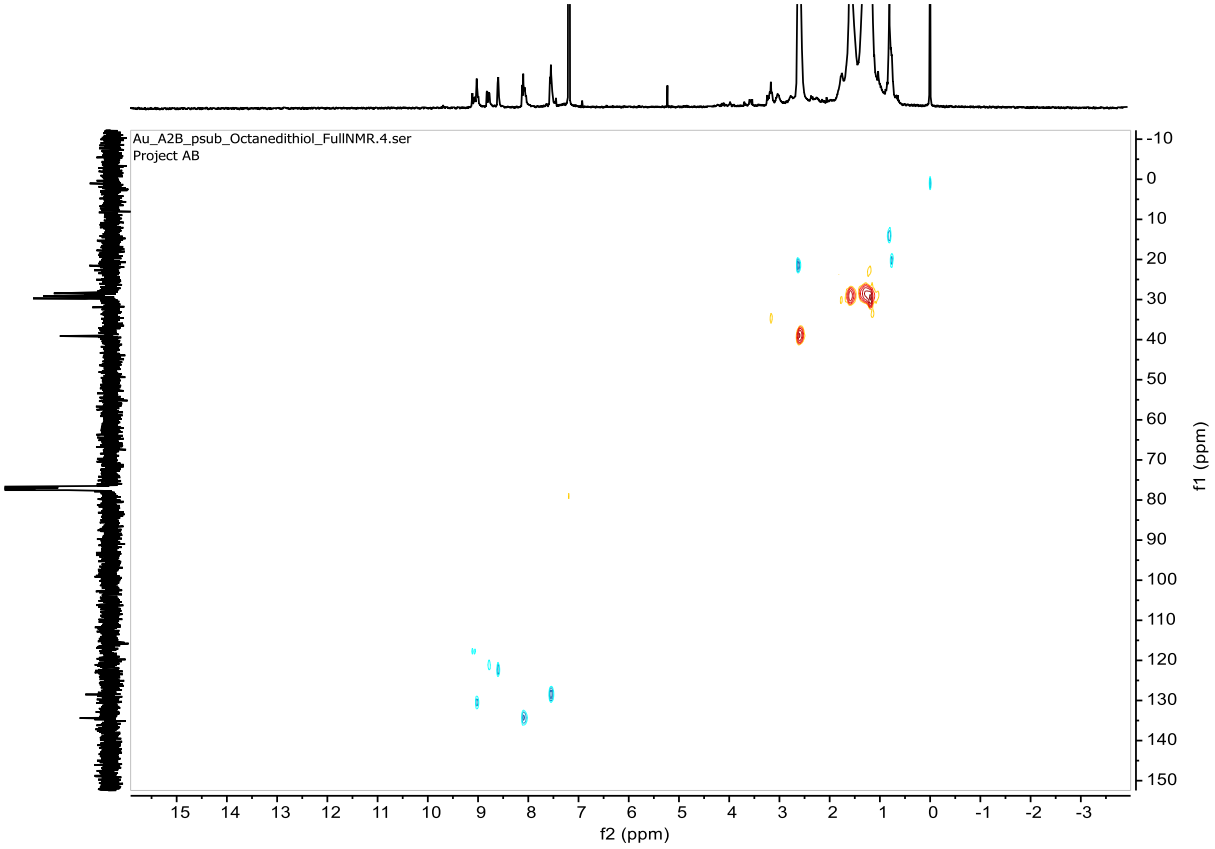
Au_A2B_psub_Octanedithiol_FullNMR.4.ser
Project AB
f2 (ppm)
f1 (ppm)

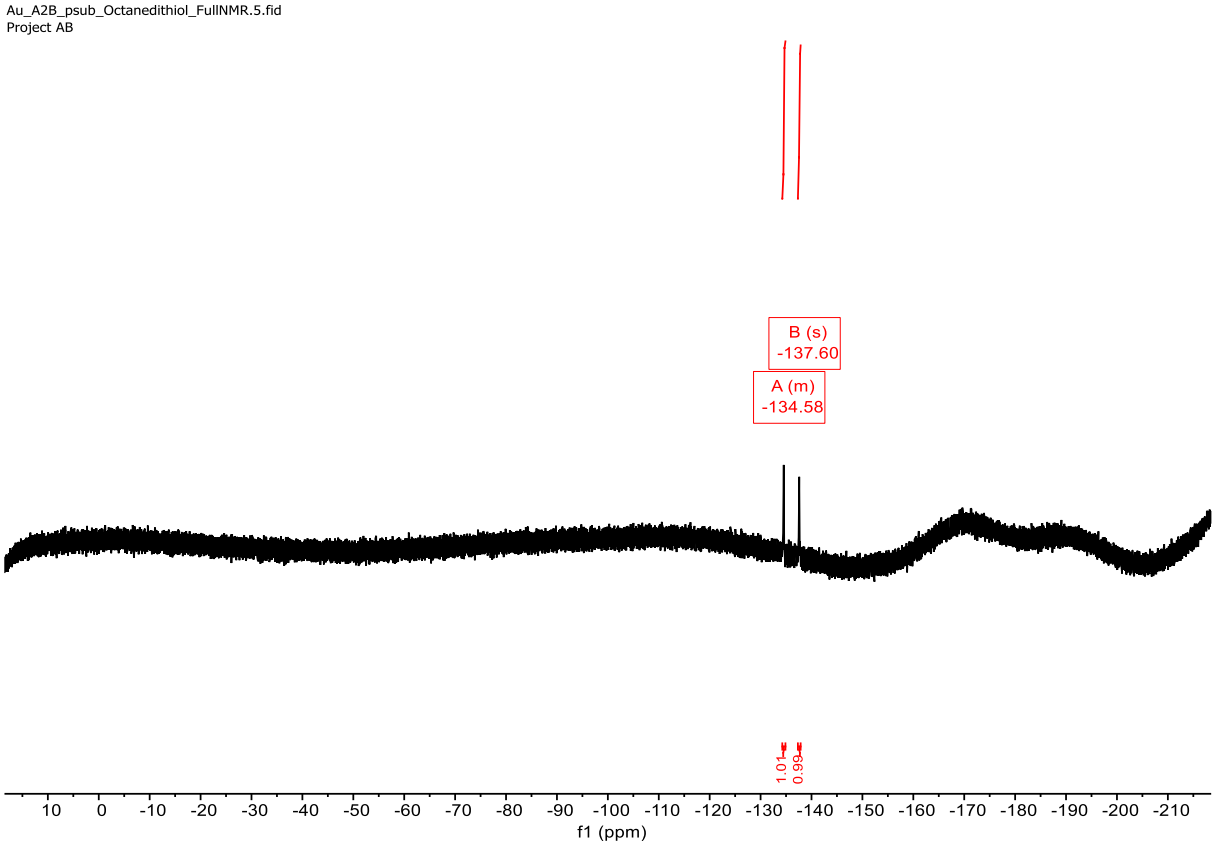
Au_A2B_psub_Octanedithiol_FullNMR.5.fid
Project AB
B (s)
-137.60
A (m)
-134.58
1.01
0.99
10 0 -10 -20 -30 -40 -50 -60 -70 -80 -90 -100 -110 -120 -130 -140 -150 -160 -170 -180 -190 -200 -210
f1 (ppm)

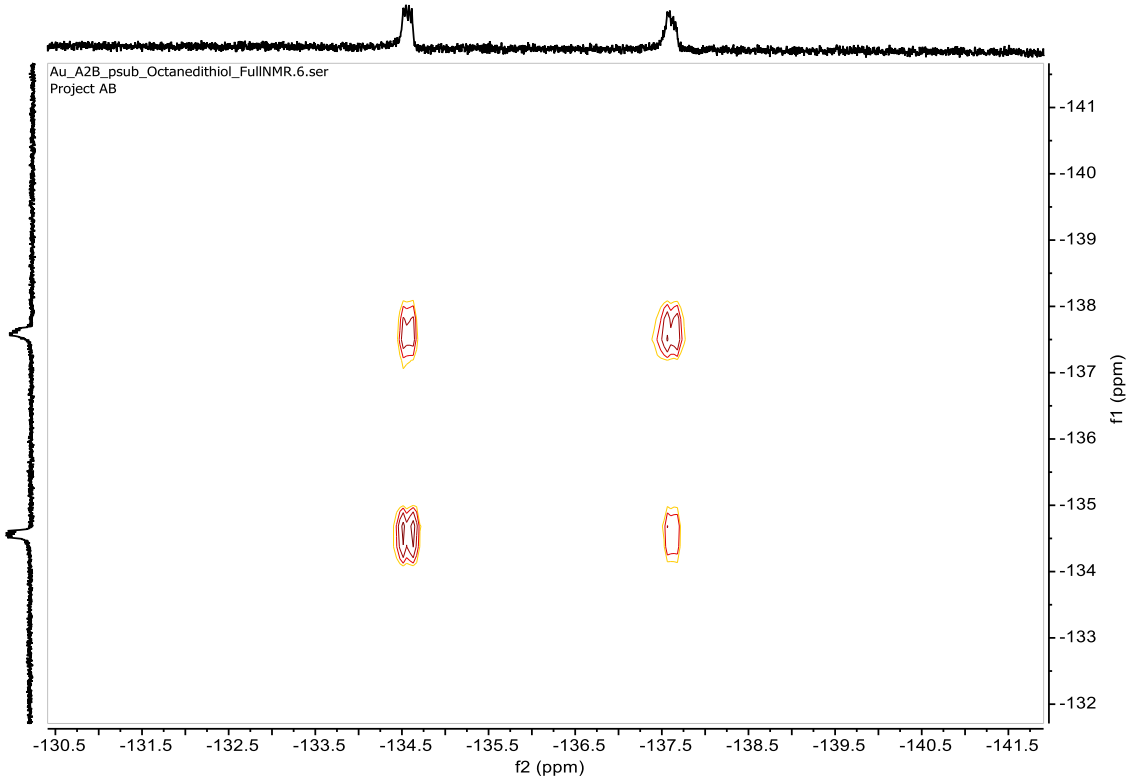
Au_A2B_psub_Octanedithiol_FullNMR.6.ser
Project AB
-141
-140
-139
-138
-137
-136
-135
-134
-133
-132
f1 (ppm)
-130.5
-131.5
-132.5
-133.5
-134.5
-135.5
-136.5
-137.5
-138.5
-139.5
-140.5
-141.5
f2 (ppm)

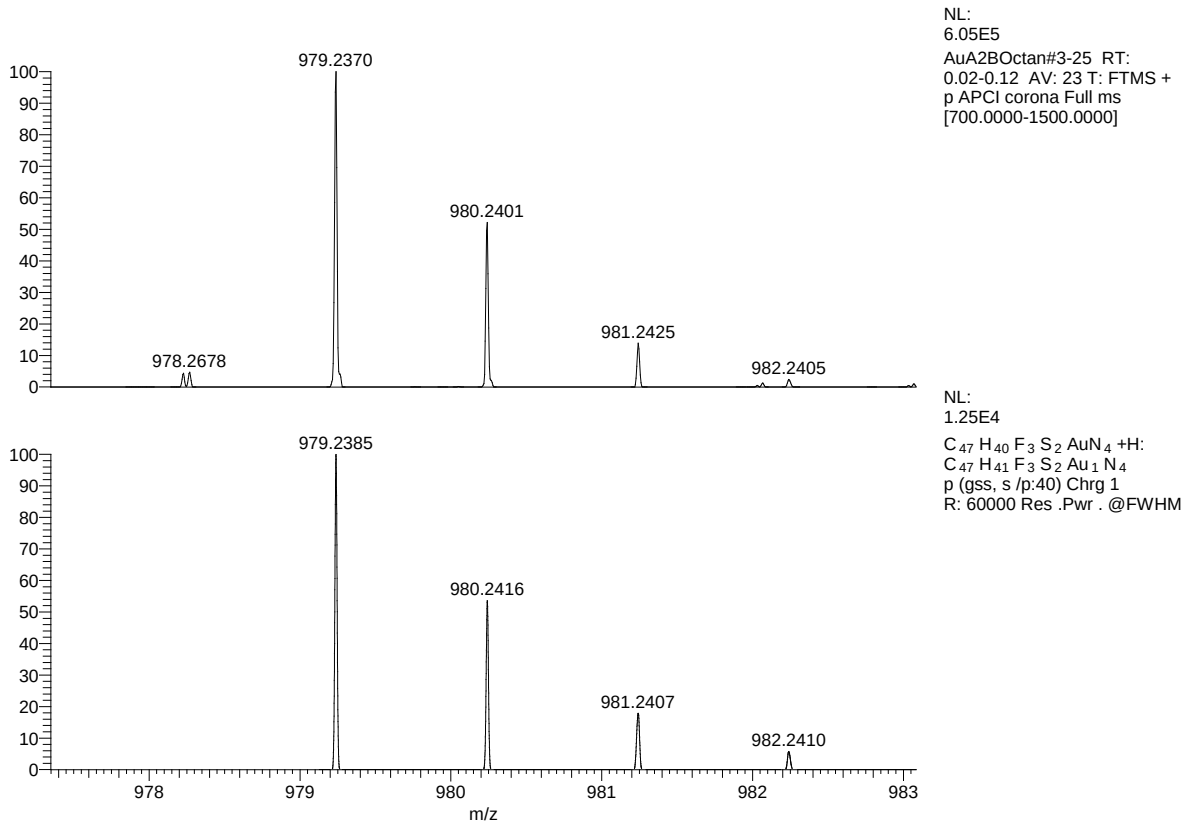
NL:
6.05E5
AuA2BOctan#3-25 RT:
0.02-0.12 AV: 23 T: FTMS +
p APCI corona Full ms
[700.0000-1500.0000]
979.2370
980.2401
981.2425
978.2678
982.2405
NL:
1.25E4
C47 H40 F3 S2 AuN4 +H:
C47 H41 F3 S2 Au1 N4
p (gss, s /p:40) Chrg 1
R: 60000 Res .Pwr . @FWHM
979.2385
980.2416
981.2407
982.2410
100
90
80
70
60
50
40
30
20
10
0
978
979
980
981
982
983
m/z

AuA2BOctan #3-25 RT: 0.02-0.12 AV: 23 NL: 6.05E5
T: FTMS + p APCI corona Full ms [700.0000-1500.0000]

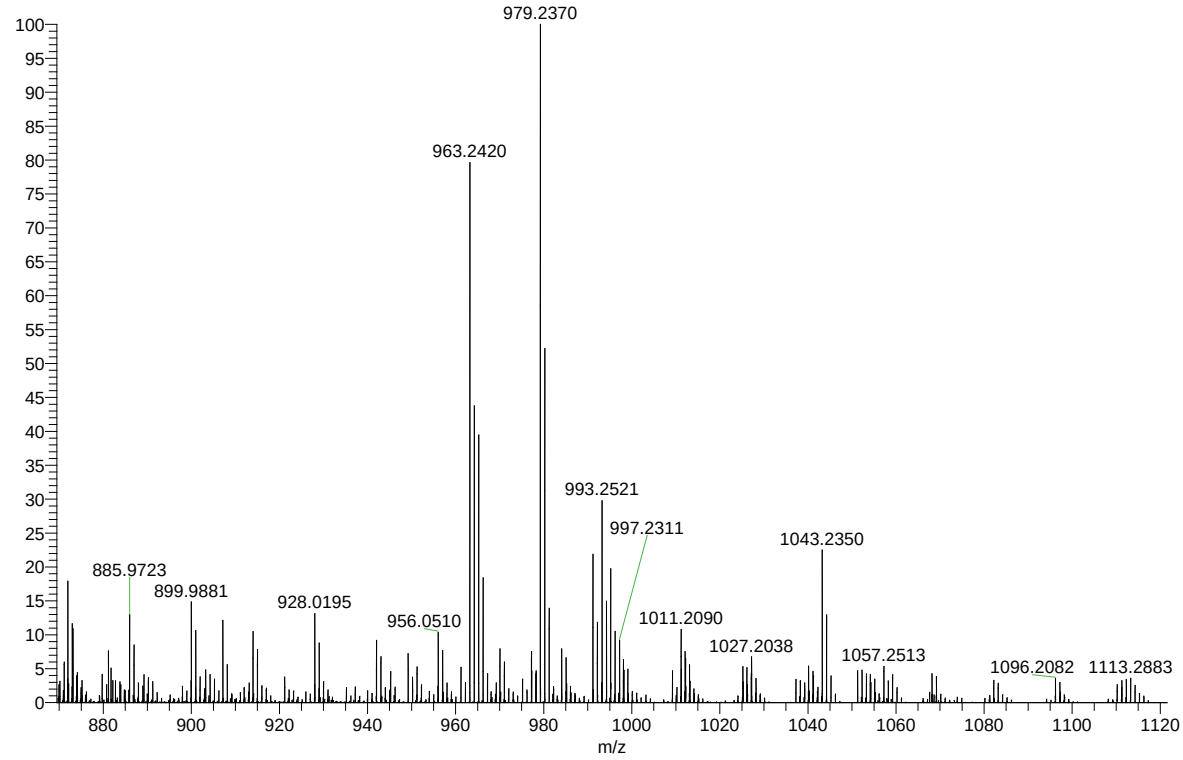

Au[5,15-Tol-10-C_6F_4-SC_3H_6SH-Corrole]

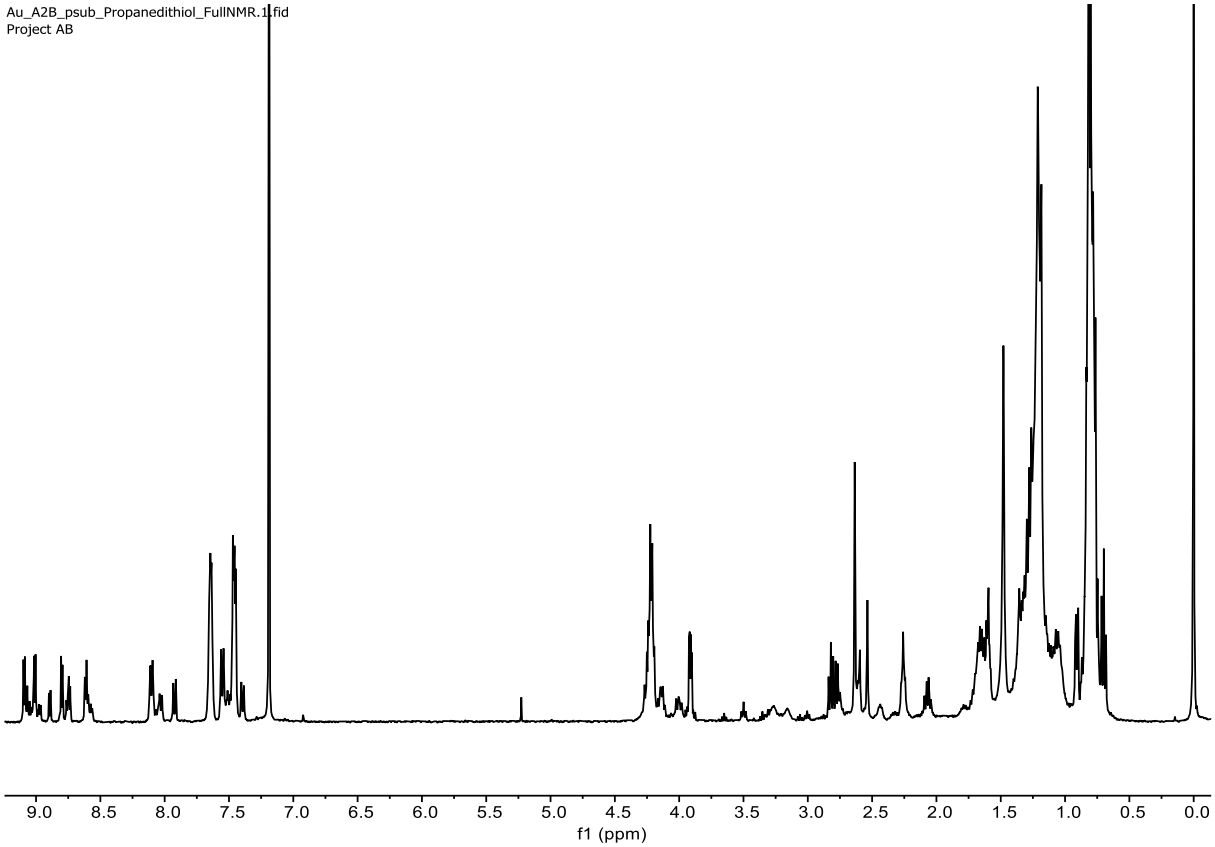

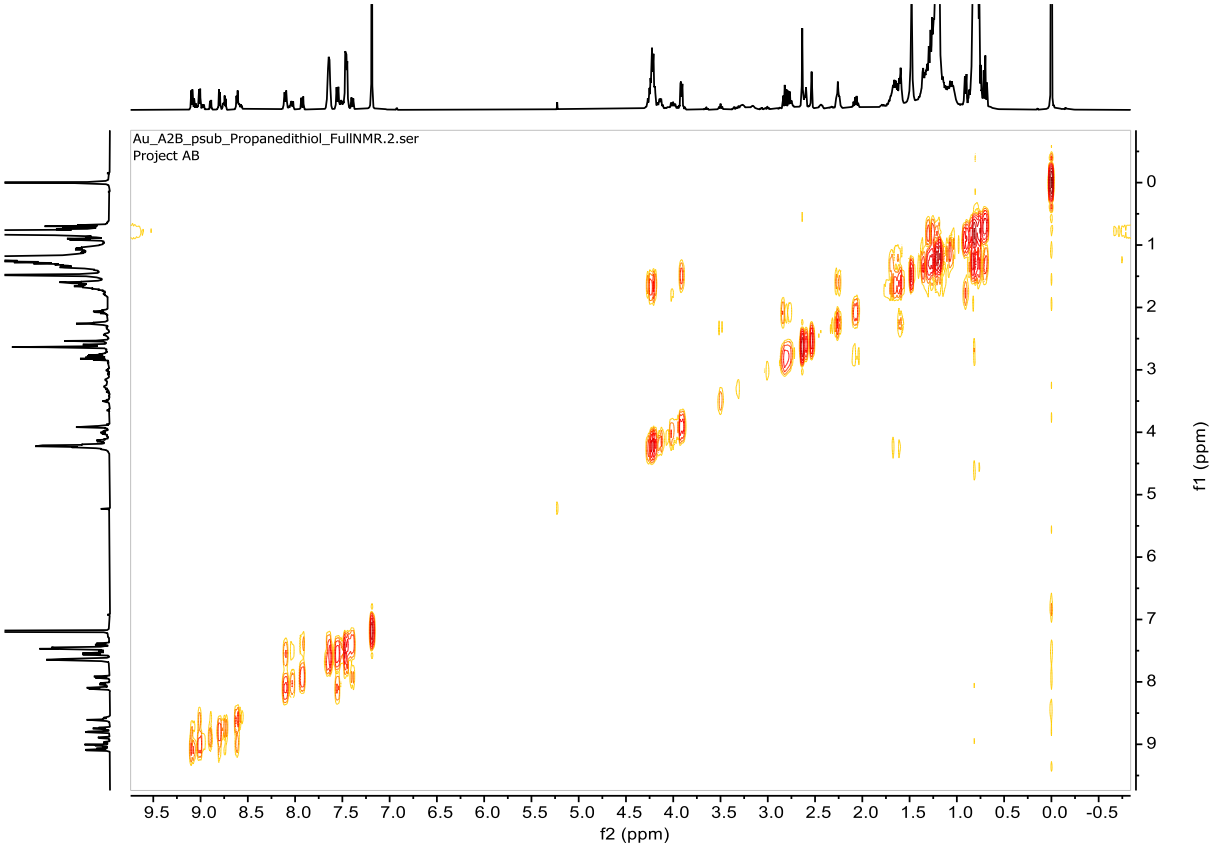
Au_A2B_psub_Propanedithiol_FullNMR.2.ser
Project AB
f2 (ppm)
f1 (ppm)

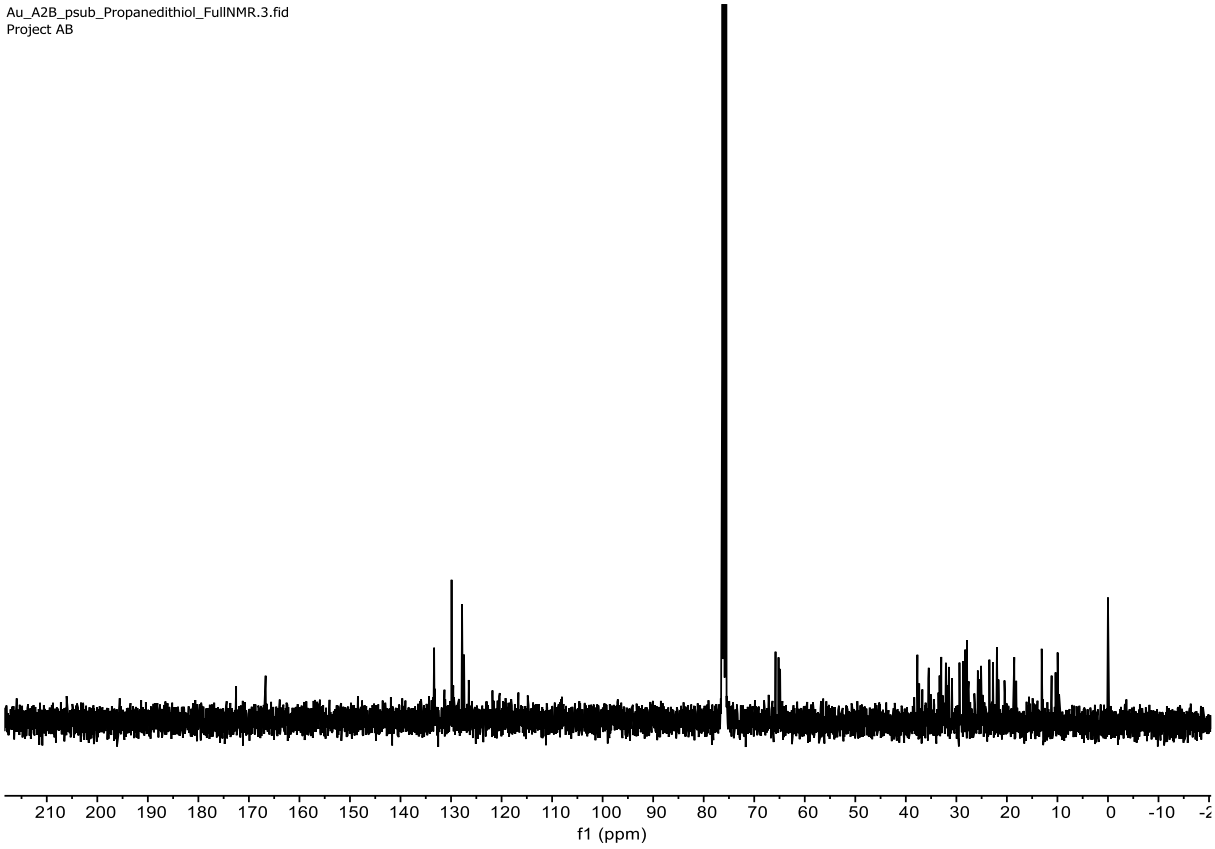
Au_A2B_psub_Propanedithiol_FullNMR.3.fid
Project AB
210 200 190 180 170 160 150 140 130 120 110 100 90 80 70 60 50 40 30 20 10 0 -10
f1 (ppm)

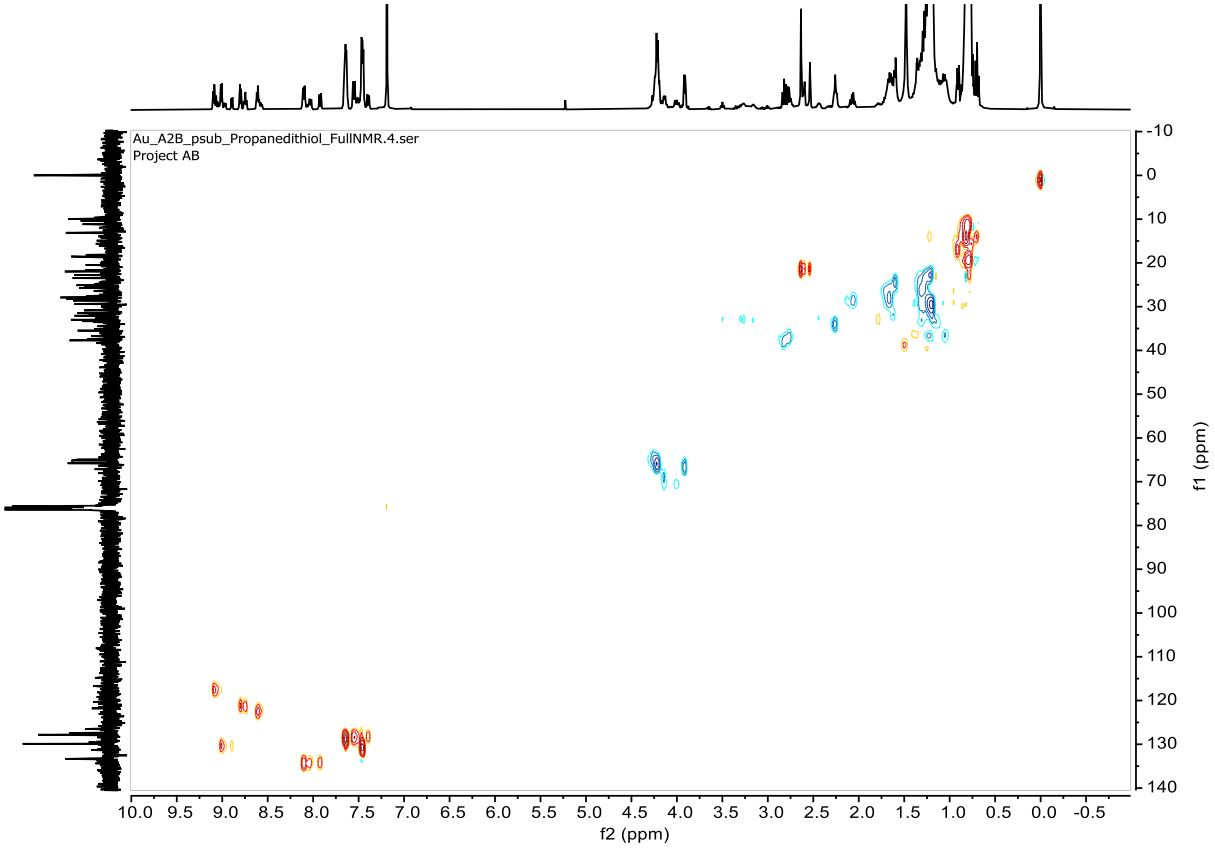
Au_A2B_psub_Propanedithiol_FullNMR.4.ser
Project AB
f2 (ppm)
f1 (ppm)


Au_A2B_psub_Propanedithiol_FullNMR.5.fid
Project AB
B (dd)
-136.86
A (m)
-134.16
C (m)
-137.17
2.00
0.83
0.51
10 0 -10 -20 -30 -40 -50 -60 -70 -80 -90 -100 -110 -120 -130 -140 -150 -160 -170 -180 -190 -200 -210
f1 (ppm)

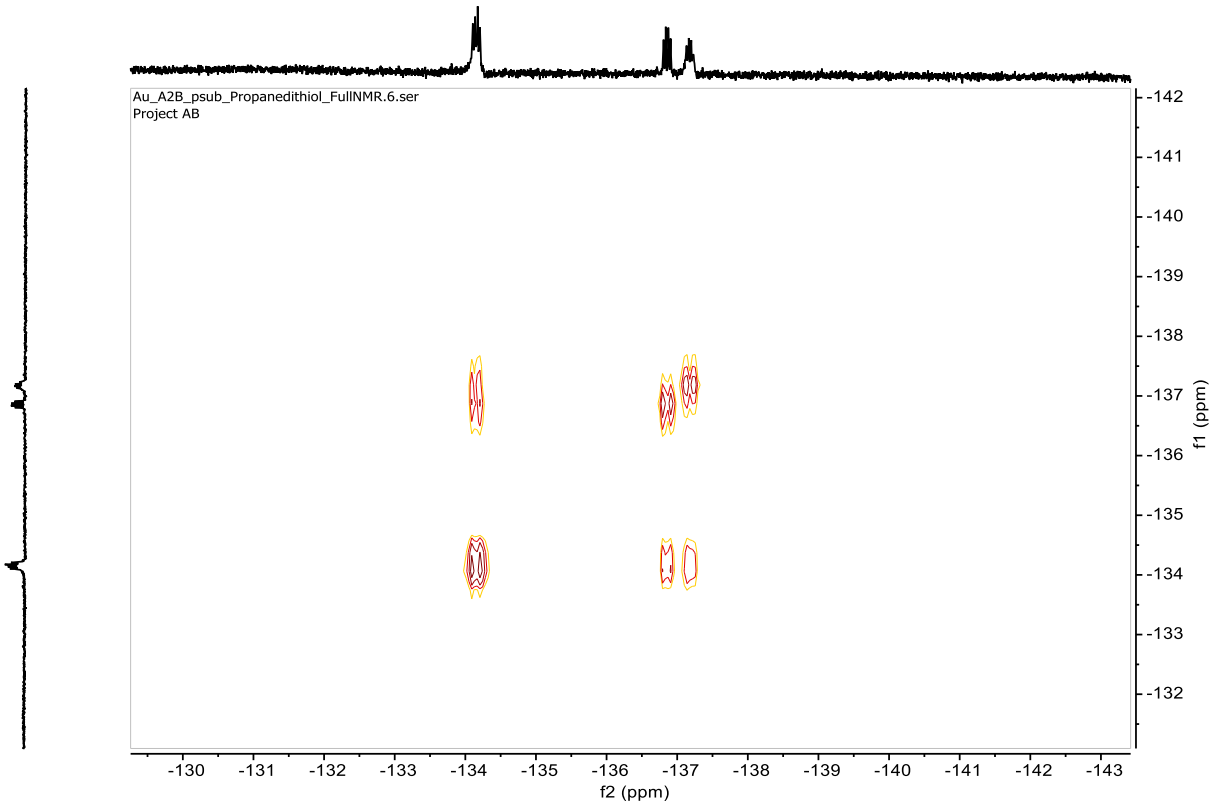
Au_A2B_psub_Propanedithiol_FullNMR.6.ser
Project AB
-142
-141
-140
-139
-138
-137
-136
-135
-134
-133
-132
f1 (ppm)
-130
-131
-132
-133
-134
-135
-136
-137
-138
-139
-140
-141
-142
-143
f2 (ppm)

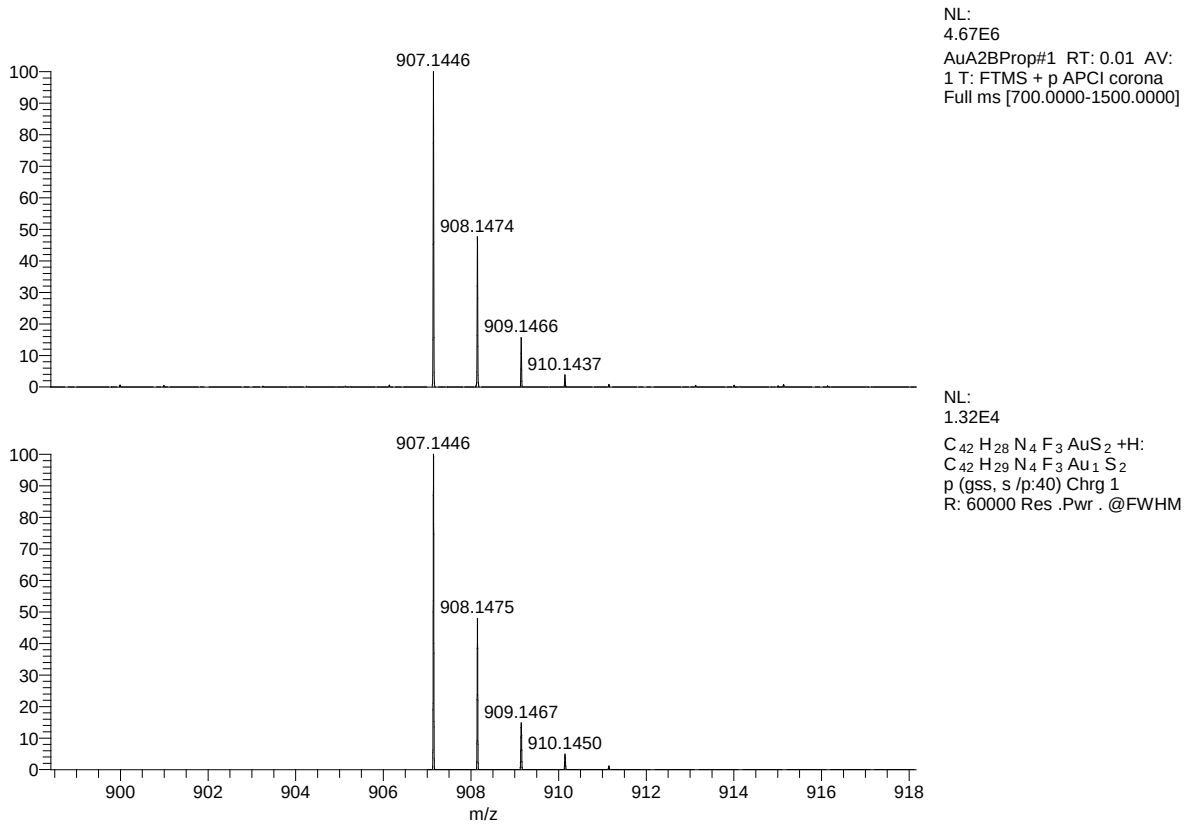
NL:
4.67E6
AuA2BProp#1 RT: 0.01 AV:
1 T: FTMS + p APCI corona
Full ms [700.0000-1500.0000]
907.1446
908.1474
909.1466
910.1437
NL:
1.32E4
C42 H28 N4 F3 AuS2 +H:
C42 H29 N4 F3 Au1 S2
p (gss, s /p:40) Chrg 1
R: 60000 Res .Pwr . @FWHM
907.1446
908.1475
909.1467
910.1450
100
90
80
70
60
50
40
30
20
10
0
900
902
904
906
908
910
912
914
916
918
m/z

AuA2BProp #1 RT: 0.01 AV: 1 NL: 4.67E6
T: FTMS + p APCI corona Full ms [700.0000-1500.0000]

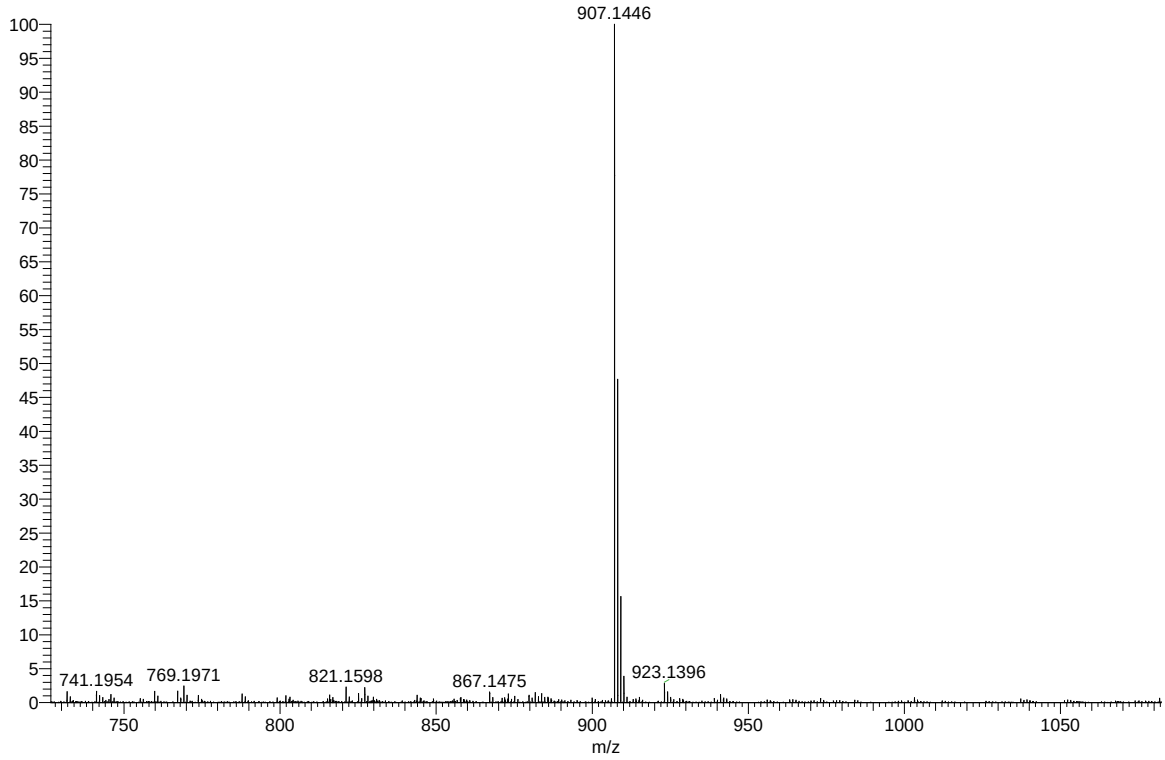

Au[5,15-Tol-10-C_6F_4-$SC_5H_{10}SH$-Corrole]

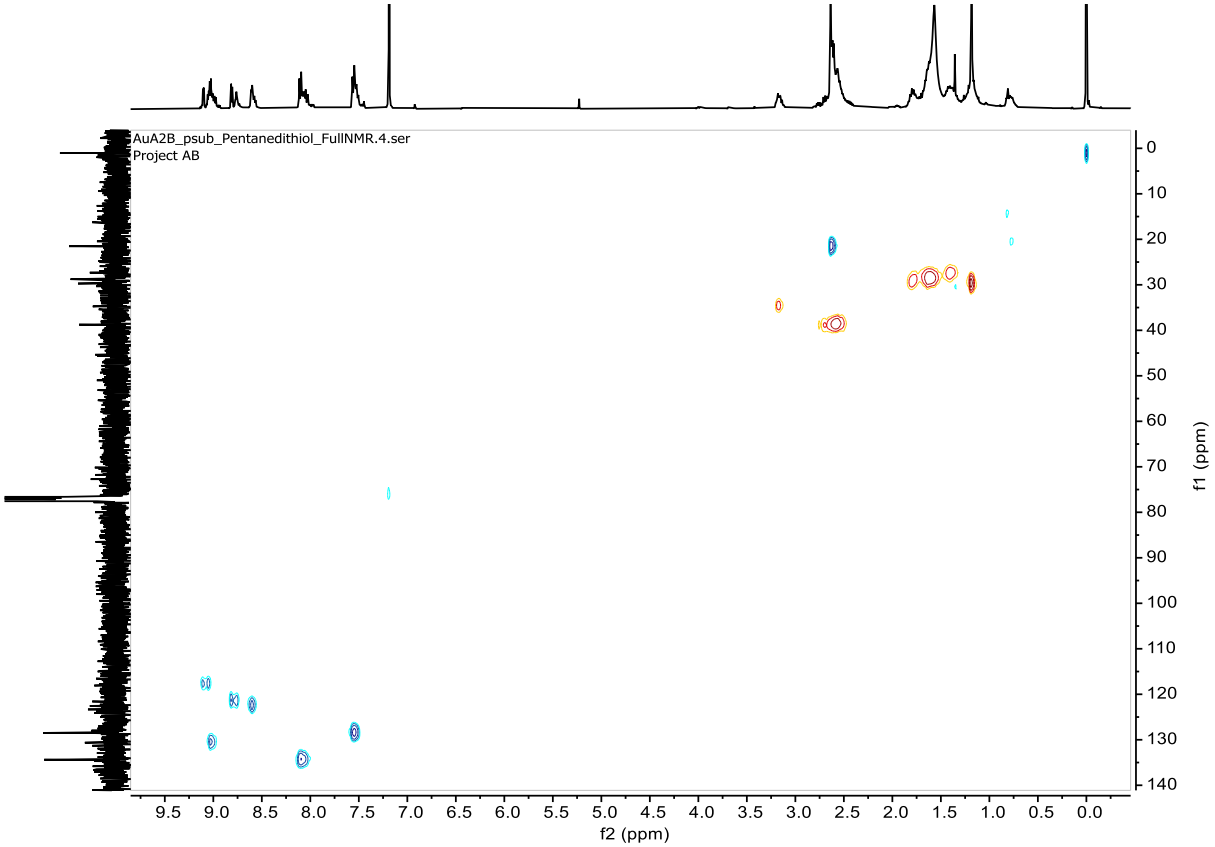

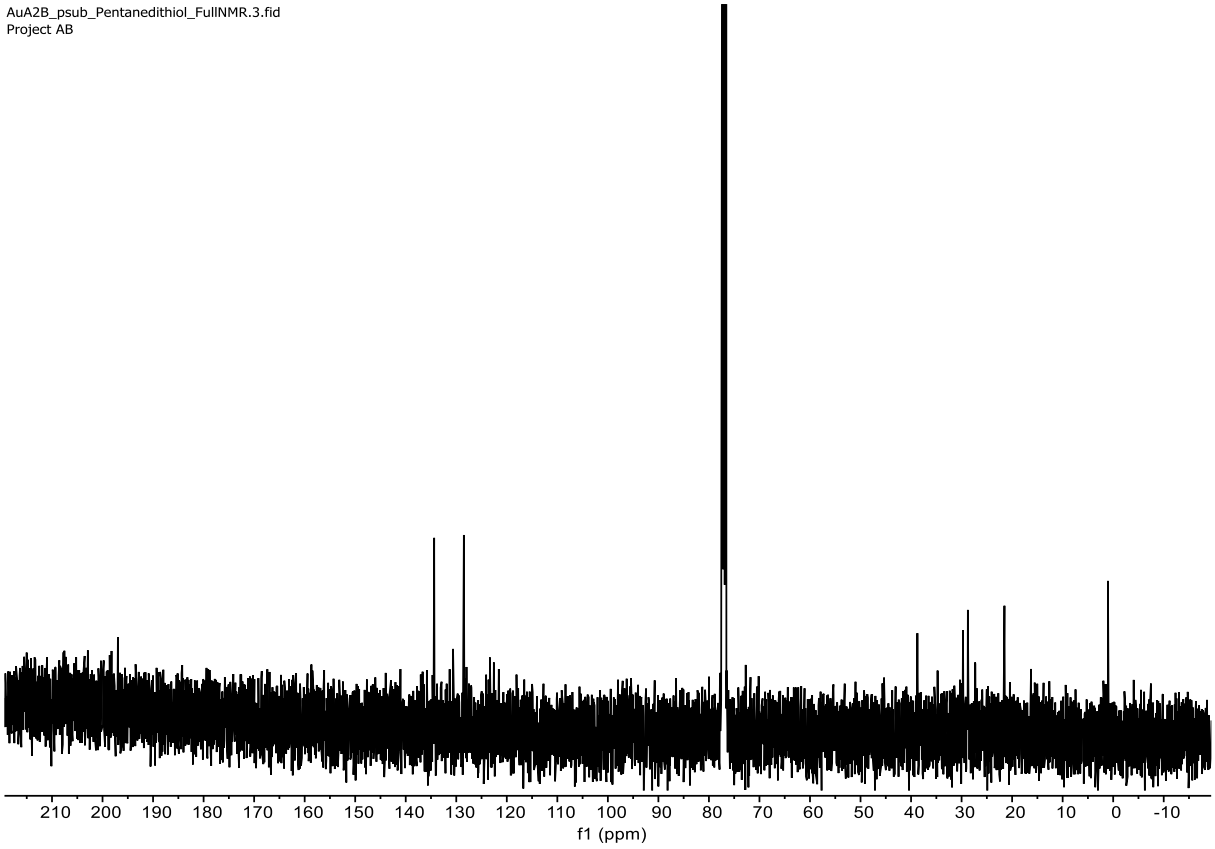
AuA2B_psub_Pentanedithiol_FullNMR.3.fid
Project AB
210 200 190 180 170 160 150 140 130 120 110 100 90 80 70 60 50 40 30 20 10 0 -10
f1 (ppm)

AuA2Bpent #43 RT: 0.20 AV: 1 NL: 1.92E7
T: FTMS + p APCI corona Full ms [700.0000-1500.0000]

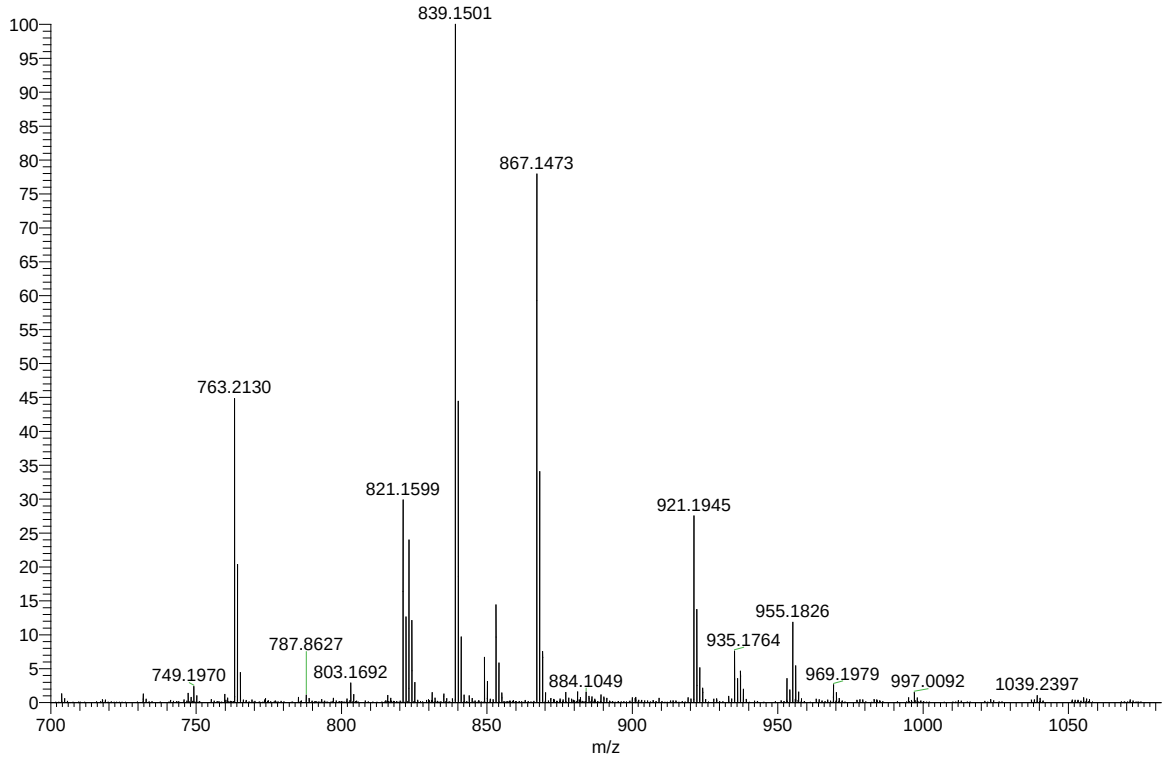

Au[5,15-Tol-10-C_6F_5-Corrole]

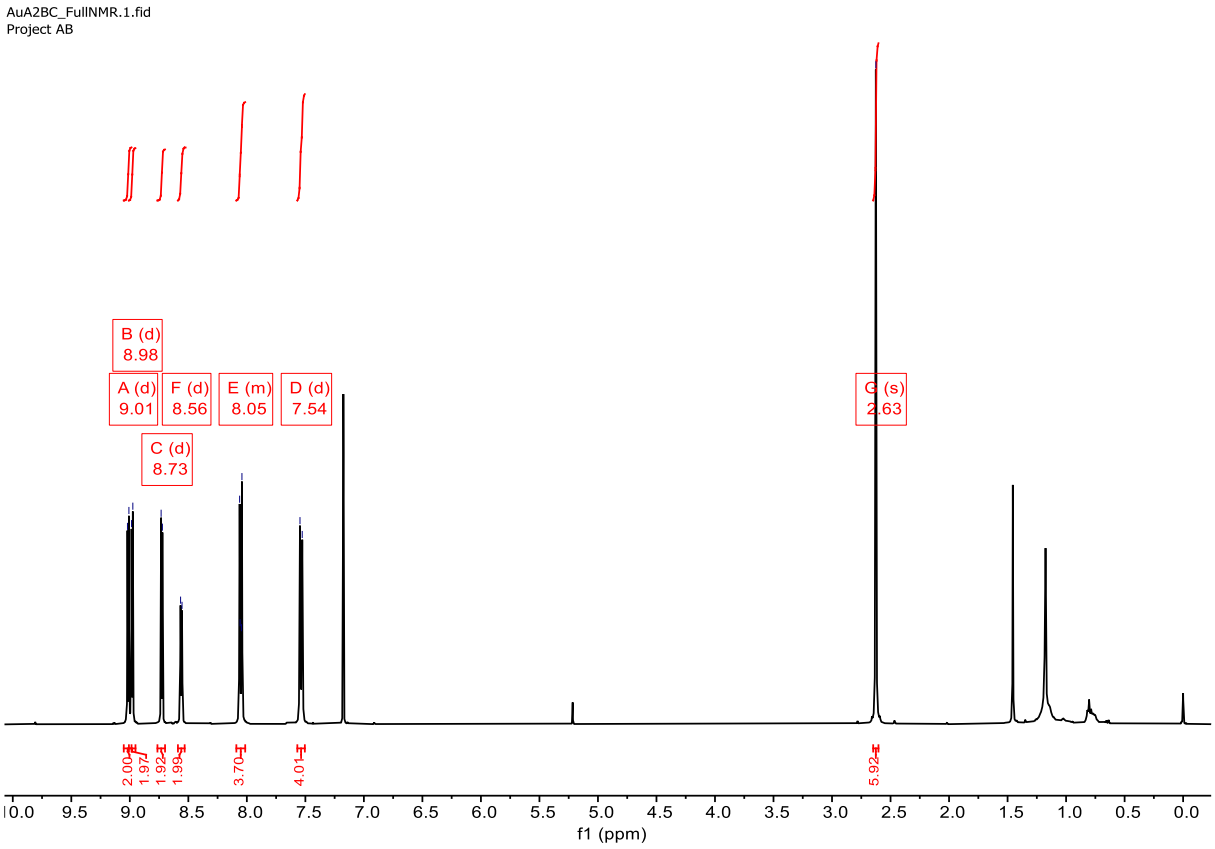

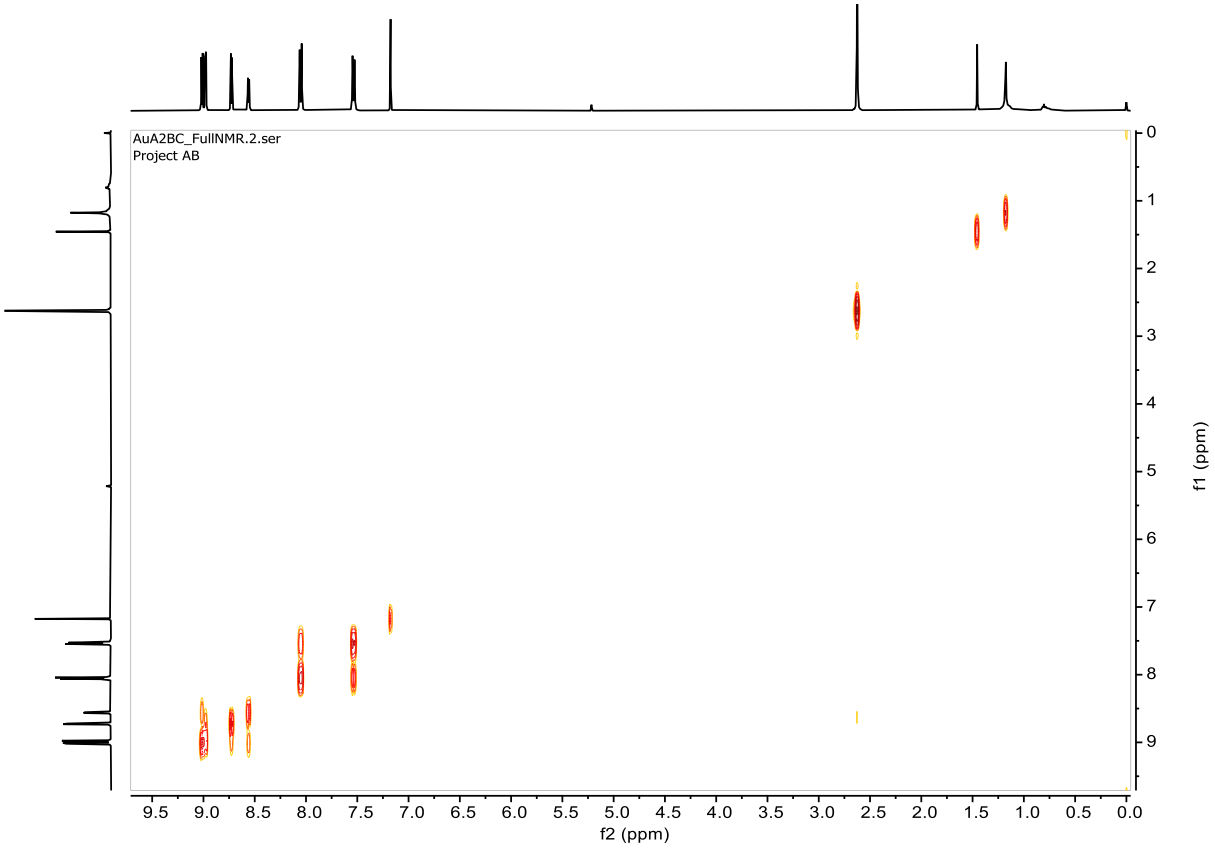
AuA2BC_FullNMR.2.ser
Project AB
f2 (ppm)
f1 (ppm)

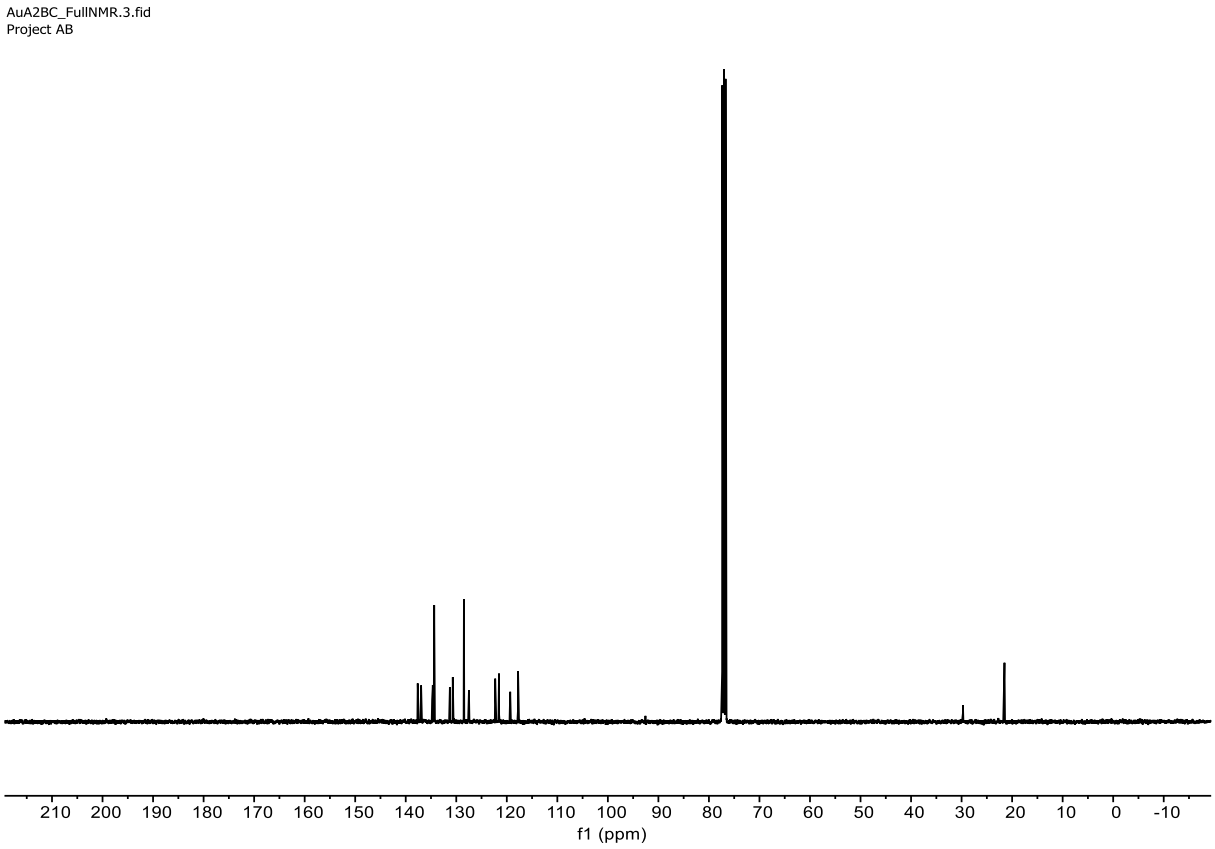
AuA2BC_FullNMR.3.fid
Project AB
210 200 190 180 170 160 150 140 130 120 110 100 90 80 70 60 50 40 30 20 10 0 -10
f1 (ppm)

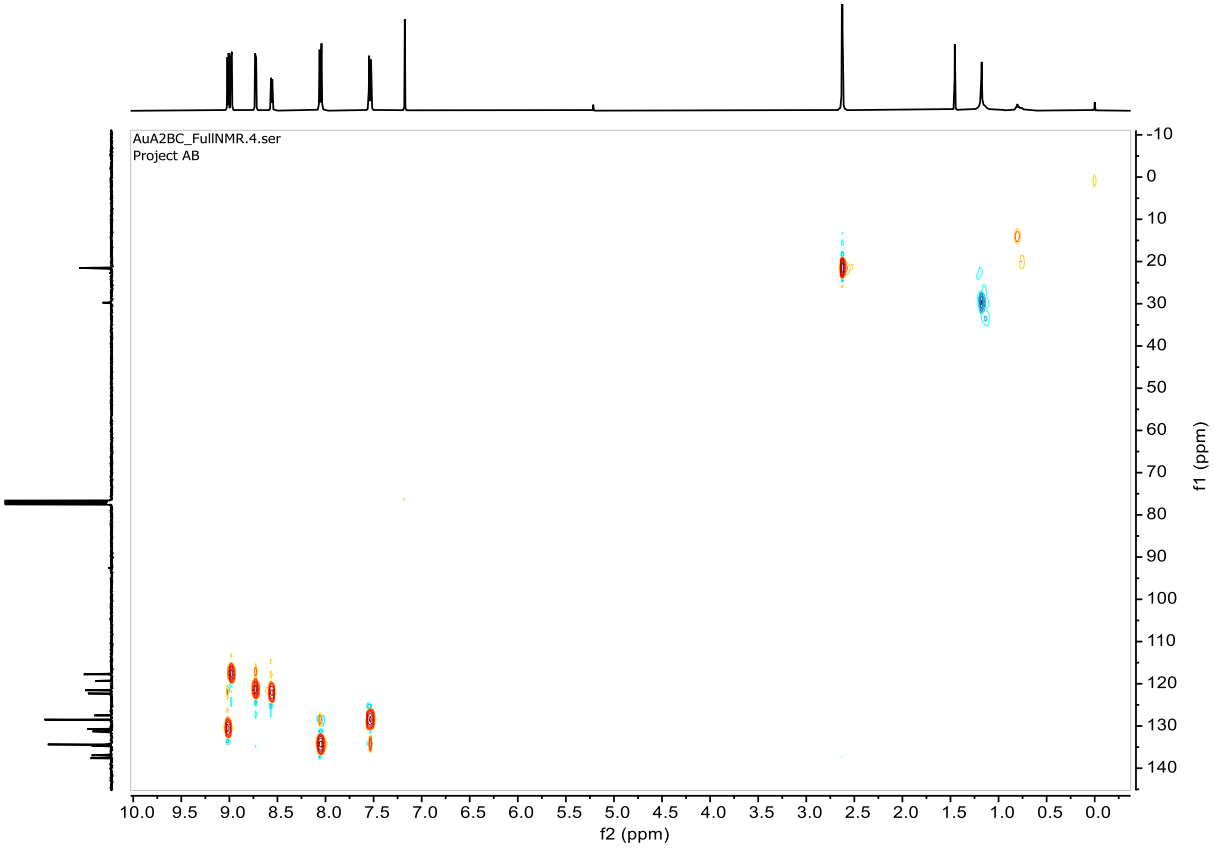
AuA2BC_FullNMR.4.ser
Project AB
10.0 9.5 9.0 8.5 8.0 7.5 7.0 6.5 6.0 5.5 5.0 4.5 4.0 3.5 3.0 2.5 2.0 1.5 1.0 0.5 0.0
f2 (ppm)
-10 0 10 20 30 40 50 60 70 80 90 100 110 120 130 140
f1 (ppm)

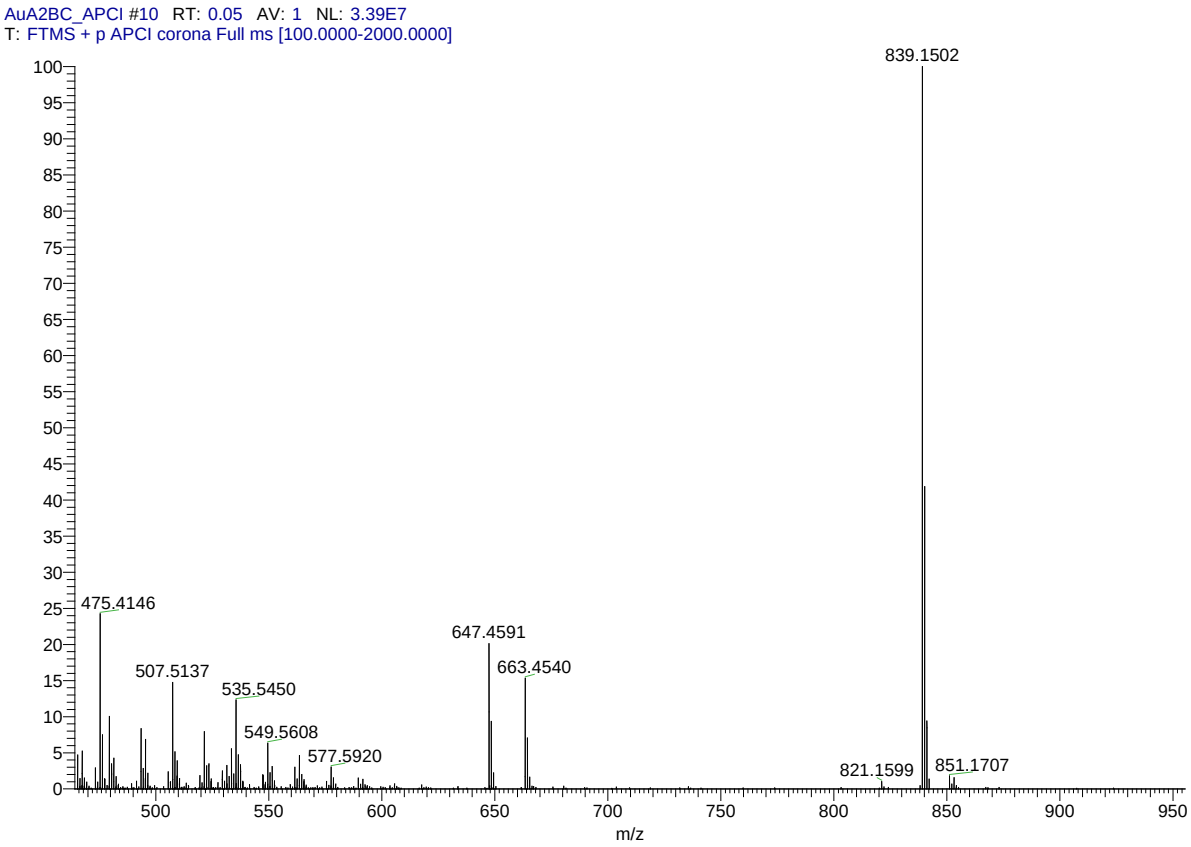
AuA2BC_APCI #10 RT: 0.05 AV: 1 NL: 3.39E7
T: FTMS + p APCI corona Full ms [100.0000-2000.0000]
839.1502
475.4146
647.4591
663.4540
507.5137
535.5450
549.5608
577.5920
821.1599
851.1707
m/z

Re[5,15-Tol-10-C_6F_5-Corrole](O)

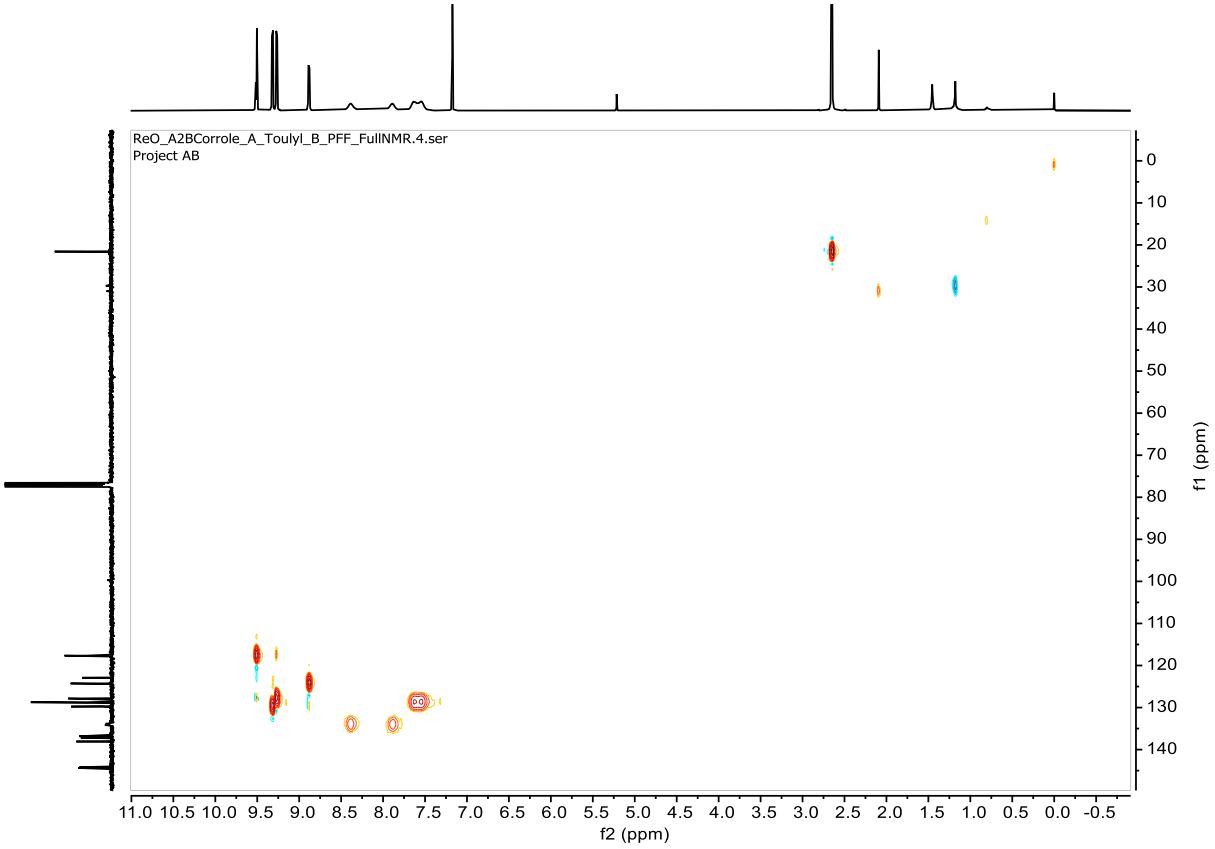

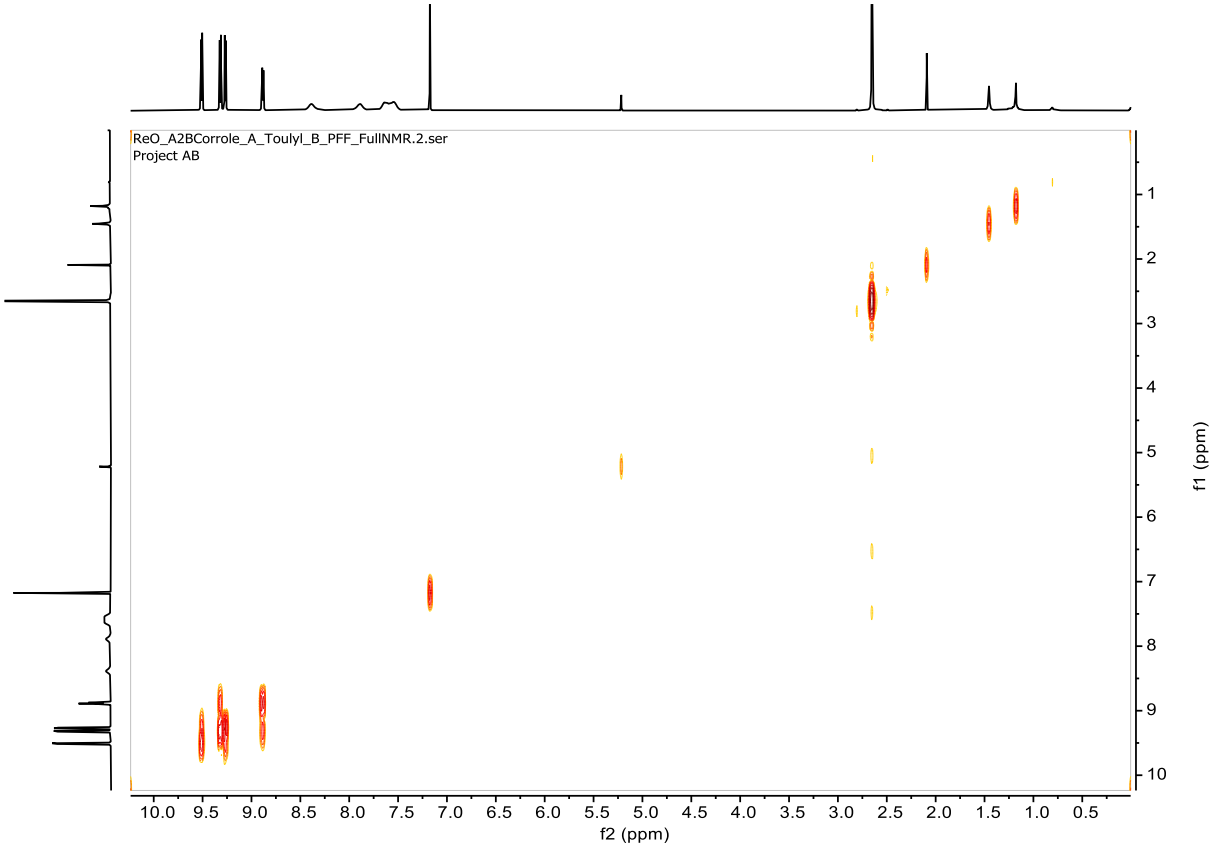
ReO_A2BCorrole_A_Toulyl_B_PFF_FullNMR.2.ser
Project AB
f2 (ppm)
f1 (ppm)

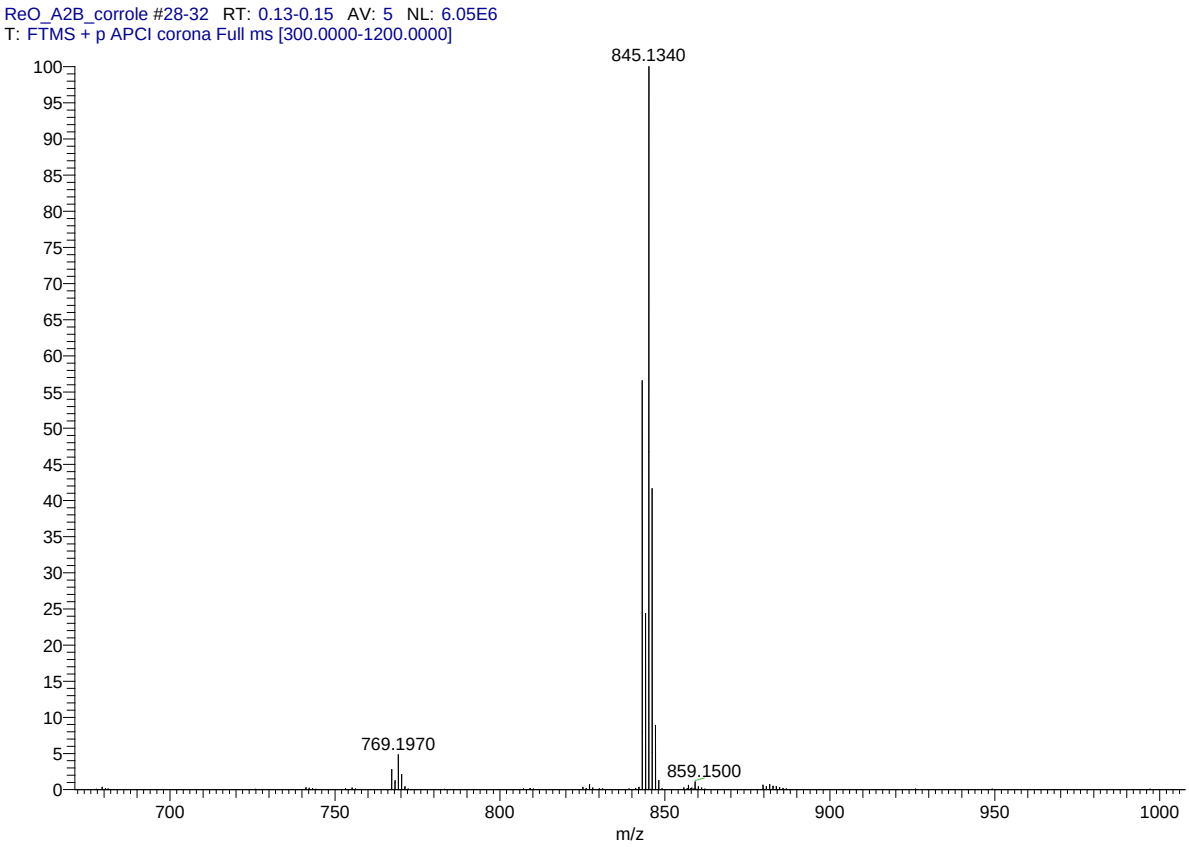
ReO_A2B_corrole #28-32 RT: 0.13-0.15 AV: 5 NL: 6.05E6
T: FTMS + p APCI corona Full ms [300.0000-1200.0000]
845.1340
769.1970
859.1500
m/z

Re[5,15-Tol-10-C_6F_4-SC_3H_6SH](O)

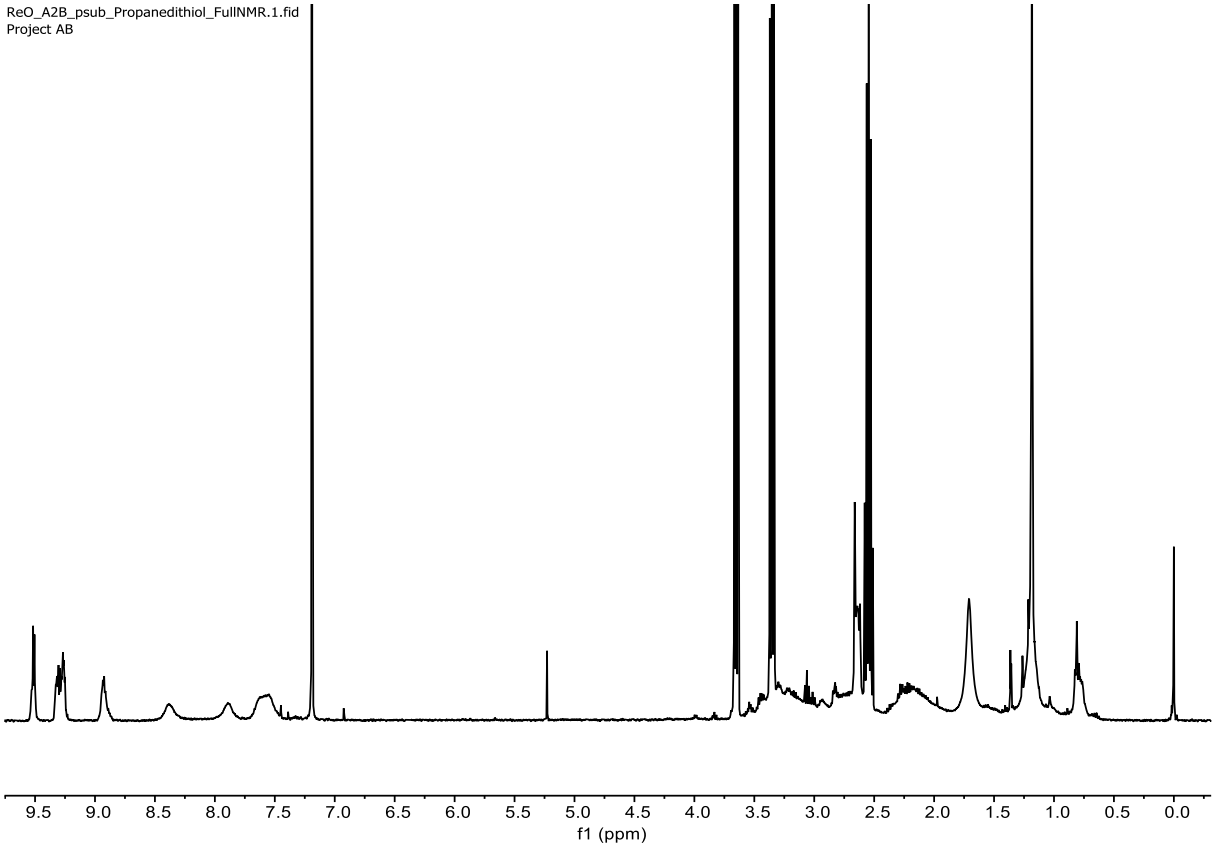

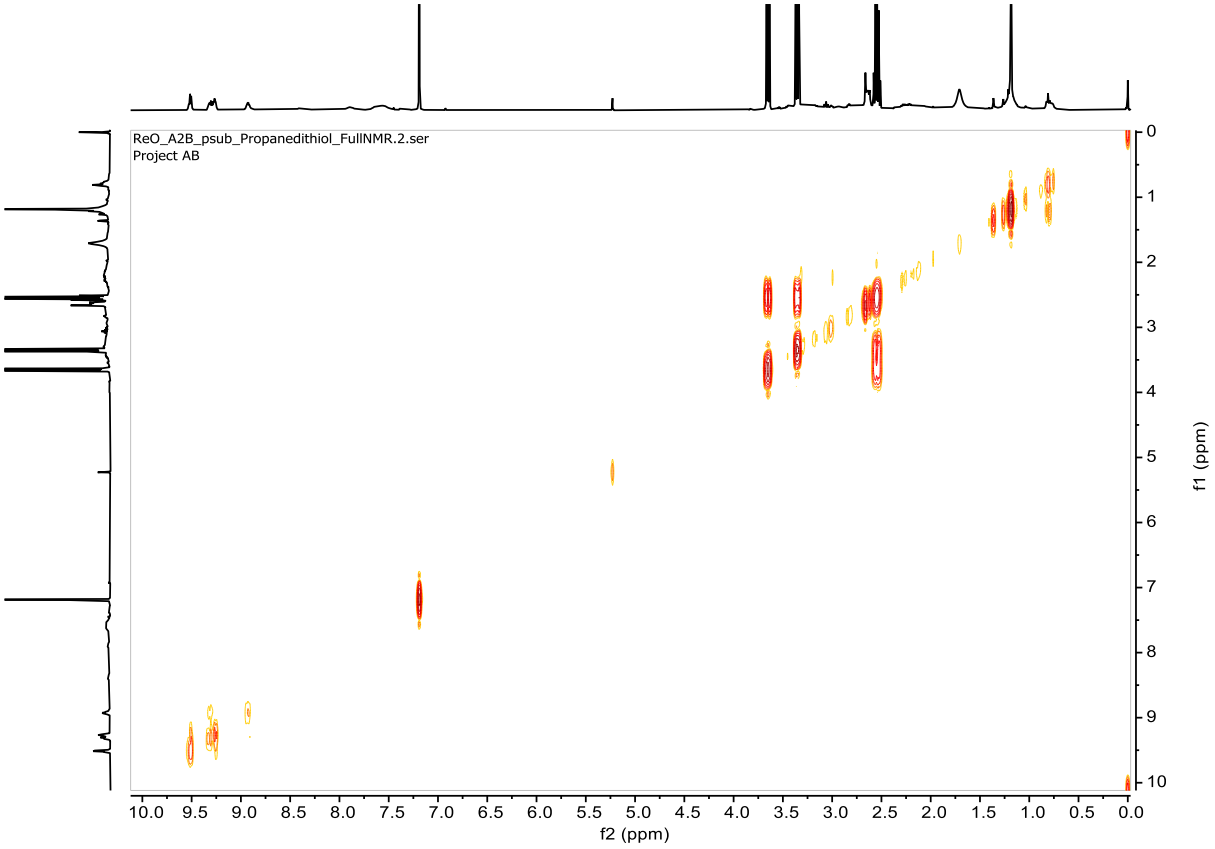
ReO_A2B_psub_Propanedithiol_FullNMR.2.ser
Project AB
f2 (ppm)
f1 (ppm)

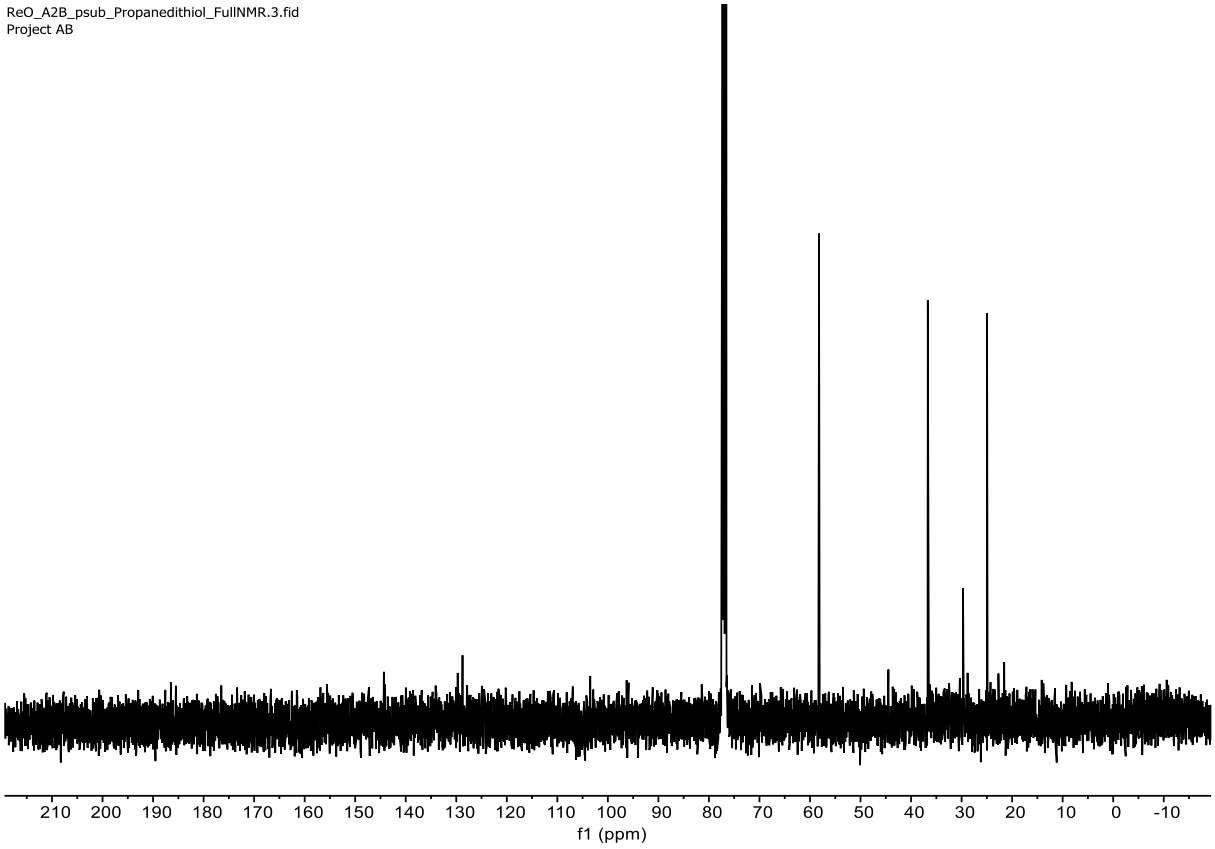
ReO_A2B_psub_Propanedithiol_FullNMR.3.fid
Project AB
210 200 190 180 170 160 150 140 130 120 110 100 90 80 70 60 50 40 30 20 10 0 -10
f1 (ppm)

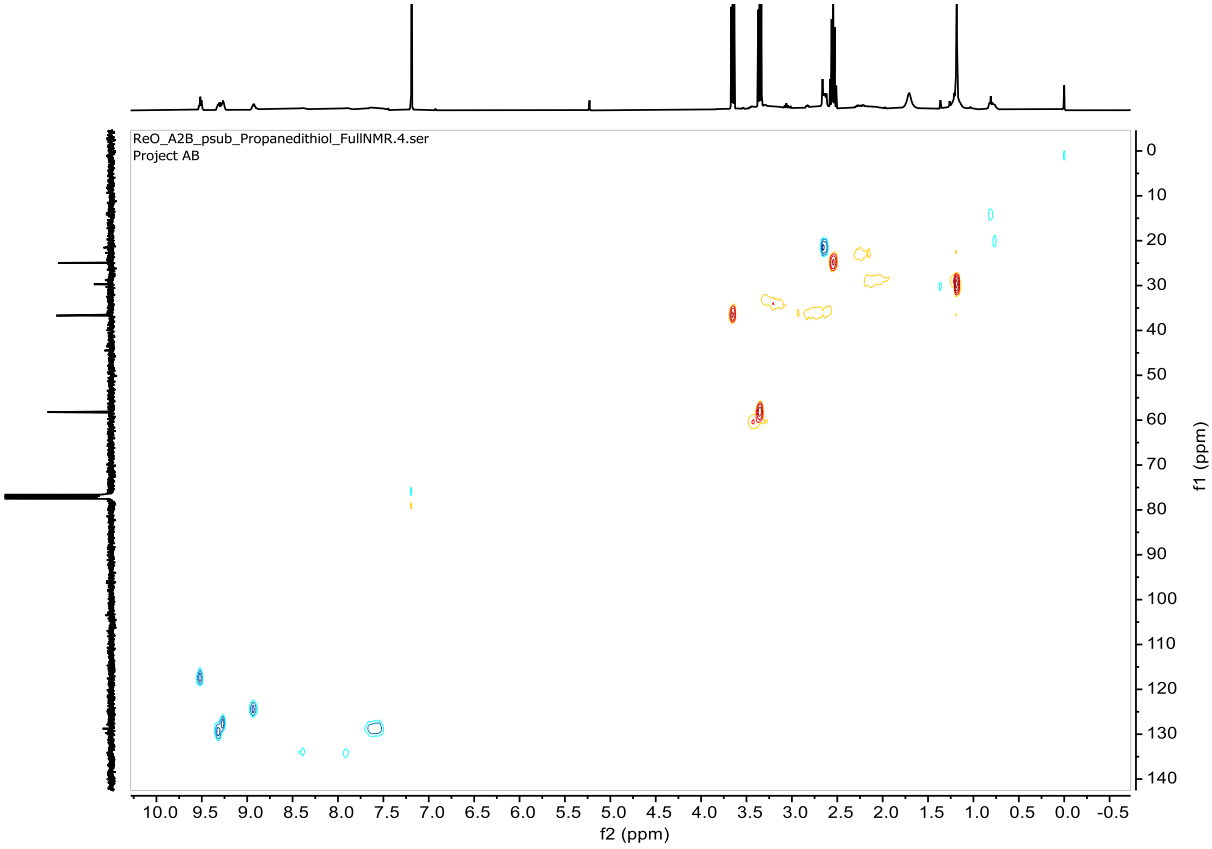
ReO_A2B_psub_Propanedithiol_FullNMR.4.ser
Project AB
f2 (ppm)
f1 (ppm)

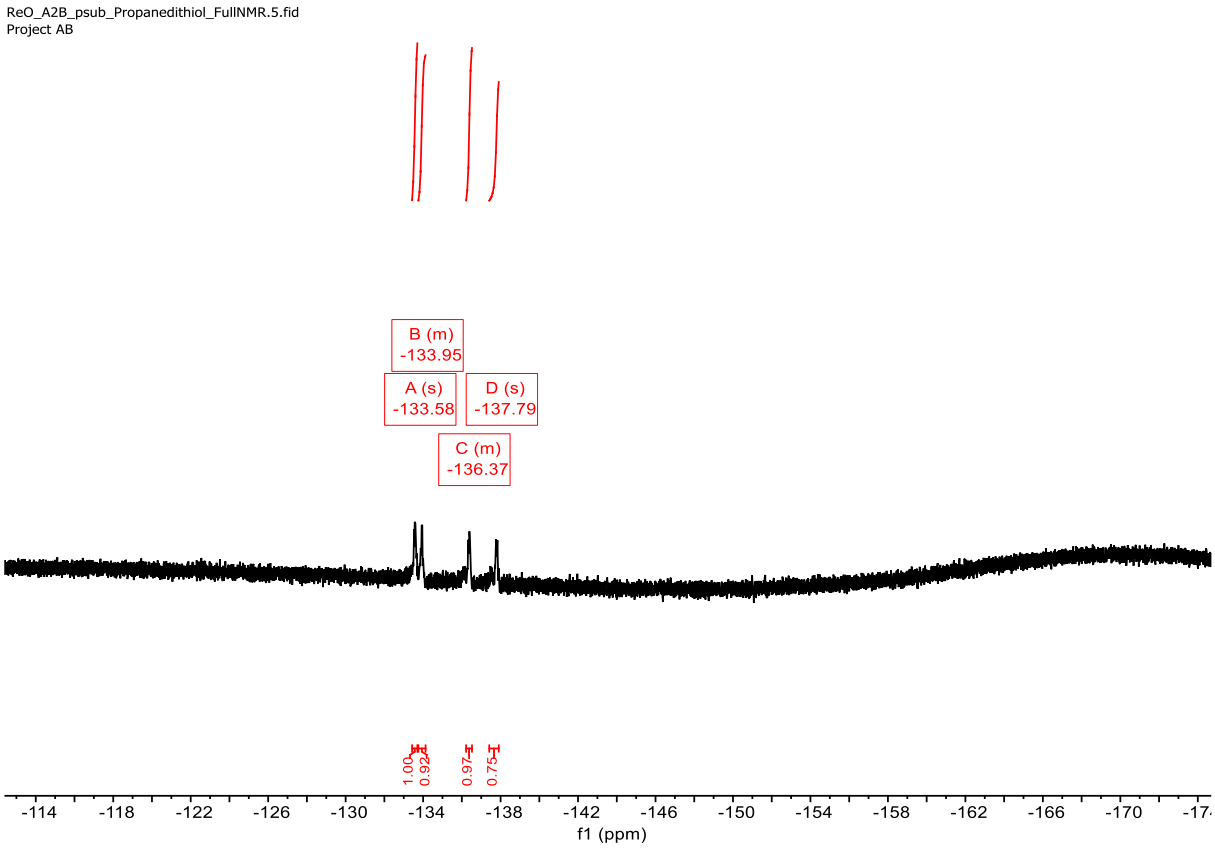
ReO_A2B_psub_Propanedithiol_FullNMR.5.fid
Project AB
B (m)
-133.95
A (s)
-133.58
D (s)
-137.79
C (m)
-136.37
1.00
0.92
0.97
0.75
-114
-118
-122
-126
-130
-134
-138
-142
-146
-150
-154
-158
-162
-166
-170
f1 (ppm)

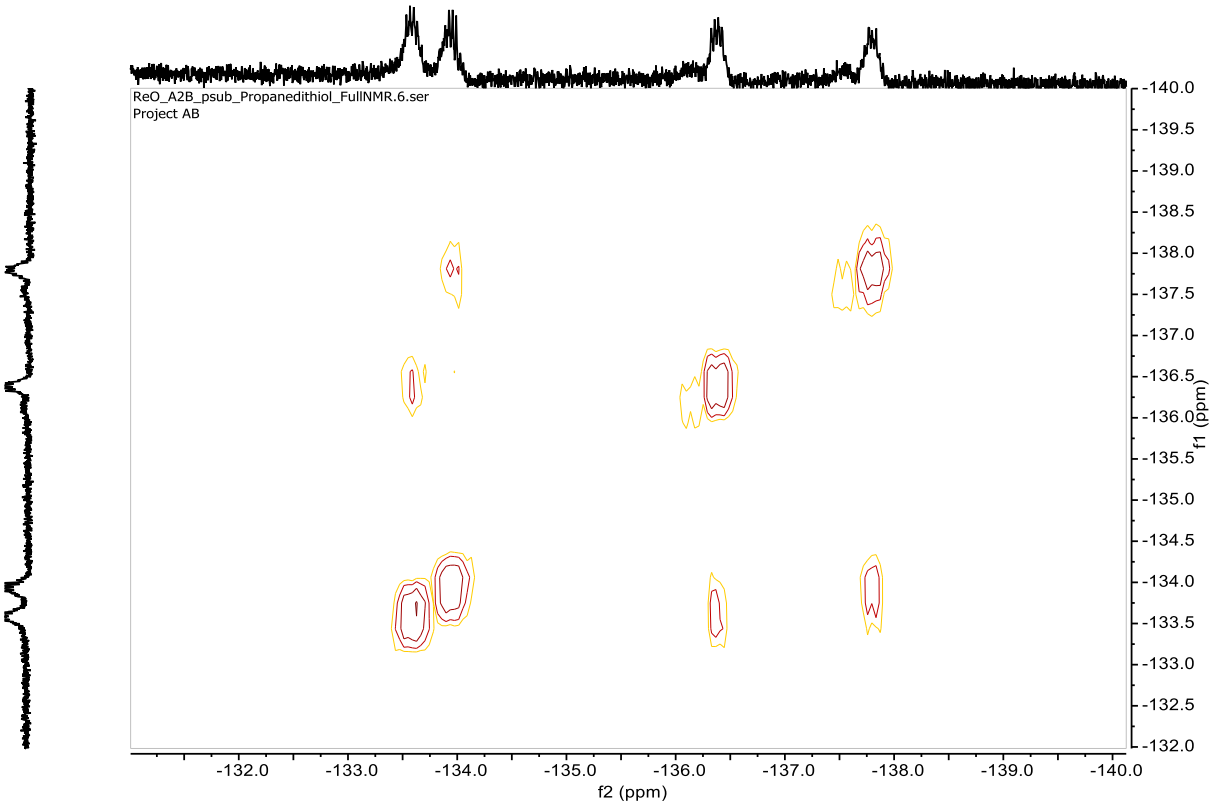
ReO_A2B_psub_Propanedithiol_FullNMR.6.ser
Project AB
-140.0
-139.5
-139.0
-138.5
-138.0
-137.5
-137.0
-136.5
-136.0
-135.5
-135.0
-134.5
-134.0
-133.5
-133.0
-132.5
-132.0
f1 (ppm)
-132.0
-133.0
-134.0
-135.0
-136.0
-137.0
-138.0
-139.0
-140.0
f2 (ppm)

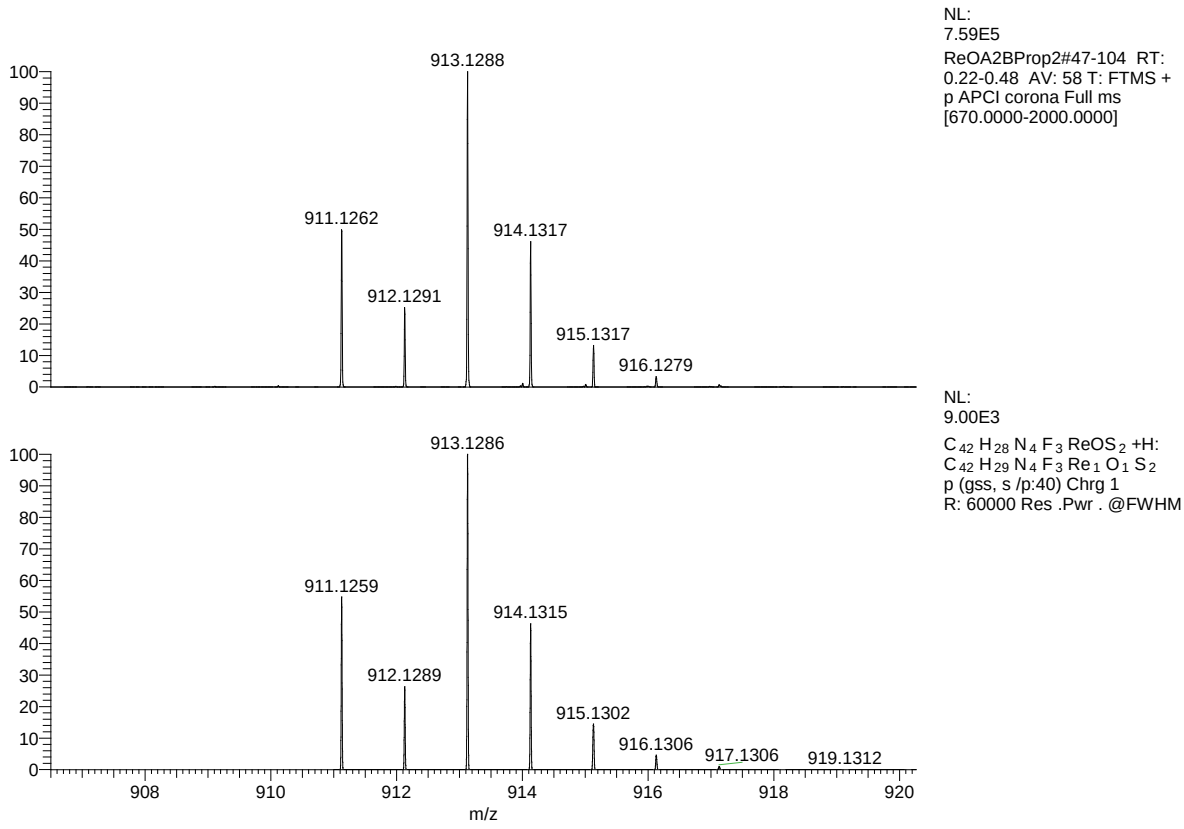
NL:
7.59E5
ReOA2BProp2#47-104 RT:
0.22-0.48 AV: 58 T: FTMS +
p APCI corona Full ms
[670.0000-2000.0000]
913.1288
911.1262
914.1317
912.1291
915.1317
916.1279
NL:
9.00E3
C42 H28 N4 F3 ReOS2 +H:
C42 H29 N4 F3 Re1 O1 S2
p (gss, s /p:40) Chrg 1
R: 60000 Res .Pwr . @FWHM
913.1286
911.1259
914.1315
912.1289
915.1302
916.1306
917.1306
919.1312
m/z

ReOA2BProp2 #47-104 RT: 0.22-0.48 AV: 58 NL: 7.59E5
T: FTMS + p APCI corona Full ms [670.0000-2000.0000]

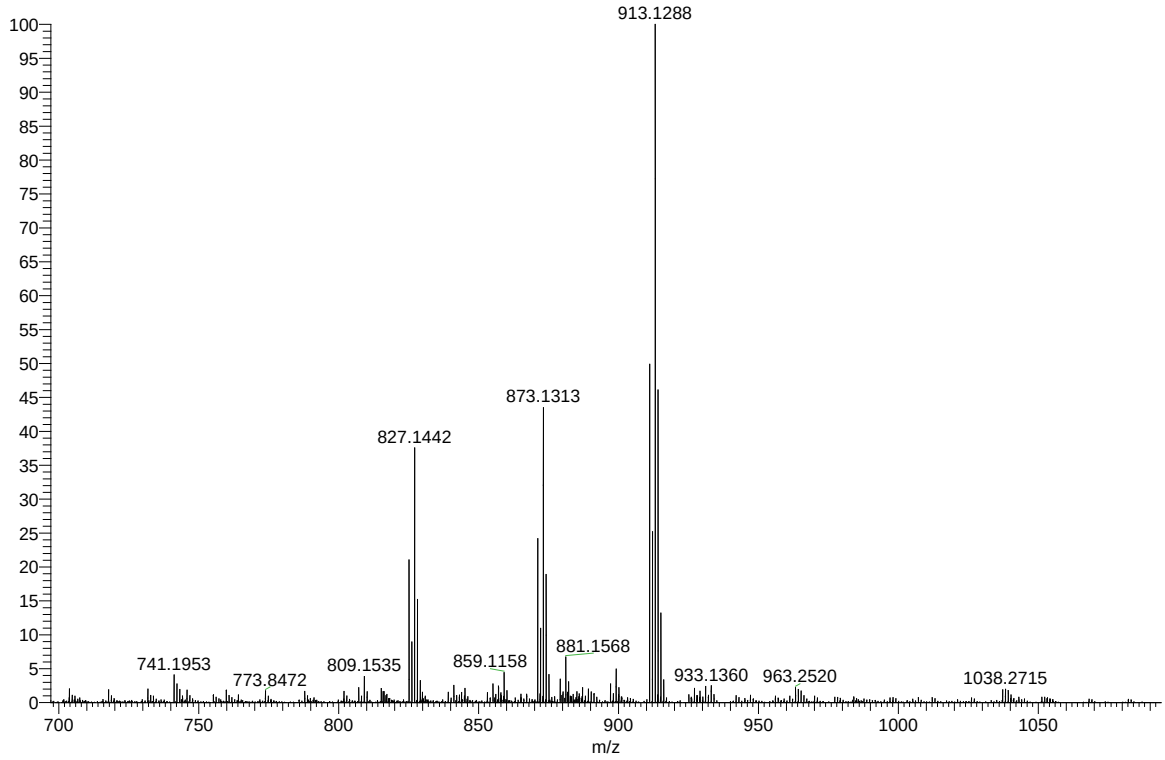

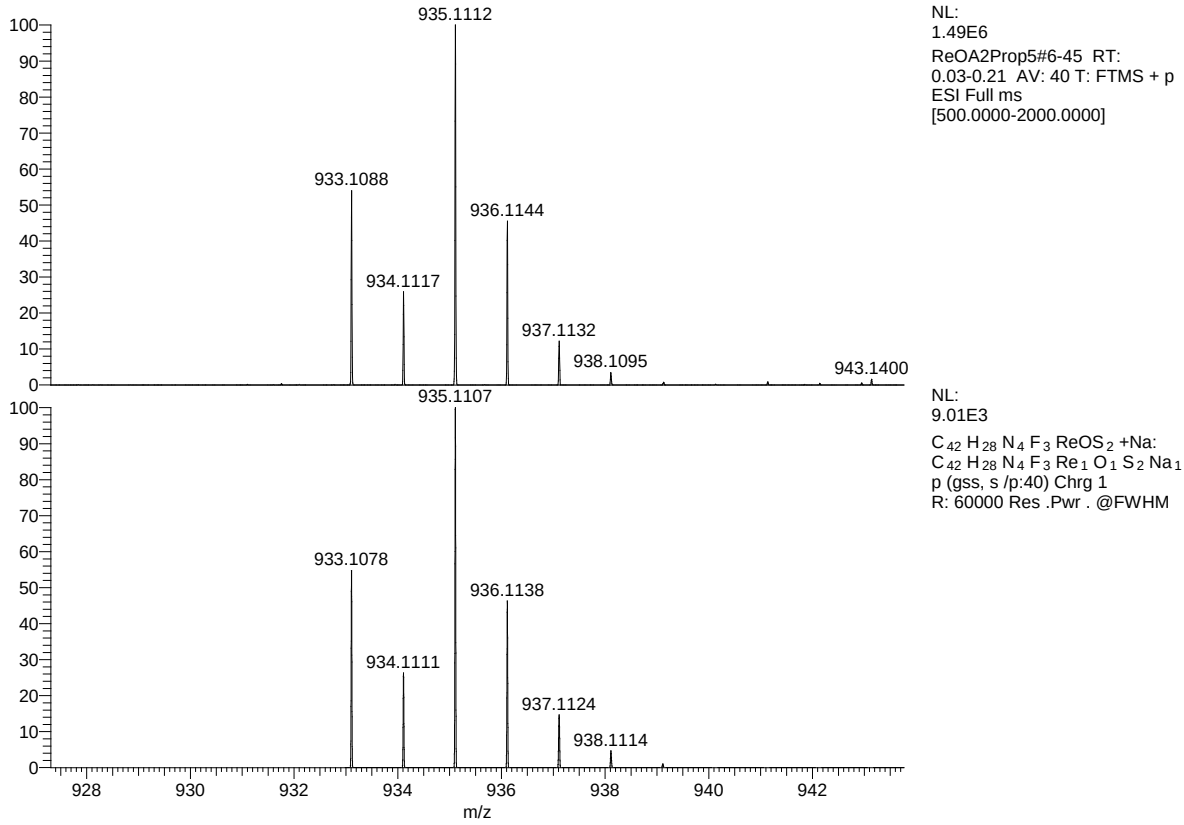
935.1112
933.1088
936.1144
934.1117
937.1132
938.1095
943.1400
NL:
1.49E6
ReOA2Prop5#6-45 RT:
0.03-0.21 AV: 40 T: FTMS + p
ESI Full ms
[500.0000-2000.0000]
935.1107
933.1078
936.1138
934.1111
937.1124
938.1114
NL:
9.01E3
C42 H28 N4 F3 ReOS2 +Na:
C42 H28 N4 F3 Re1 O1 S2 Na1
p (gss, s /p:40) Chrg 1
R: 60000 Res .Pwr . @FWHM
m/z

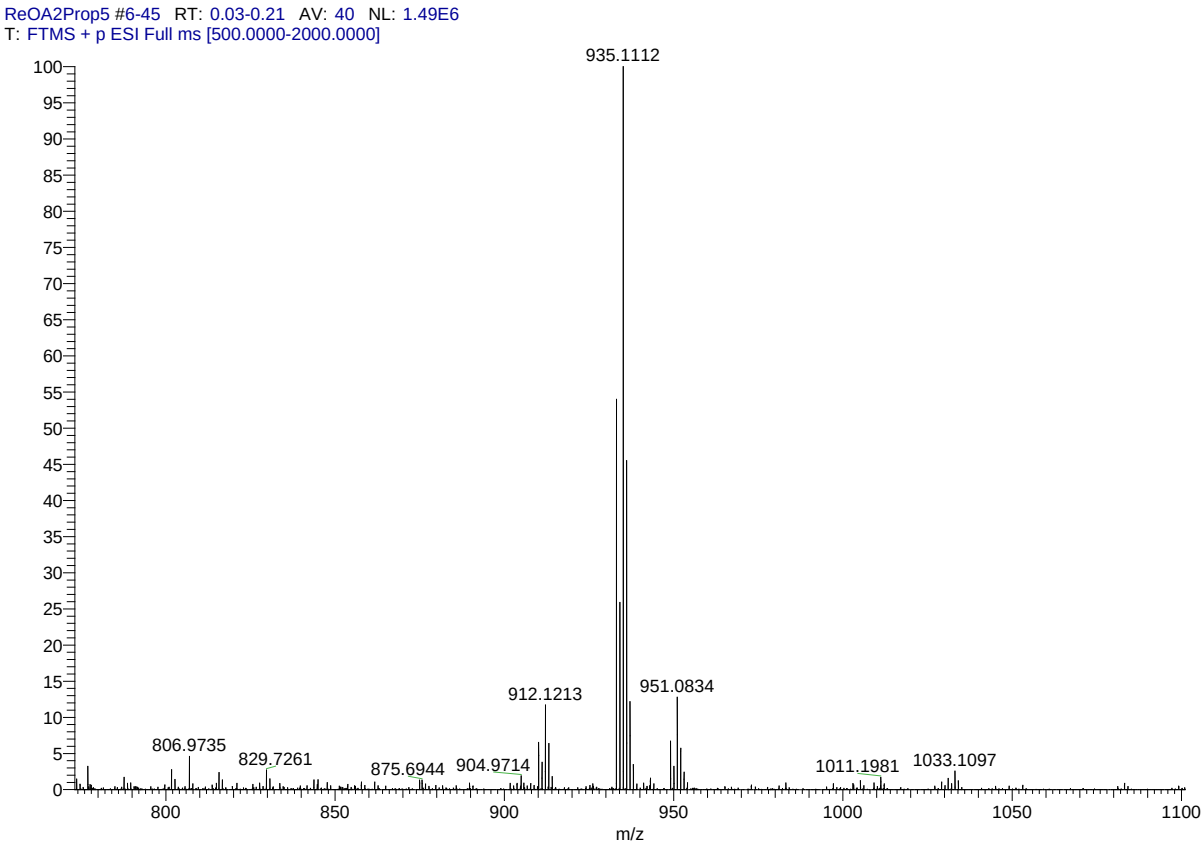
ReOA2Prop5 #6-45 RT: 0.03-0.21 AV: 40 NL: 1.49E6
T: FTMS + p ESI Full ms [500.0000-2000.0000]
935.1112
912.1213
951.0834
806.9735
829.7261
875.6944
904.9714
1011.1981
1033.1097
m/z

Re[5,15-Tol-10-C_6F_4-$SC_5H_{10}SH$-Corrole](O)

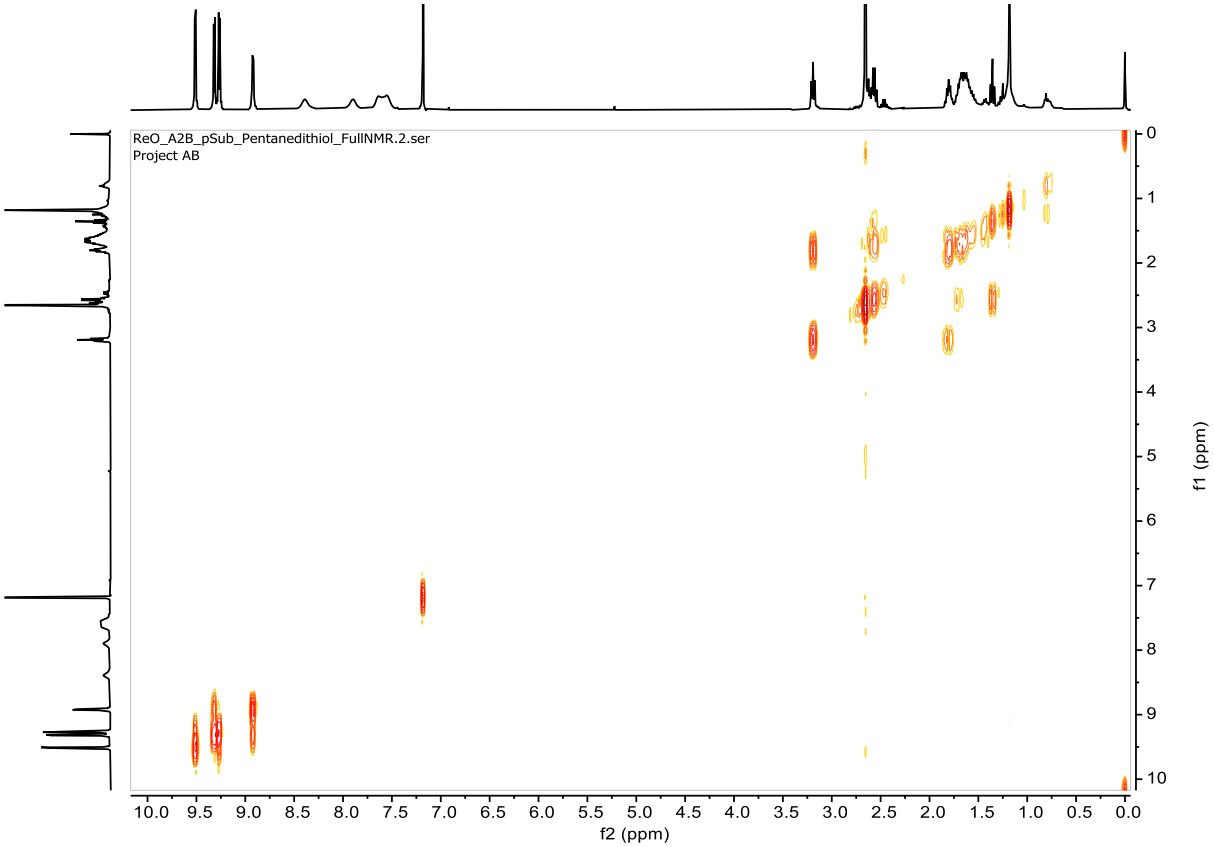

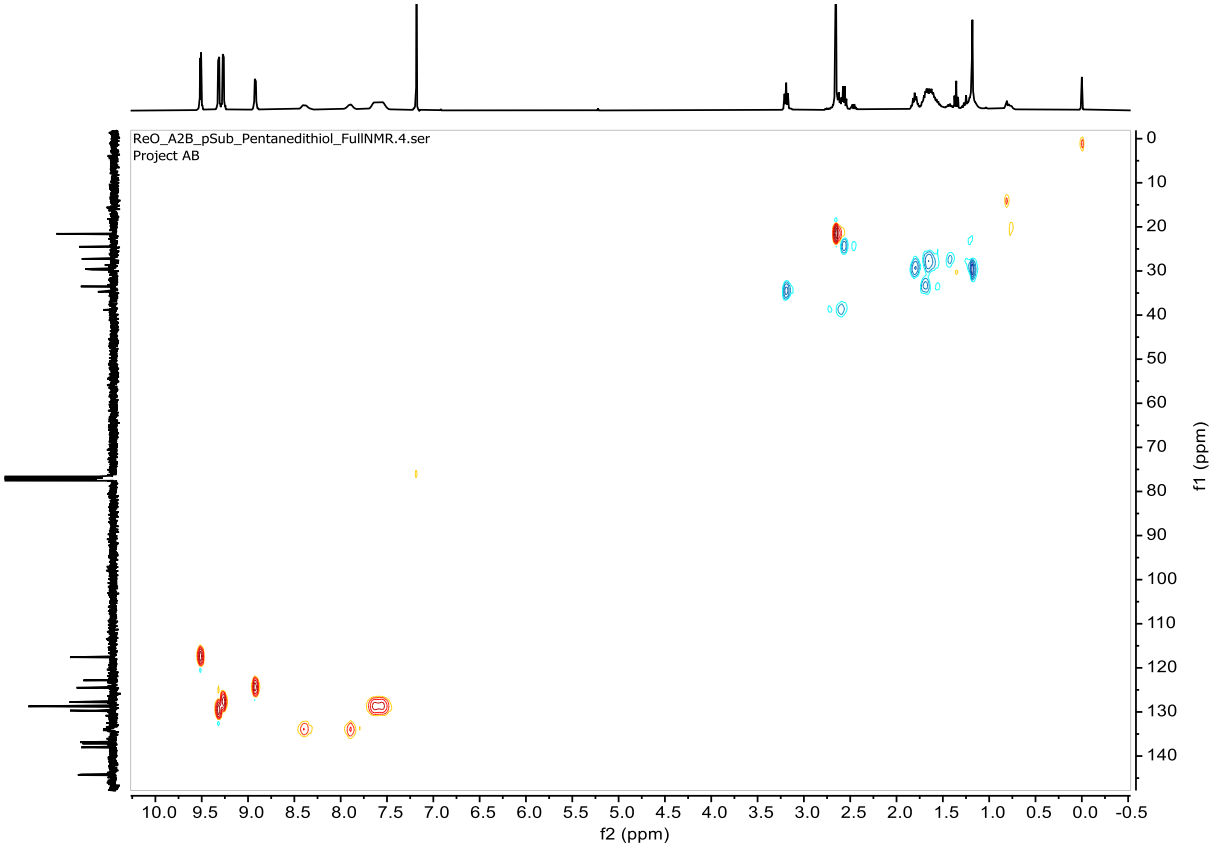
ReO_A2B_pSub_Pentanedithiol_FullNMR.4.ser
Project AB
f2 (ppm)
f1 (ppm)

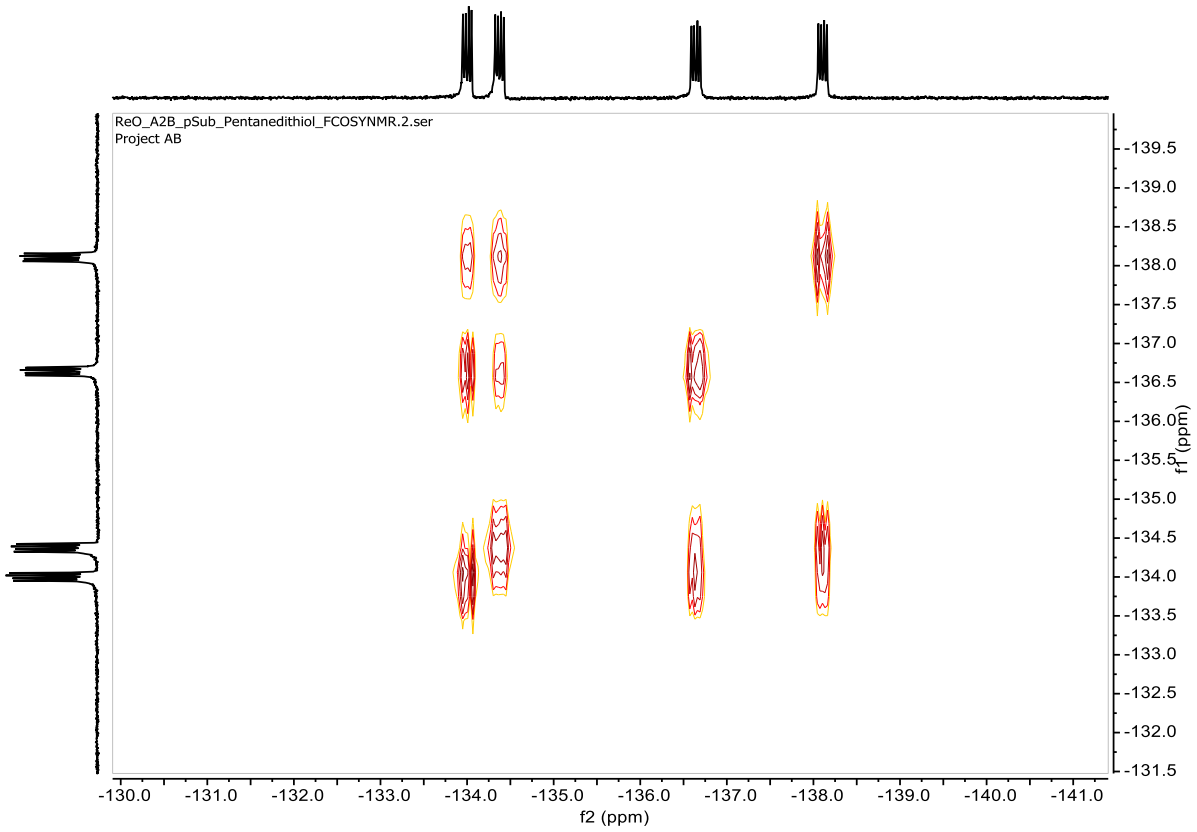
ReO_A2B_pSub_Pentanedithiol_FCOSYNMR.2.ser
Project AB
-139.5
-139.0
-138.5
-138.0
-137.5
-137.0
-136.5
-136.0
-135.5
-135.0
-134.5
-134.0
-133.5
-133.0
-132.5
-132.0
-131.5
f1 (ppm)
-130.0
-131.0
-132.0
-133.0
-134.0
-135.0
-136.0
-137.0
-138.0
-139.0
-140.0
-141.0
f2 (ppm)

ReOA2BPent #4-125 RT: 0.02-0.60 AV: 122 NL: 1.67E5
T: FTMS + p ESI Full ms [600.0000-2000.0000]

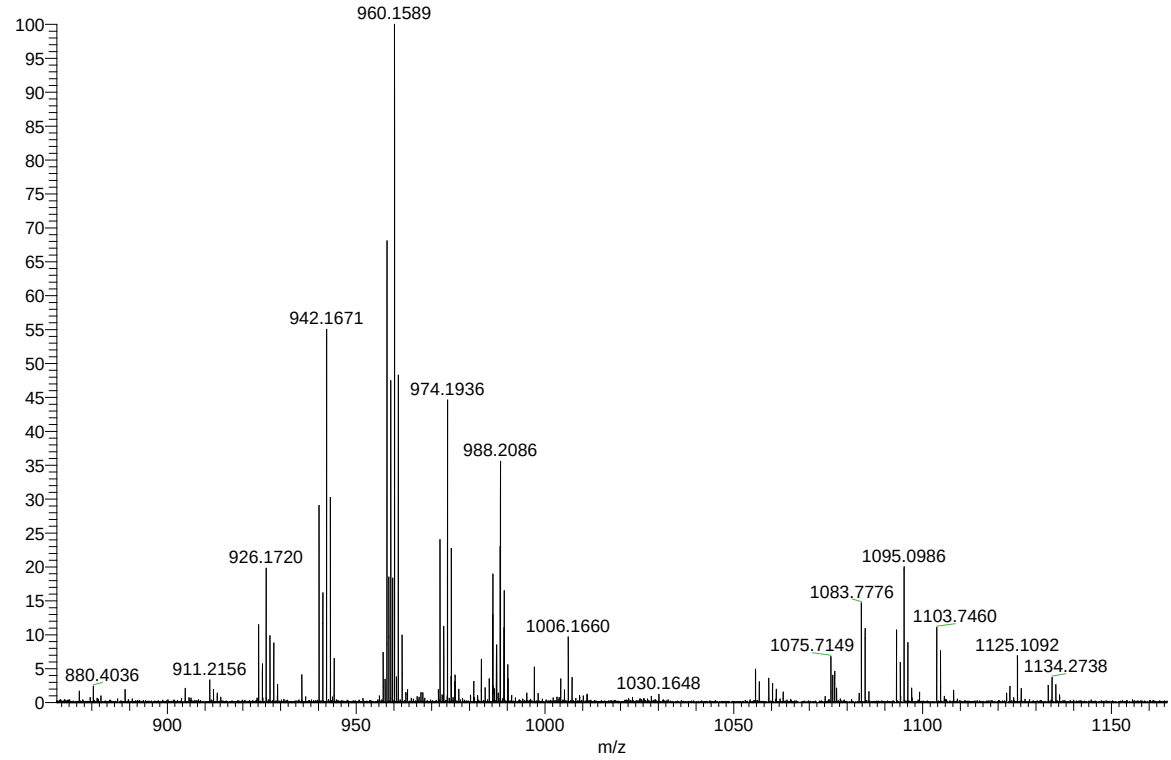

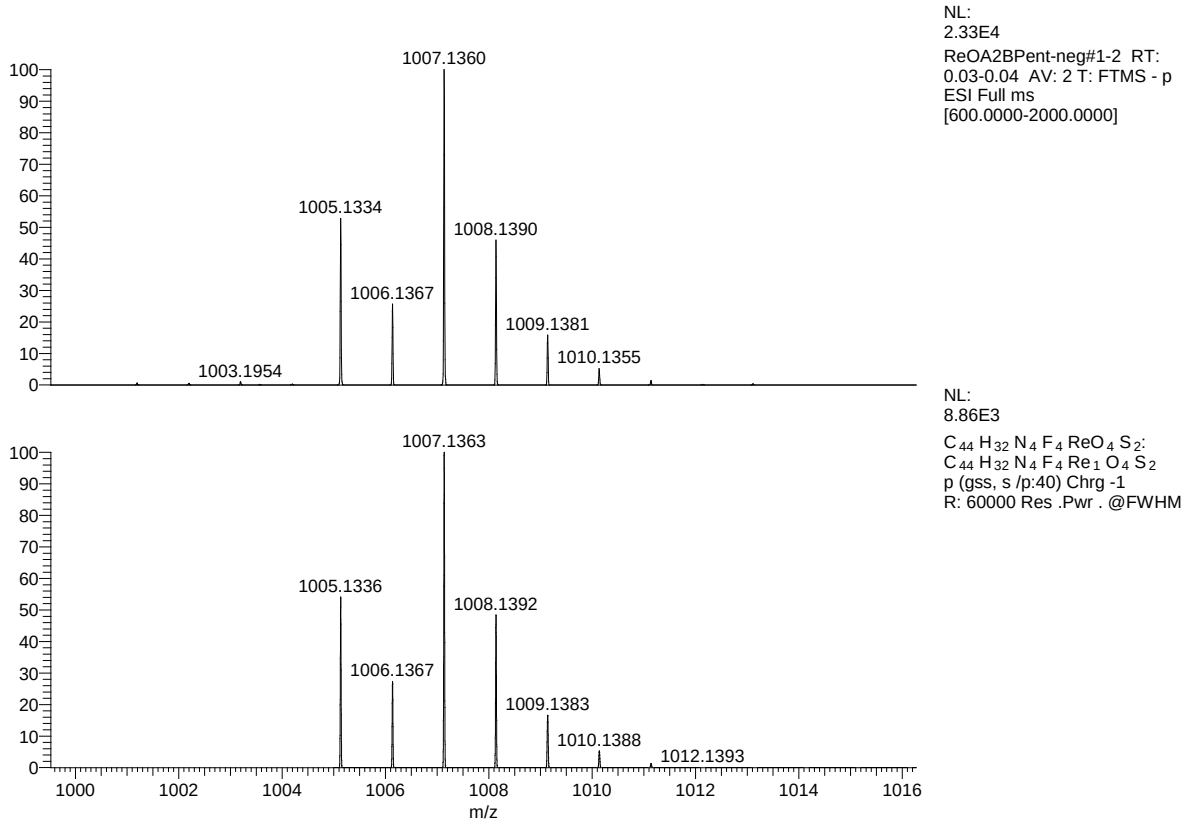
NL:
2.33E4
ReOA2BPent-neg#1-2 RT:
0.03-0.04 AV: 2 T: FTMS - p
ESI Full ms
[600.0000-2000.0000]
1007.1360
1005.1334
1008.1390
1006.1367
1009.1381
1010.1355
1003.1954
NL:
8.86E3
C44 H32 N4 F4 ReO4 S2:
C44 H32 N4 F4 Re1 O4 S2
p (gss, s /p:40) Chrg -1
R: 60000 Res .Pwr . @FWHM
1007.1363
1005.1336
1008.1392
1006.1367
1009.1383
1010.1388
1012.1393
m/z

ReOA2BPent-neg #1-2 RT: 0.03-0.04 AV: 2 NL: 2.33E4
T: FTMS - p ESI Full ms [600.0000-2000.0000]

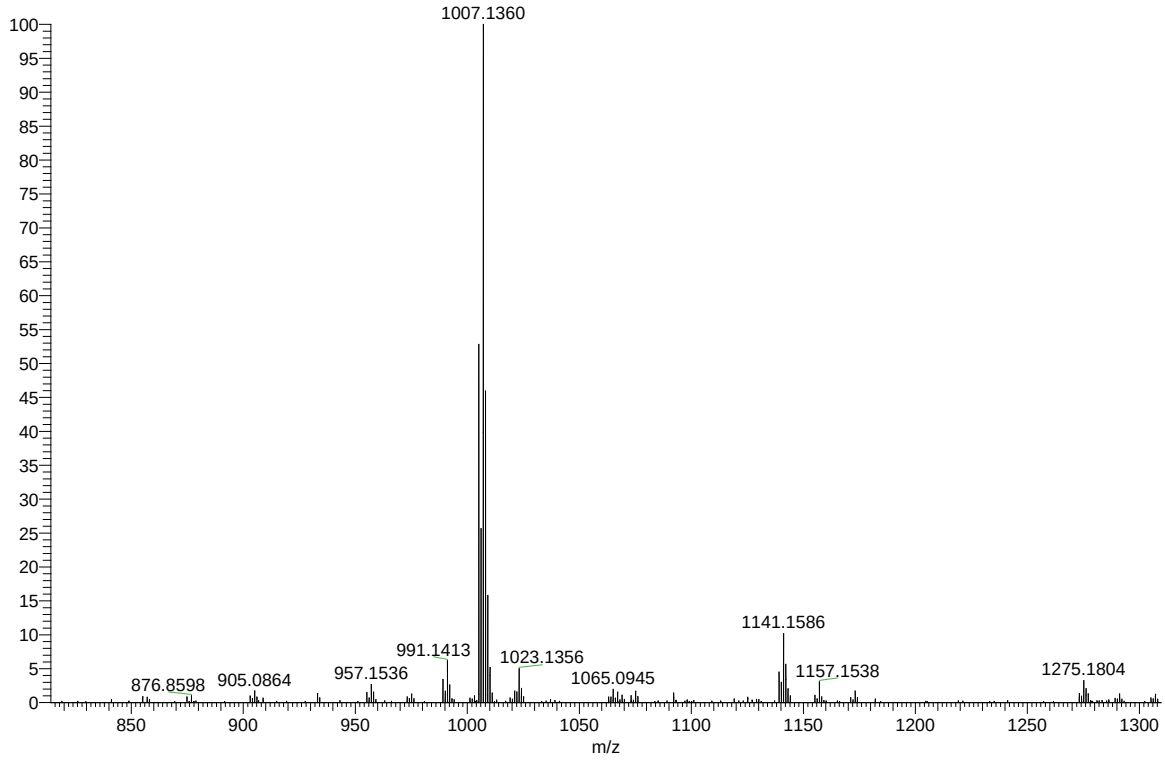

Re[5,15-Tol-10-C_6F_4-SC_8H_{16}SH-Corrole](O)

ReO_A2B_A_paraMethylPhenyl_B_Pentafluoro_para-octanedithiol.1.fid
Project AB

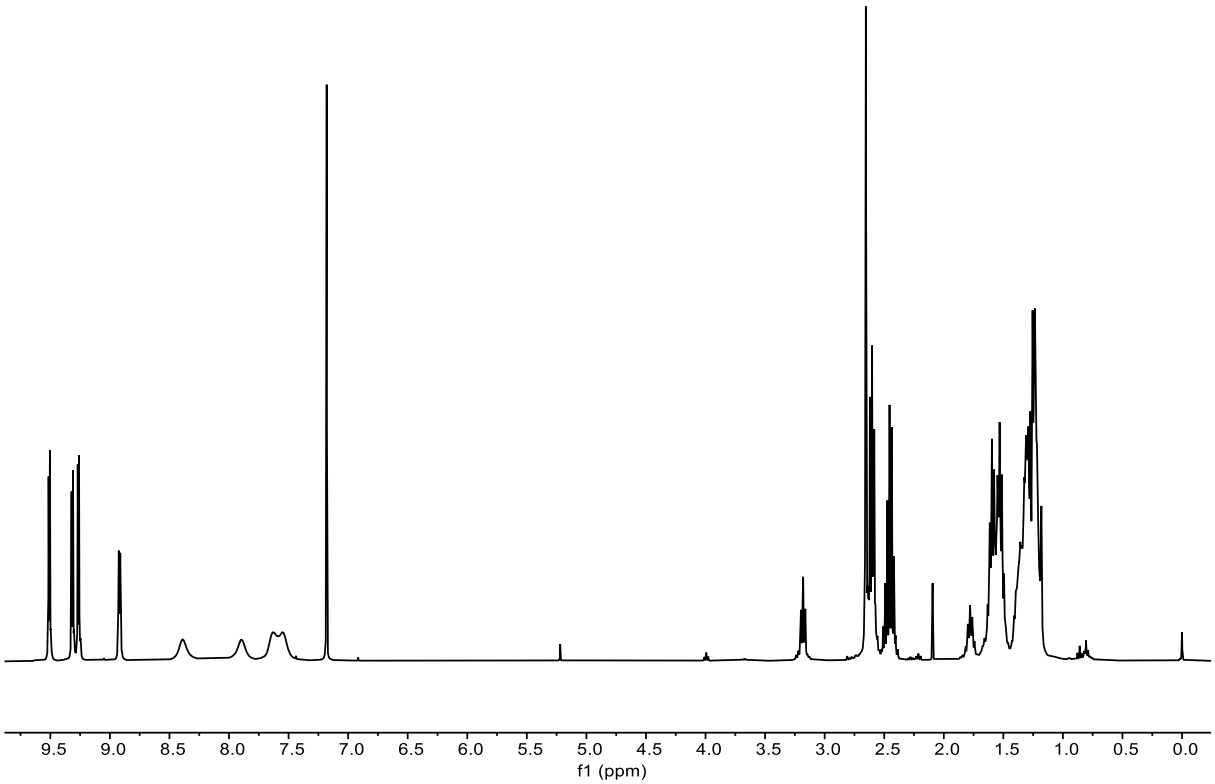

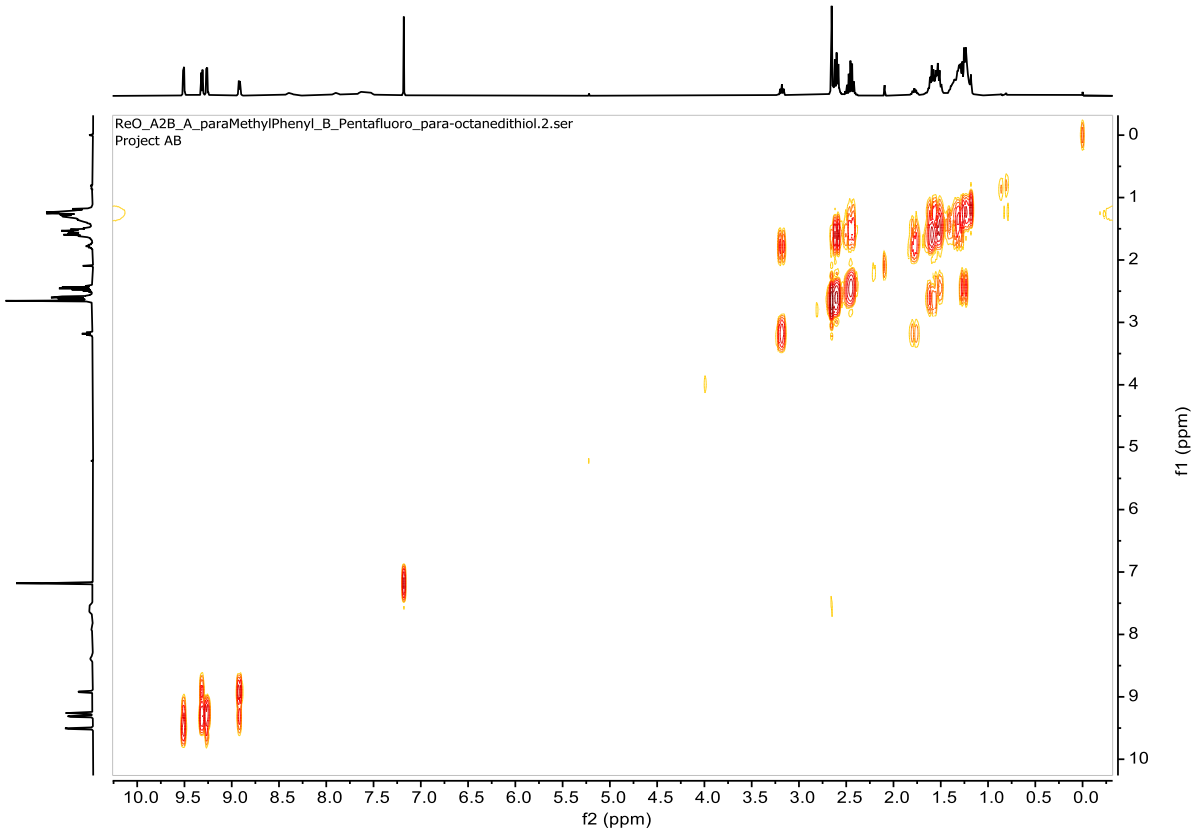
ReO_A2B_A_paraMethylPhenyl_B_Pentafluoro_para-octanedithiol.2.ser
Project AB
10.0 9.5 9.0 8.5 8.0 7.5 7.0 6.5 6.0 5.5 5.0 4.5 4.0 3.5 3.0 2.5 2.0 1.5 1.0 0.5 0.0
f2 (ppm)
0 1 2 3 4 5 6 7 8 9 10
f1 (ppm)

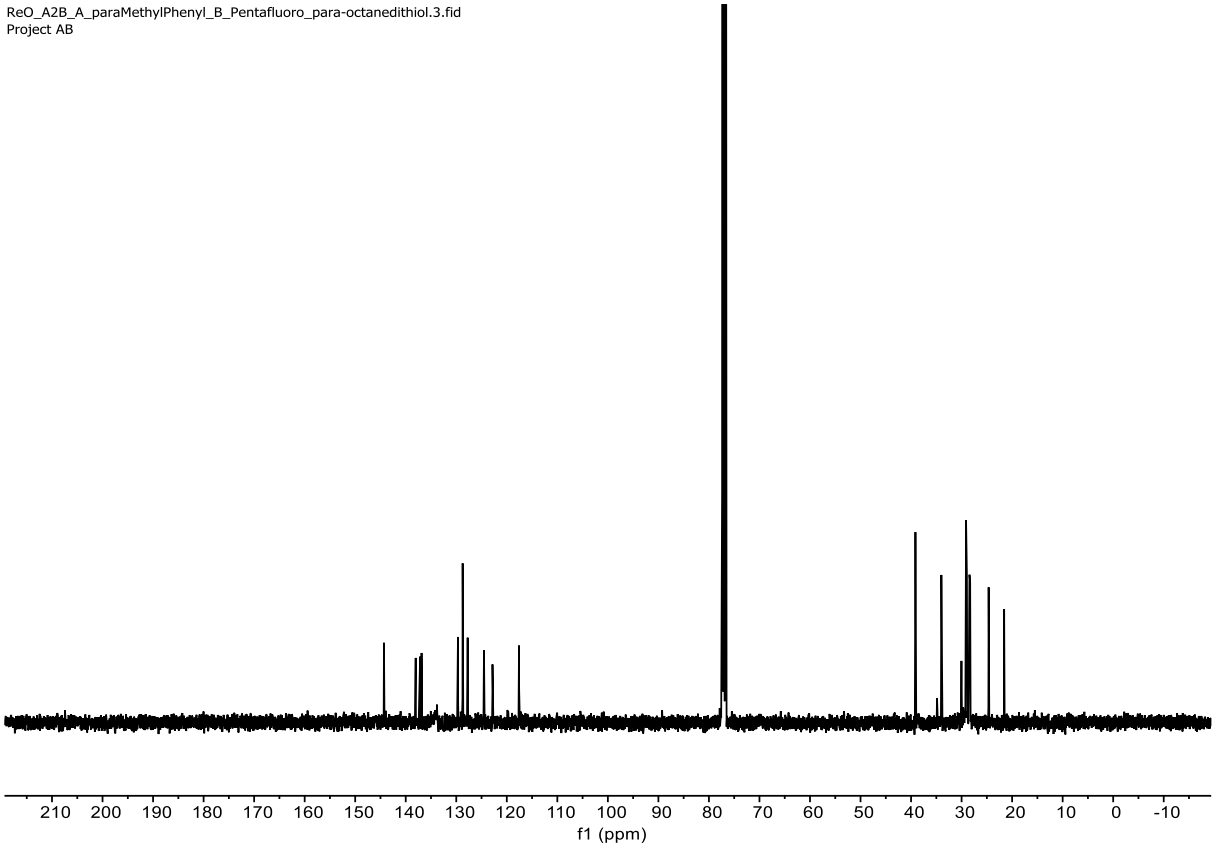
ReO_A2B_A_paraMethylPhenyl_B_Pentafluoro_para-octanedithiol.3.fid
Project AB
210 200 190 180 170 160 150 140 130 120 110 100 90 80 70 60 50 40 30 20 10 0 -10
f1 (ppm)

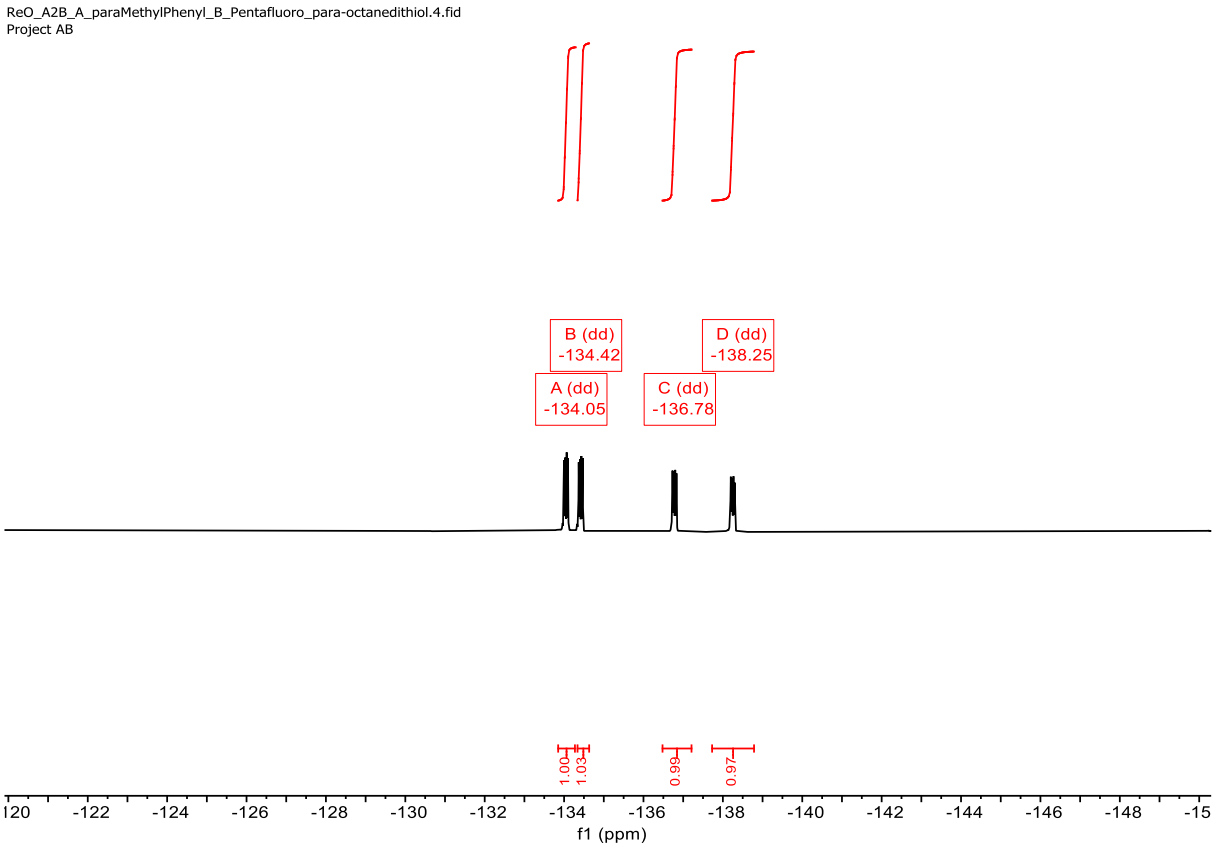
ReO_A2B_A_paraMethylPhenyl_B_Pentafluoro_para-octanedithiol.4.fid
Project AB
B (dd)
-134.42
D (dd)
-138.25
A (dd)
-134.05
C (dd)
-136.78
1.00
1.03
0.99
0.97
120
-122
-124
-126
-128
-130
-132
-134
-136
-138
-140
-142
-144
-146
-148
-15
f1 (ppm)

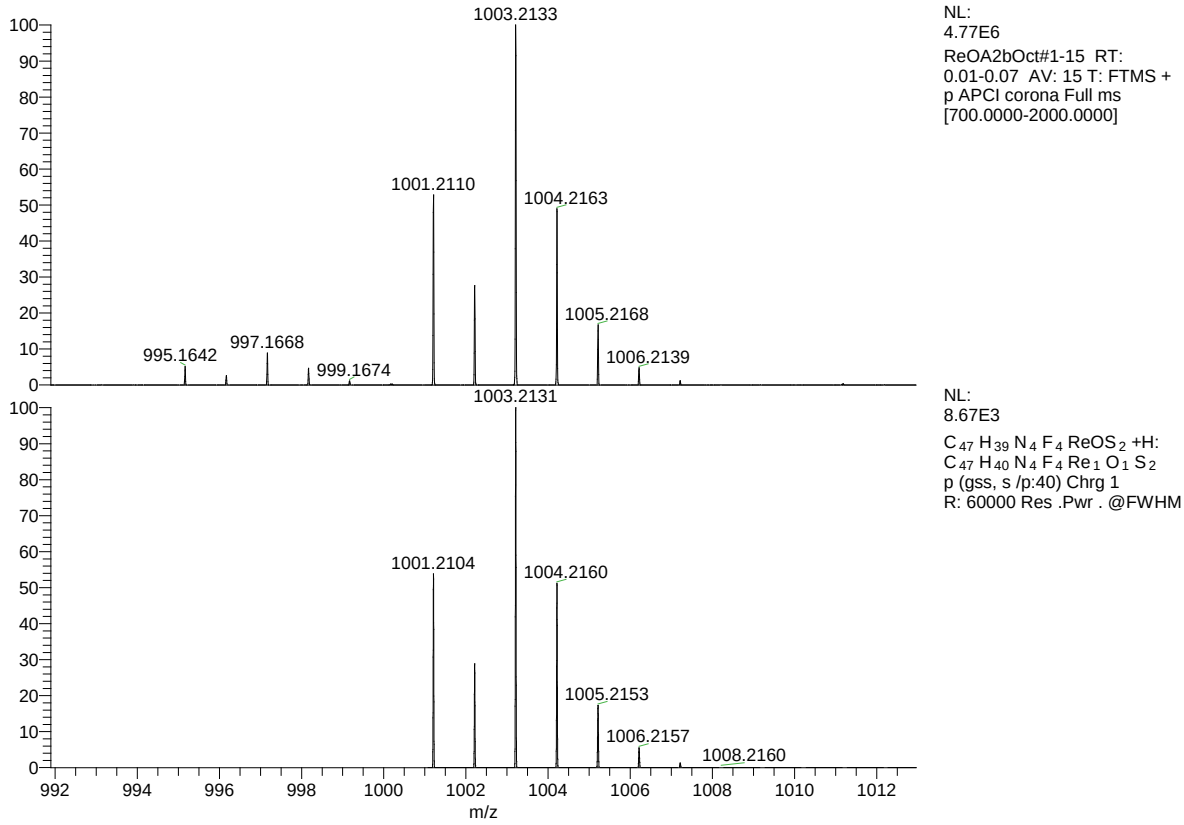
1003.2133
1001.2110
1004.2163
1005.2168
995.1642
997.1668
999.1674
1006.2139
NL:
4.77E6
ReOA2bOct#1-15 RT:
0.01-0.07 AV: 15 T: FTMS +
p APCI corona Full ms
[700.0000-2000.0000]
1003.2131
1001.2104
1004.2160
1005.2153
1006.2157
1008.2160
NL:
8.67E3
C47 H39 N4 F4 ReOS2 +H:
C47 H40 N4 F4 Re1 O1 S2
p (gss, s /p:40) Chrg 1
R: 60000 Res .Pwr . @FWHM
m/z

ReOA2bOct #1-15 RT: 0.01-0.07 AV: 15 NL: 6.74E6
T: FTMS + p APCI corona Full ms [700.0000-2000.0000]

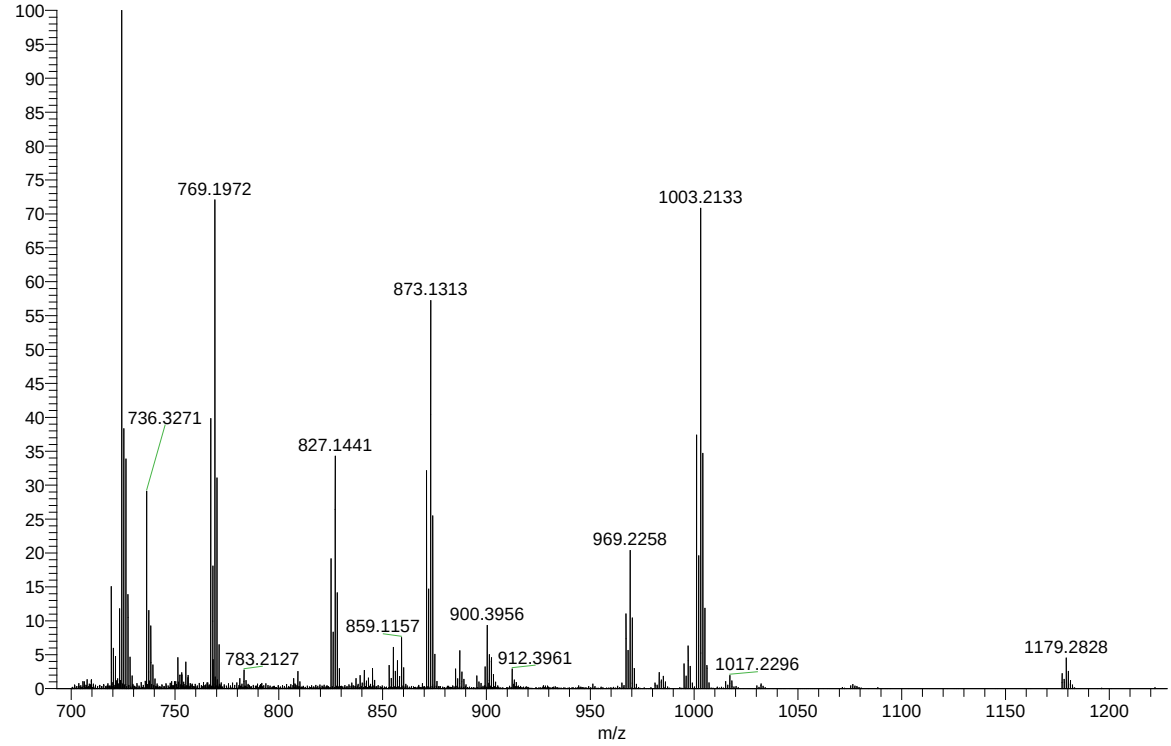

Supporting Information

Influence of Fluorinated Substituents on the Near-Infrared Phosphorescence of 5d Metallocorroles

Krister Engedal Johannesen,[a] Martin Amund Langaas Johansen,[a] Rune F. Einrem,[a] Laura M[c]Cormick M[c]Pherson,[b] Sergey M. Borisov*,[c] and Abhik Ghosh*,[a]

[a]Department of Chemistry, UiT – The Arctic University of Norway, 9037 Tromsø, Norway; [b]EPSRC National Crystallography Service, School of Chemistry, University of Southampton, Highfield, Southampton, SO17 1BJ, UK
[c]Institute of Analytical Chemistry and Food Chemistry, Graz University of Technology, Stremayrgasse 9, 8010 Graz, Austria

Content **Page**

A. ^{1}H and ^{19}F NMR spectra

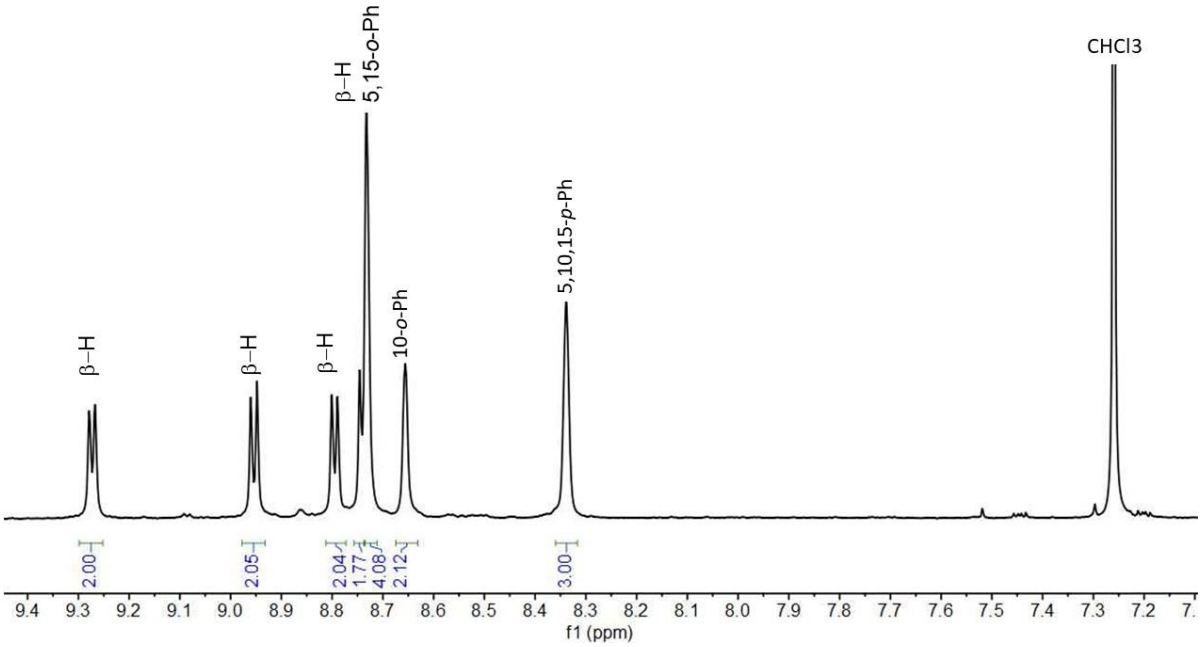

Figure S1. ^{1}H NMR spectrum of Au[T(3,5-CF_3)PC].

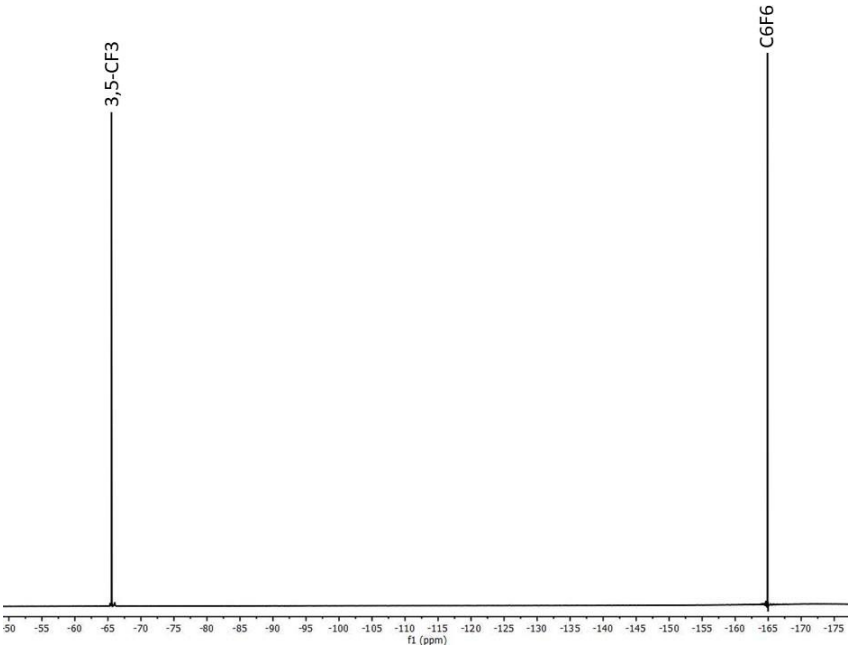

Figure S2. ^{19}F NMR spectrum of Au[T(3,5-CF_3)PC].

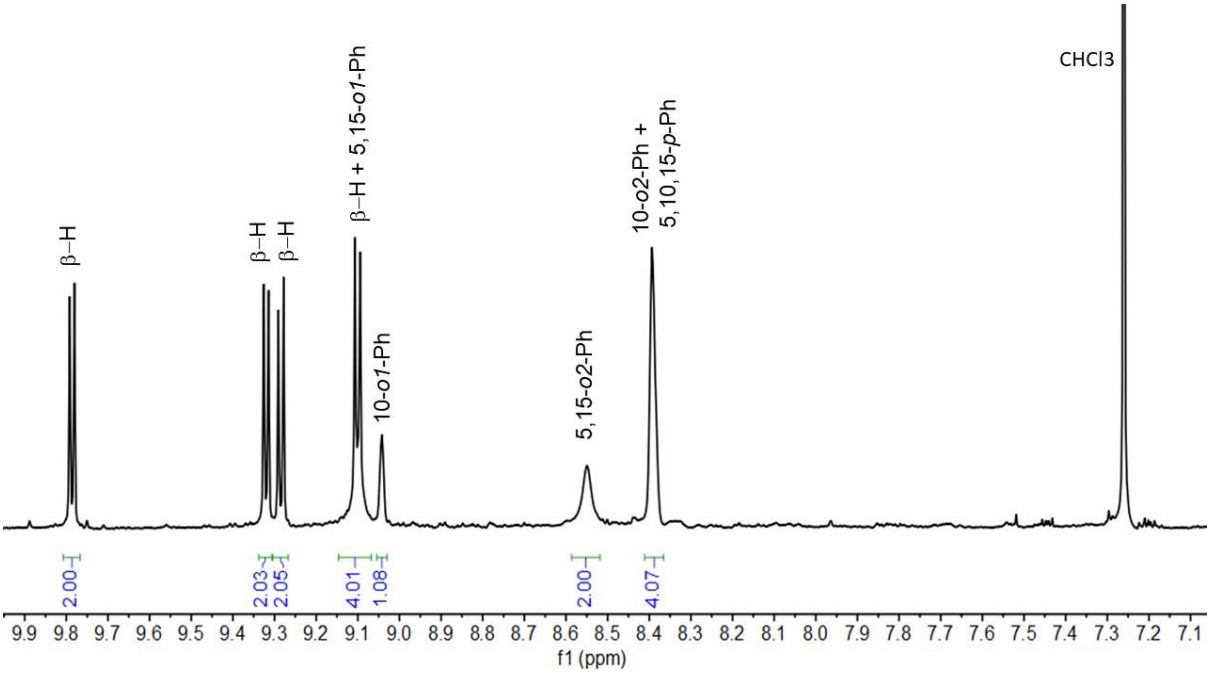

Figure S3. ^{1}H NMR spectrum of Re[T(3,5-CF_3)PC](O).

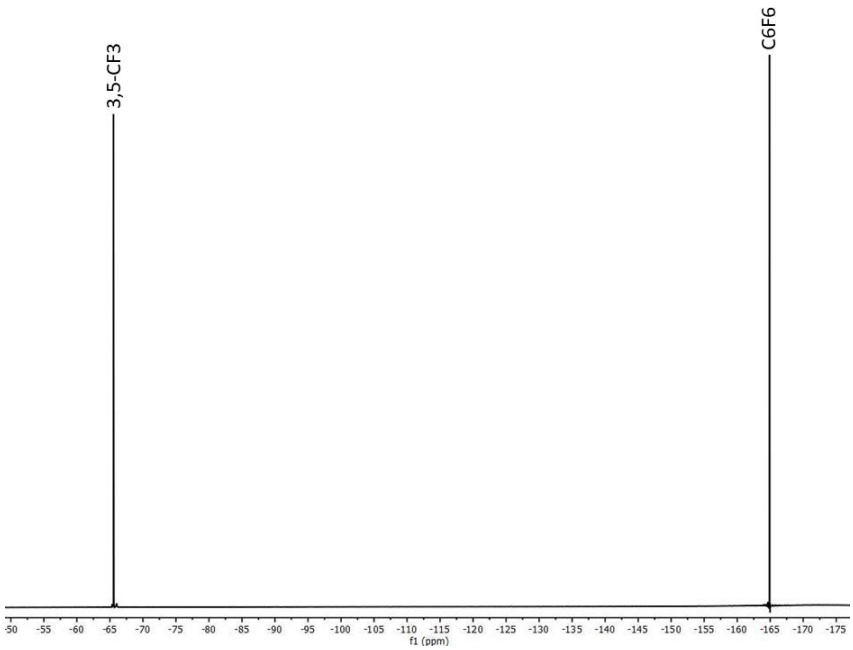

Figure S4. ^{19}F NMR spectrum of Re[T(3,5-CF_3)PC](O).

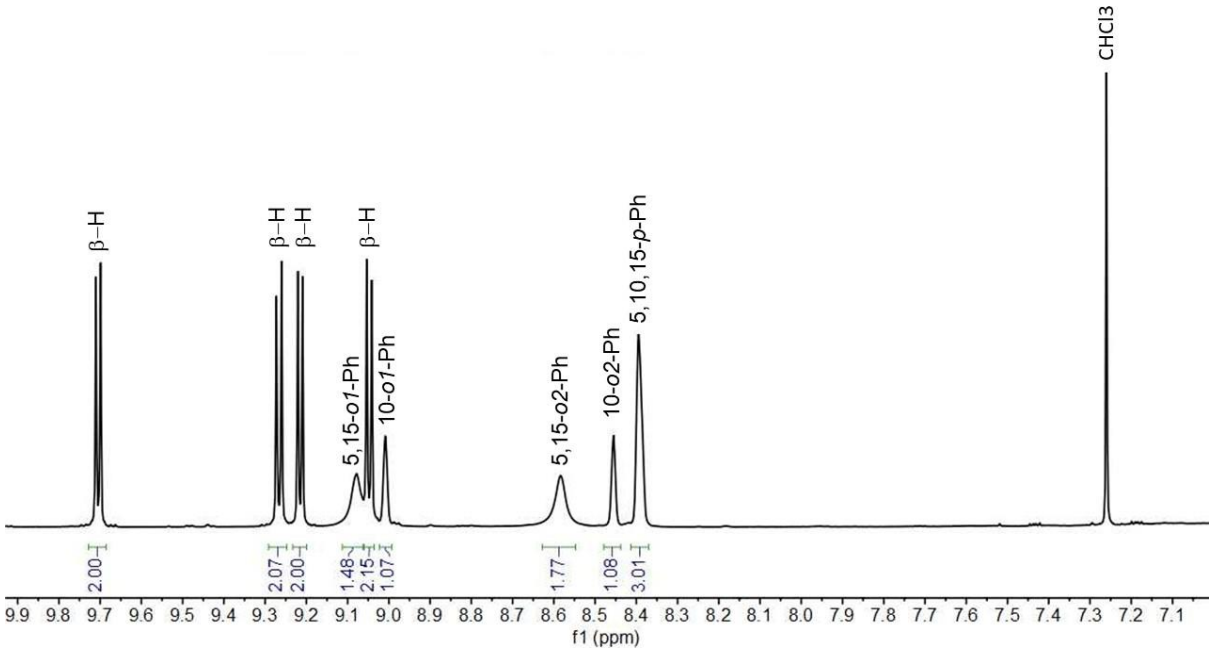

Figure S5. ^{1}H NMR spectrum of Os[T(3,5-CF_3)PC](N).

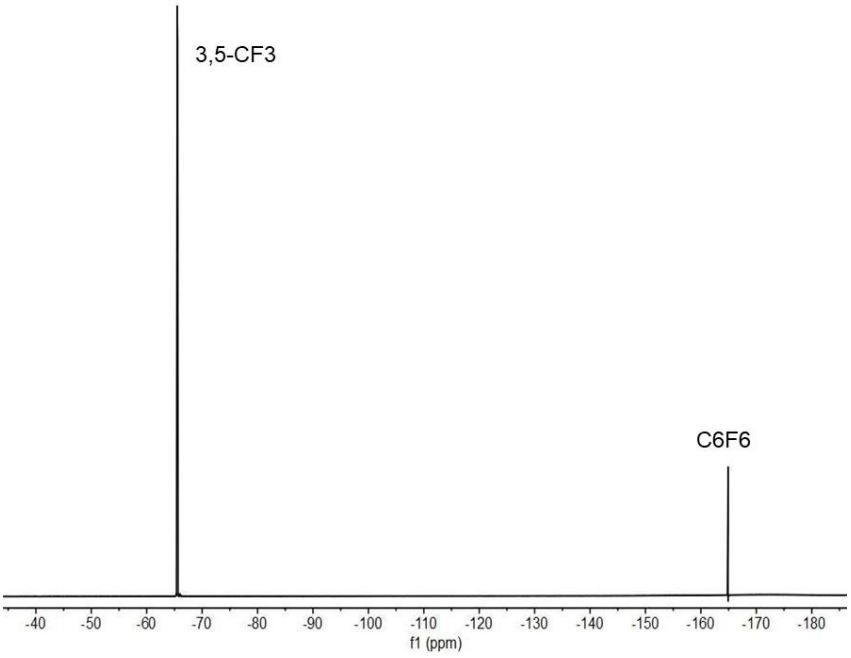

Figure S6. ^{19}F NMR spectrum of Os[T(3,5-CF_3)PC](N).

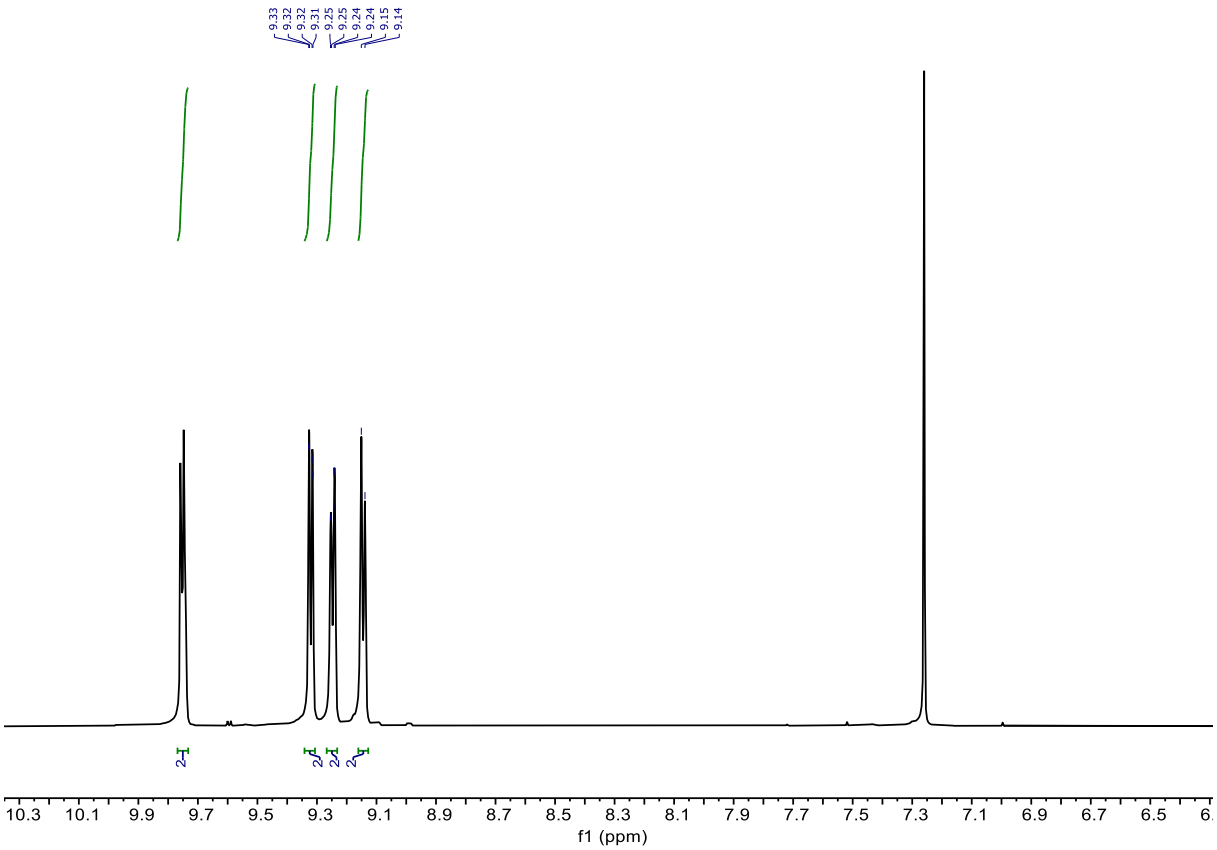

Figure S7. ^{1}H NMR spectrum of Re[TPFPC](O).

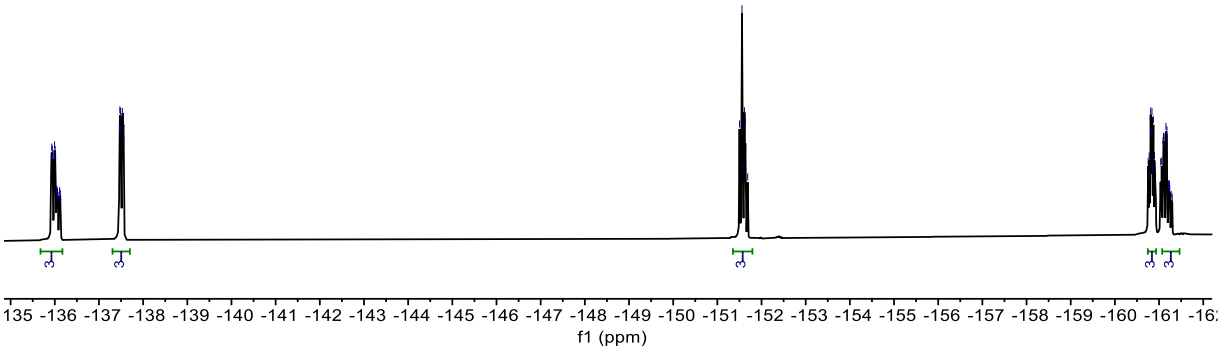

Figure S8. ^{19}F NMR spectrum of Re[TPFPC](O).

B. ESI mass spectra

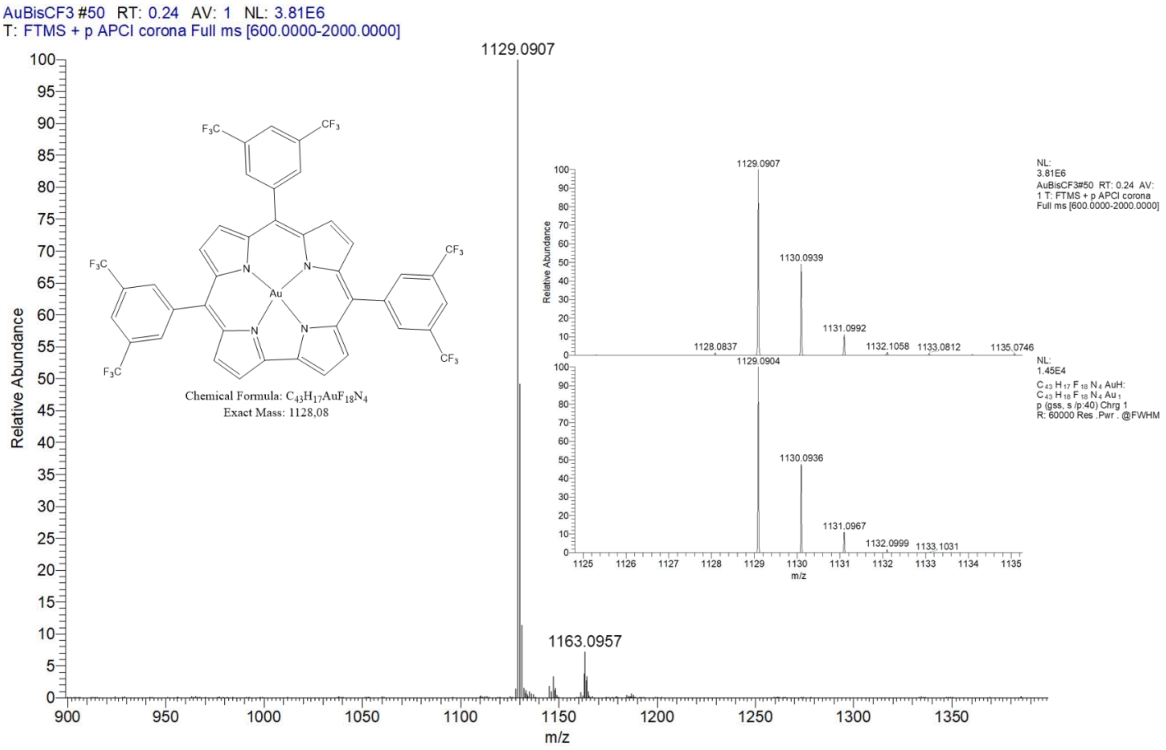

Figure S9. ESI-MS of Au[T3,5-CF_3PC]. Detail of $[M+H]^+$ (above), with simulation (below).

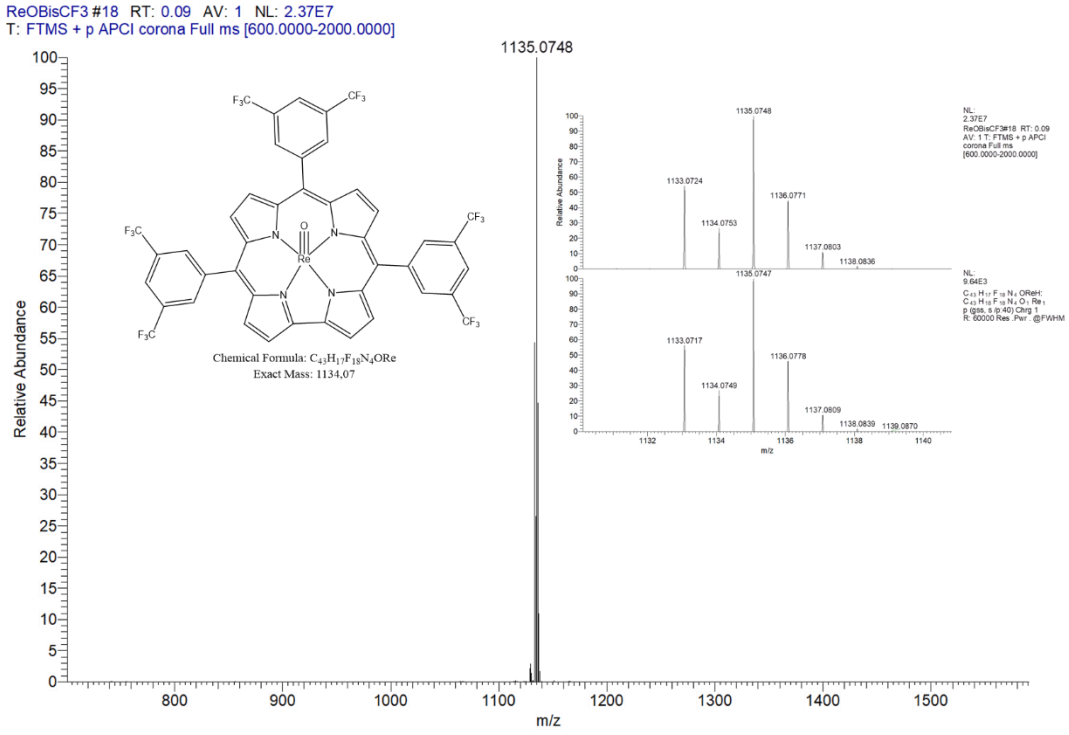

Figure S10. ESI-MS of Re[T(3,5-CF_3P)C](O). Detail of $[M+H]^+$ (above), with simulation (below).

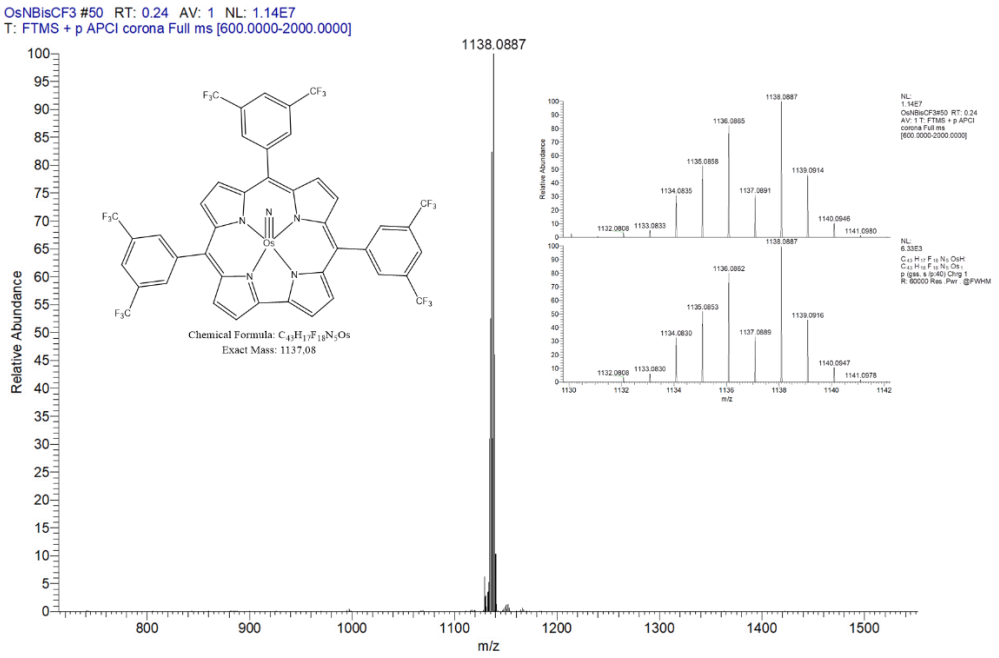

Figure S11. ESI-MS of Os[T(3,5-CF_3P)C](N), $[M+H]^+$.

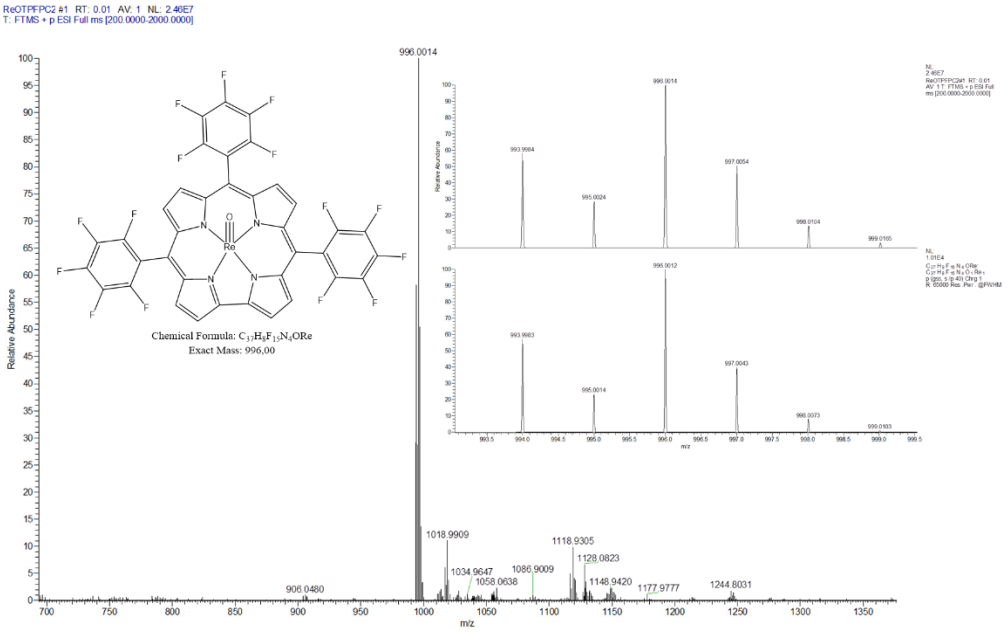

Figure S12. ESI-MS of Re[TPFPC](O).

C. Additional optical and photophysical measurements

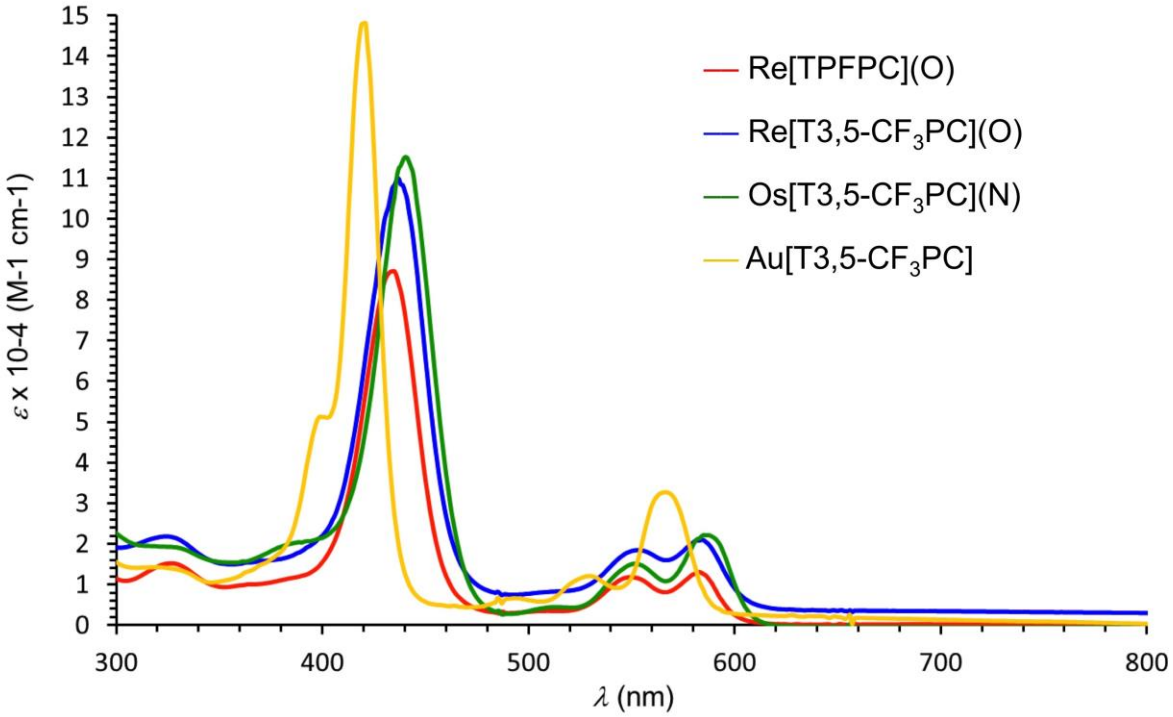

Figure S13. UV-vis spectra of Re[TPFPC](O), Re[T3,5-CF_3PC](O), Os[T3,5-CF_3PC](N) and Au[T3,5-CF_3PC].

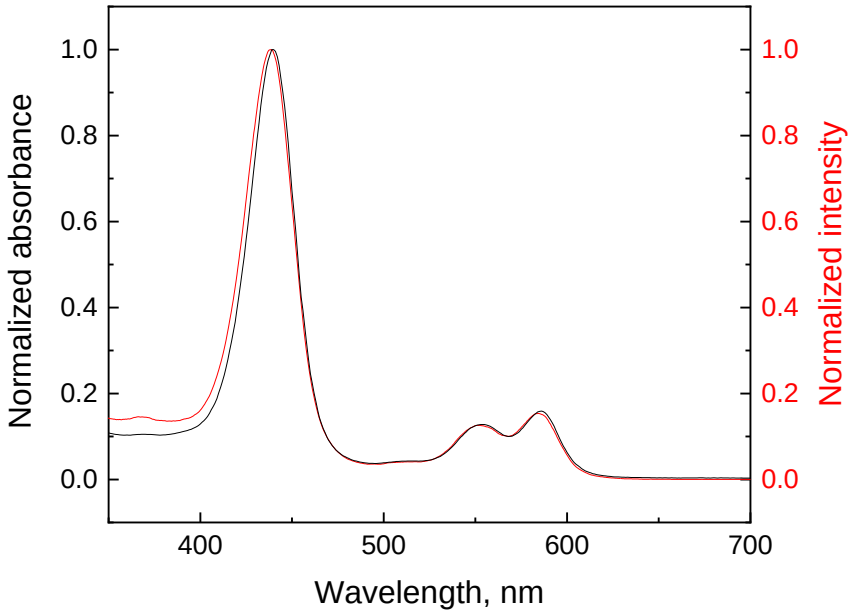

Figure S14. Normalized absorption and excitation spectra (λ_{em} = 760 nm) of Re[T3,5-CF_3PC](O) in toluene. The excitation spectrum was acquired under anoxic conditions.

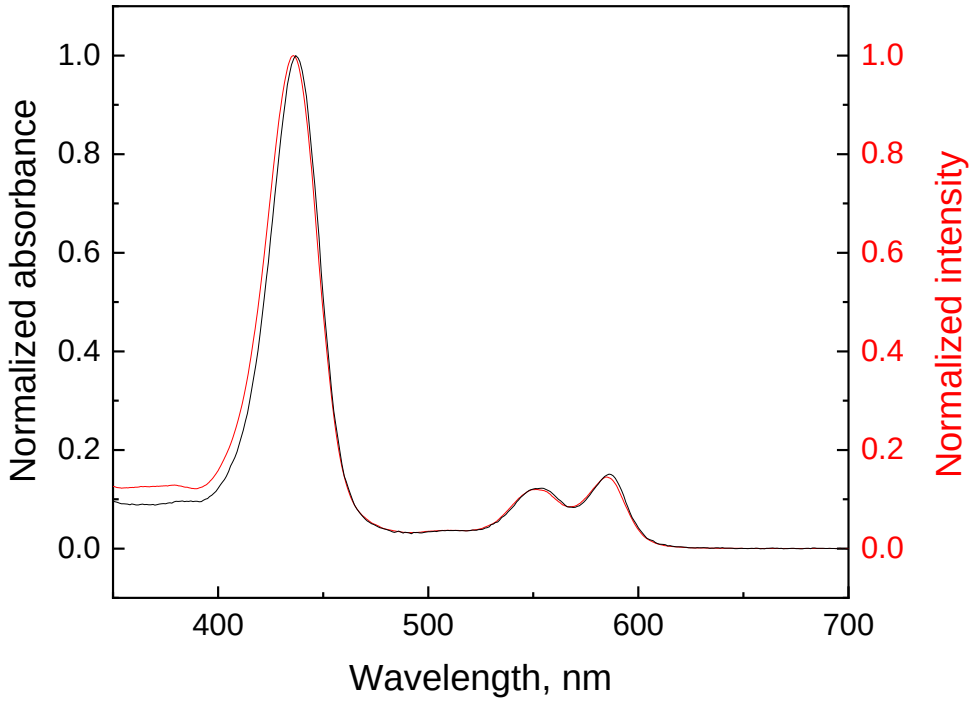

Figure S15. Normalized absorption and excitation spectra (λ_{em} = 753 nm) of Re[TPFPC](O) in toluene. The excitation spectrum was acquired under anoxic conditions.

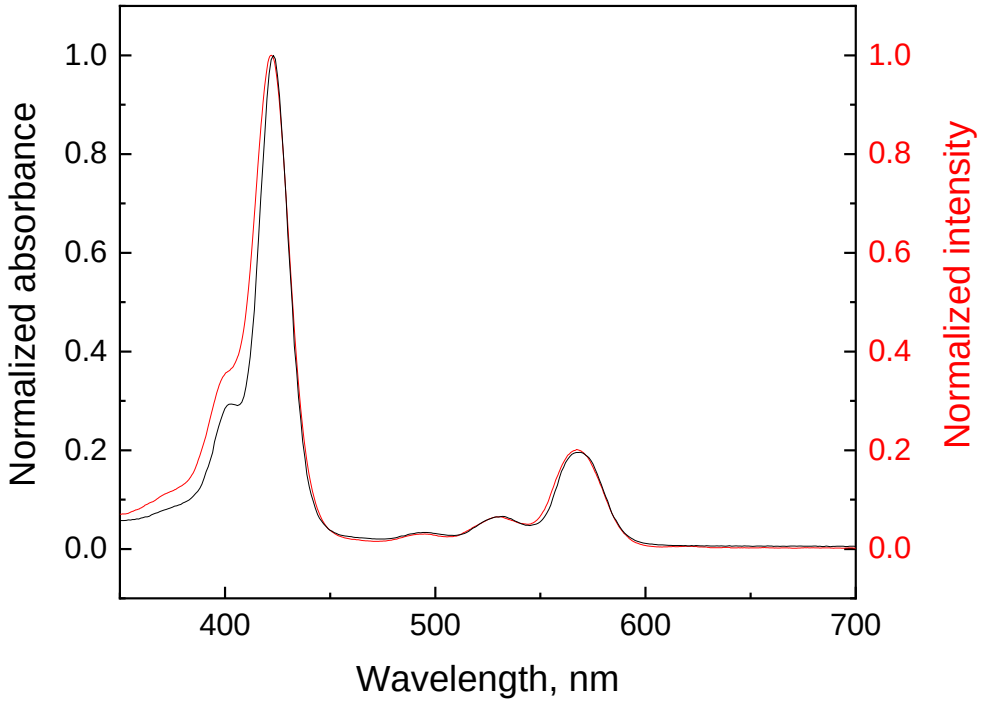

Figure S16. Normalized absorption and excitation spectra (λ_{em} = 777 nm) of Au[T3,5-CF_3PC] in toluene. The excitation spectrum was acquired under anoxic conditions.

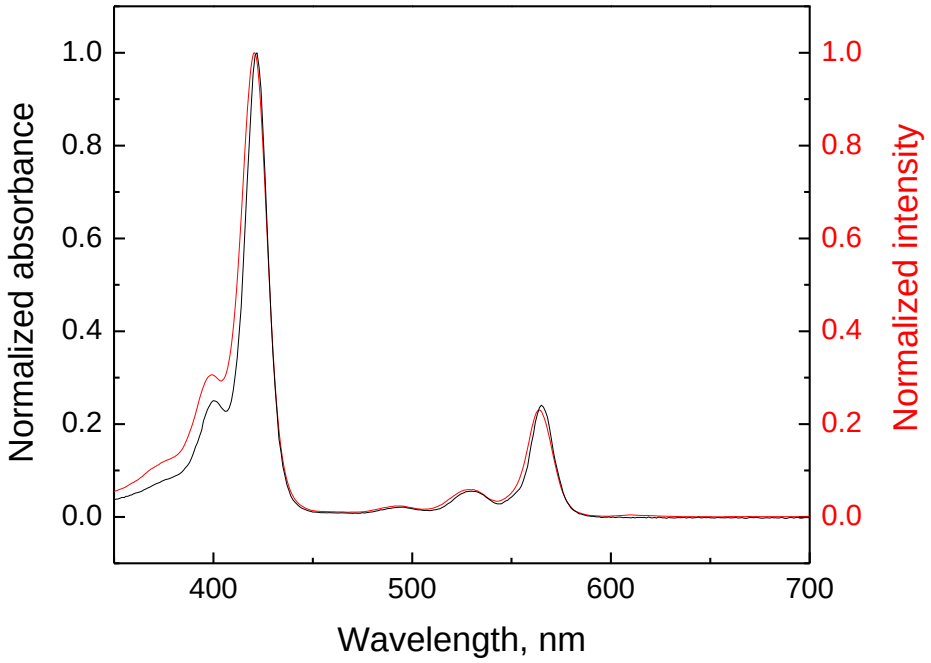

Figure S17. Normalized absorption and excitation spectra (λ_{em} = 751 nm) of Au[TPFPC] in toluene. The excitation spectrum was acquired under anoxic conditions.

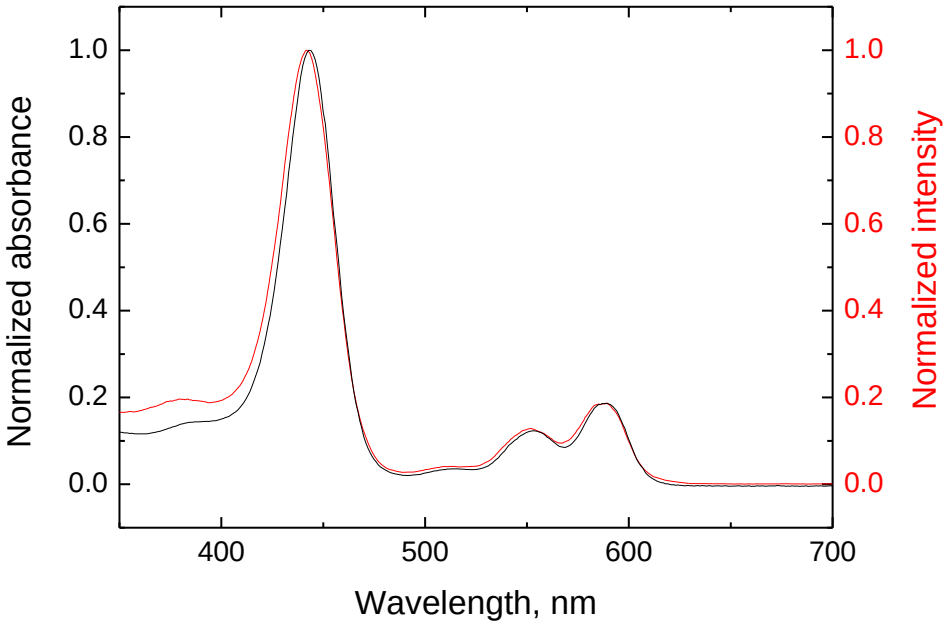

Figure S18. Normalized absorption and excitation spectra (λ_{em} = 751 nm) of Os[T3,5-CF_3PC](N) in toluene. The excitation spectrum was acquired under anoxic conditions.

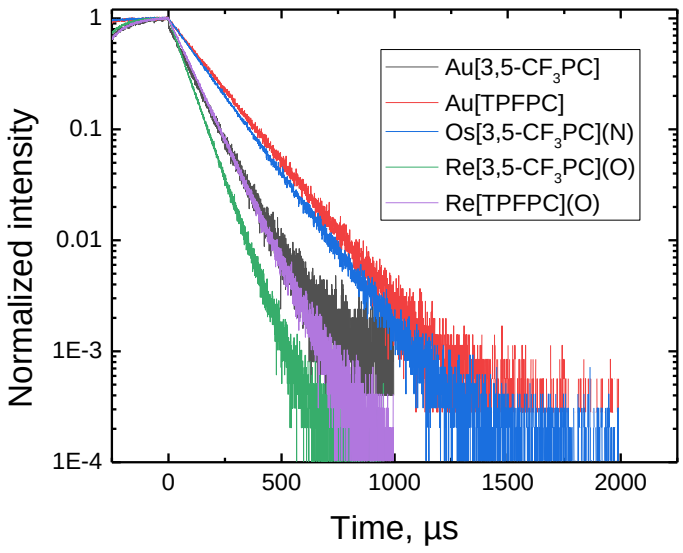

Figure S19. Luminescence decays (anoxic toluene, 23 °C) of new Au, OsN and ReO complexes with fluorinated substituents.

Influence of Fluorinated Substituents on the Near-Infrared Phosphorescence of 5d Metallocorroles

Krister Engedal Johannessen,[a] Martin Amund Langaas Johansen,[a] Rune F. Einrem,[a] Laura M[c]Cormick M[c]Pherson,[b] Abraham B. Alemayehu,*[,a] Sergey M. Borisov*[,c] and Abhik Ghosh*[,a]

[a]Department of Chemistry, UiT – The Arctic University of Norway, 9037 Tromsø, Norway;
[b]EPSRC National Crystallography Service, School of Chemistry, University of Southampton, Highfield, Southampton, SO17 1BJ, UK
[c]Institute of Analytical Chemistry and Food Chemistry, Graz University of Technology, Stremayrgasse 9, 8010 Graz, Austria

Abstract. The influence of fluorinated substituents on the luminescent properties of rhenium-oxo, osmium-nitrido and gold triarylcorroles was studied via a comparison of four ligands: triphenylcorrole (TPC), tris(*p*-trifluoromethylphenyl)corrole (T*p*CF_3PC), tris{3,5-bis(trifluoromethyl)}corrole (T3,5-CF_3PC), and tris(pentafluorophenyl)corrole (TPFPC). For each metal series examined, fluorinated substituents were found to enhance the luminescent properties, with the phosphorescence quantum yields and triplet decay times increasing in the order TPC < T*p*CF_3PC < T3,5-CF_3PC < TPFPC. Among the 11 complexes examined, the highest phosphorescence quantum yield, 2.2%, was recorded for Re[TPFPC](O).

INTRODUCTION

The last decade has witnessed the emergence of a unique class of transition metal complexes – the 5d metallocorroles.[1] Their uniqueness derives from their size-mismatched nature, which involves a large 5d ion encapsulated by a sterically constrained, macrocyclic corrole ligand.[2,3,4] In spite of the steric strain inherent in their structures, the middle and late 5d transition metal (Re,[5,6,7,8,9] Os,[10,11,12] Ir,[13] Pt,[14,15] and Au[16,17,1819,20,21,22,23]) corroles have proved thermally and photochemically rugged. Furthermore, their photophysical properties are conducive to applications as photosensitizers, most notably in photodynamic therapy and oxygen sensing.[24,25,26,27,28,29,30,31,32,33,34,35,36] Interestingly, in the course of our photophysical studies on 5d metallotriarylcorroles, we repeatedly observed somewhat higher phosphorescence quantum yields for tris{(*p*-trifluoromethyl)phenyl}corrole complexes than for their more electron-rich counterparts.[27,31-33] The observation made us wonder whether fluorinated substituents might have a beneficial effect on the luminescence properties of 5d metallocorroles. A photophysical study was accordingly carried out on the complexes depicted in **Chart 1**, except for the M = OsN, Ar = C_6F_5 case, which was not studied because of synthetic difficulties. We found that fluorinated substituents indeed appear to have a beneficial effect on the luminescence properties of the complexes, significantly increasing both the phosphorescence quantum yields and triplet decay times.

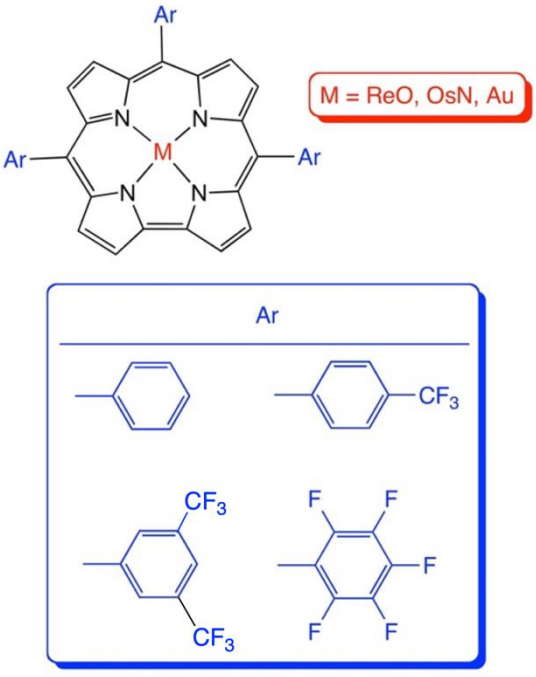

Chart 1. Molecules studied in this work.

Results and discussion

The influence of fluorinated substituents on the luminescent properties of rhenium-oxo, osmium-nitrido and gold triarylcorroles was studied via a comparison of four ligands: triphenylcorrole (TPC), tris(*p*-trifluoromethylphenyl)corrole (T*p*CF_3PC), tris{3,5-bis(trifluoromethyl)}corrole (T3,5-CF_3PC), and tris(pentafluorophenyl)corrole (TPFPC). The majority of the compounds have been previously synthesized;[5,10,18] four new compounds were synthesized specifically for this study, namely Re[T3,5-CF_3PC](O), Os[T3,5-CF_3PC](N), Au[T3,5-CF_3PC], and Re[TPFPC](O). Unfortunately, Os[TPFPC](N) could not be synthesized because the azide used as part of the synthetic protocol[10] resulted in nucleophilic displacement of the *para*-fluorines in the TPFPC ligand. Aside from that, the syntheses of the new compounds proved uneventful and one, Re[T3,5-CF_3PC](O), yielded a single-crystal X-ray structure (Figure 1 and Table 1). Key photophysical and electrochemical properties of the compounds are listed in Table 2.

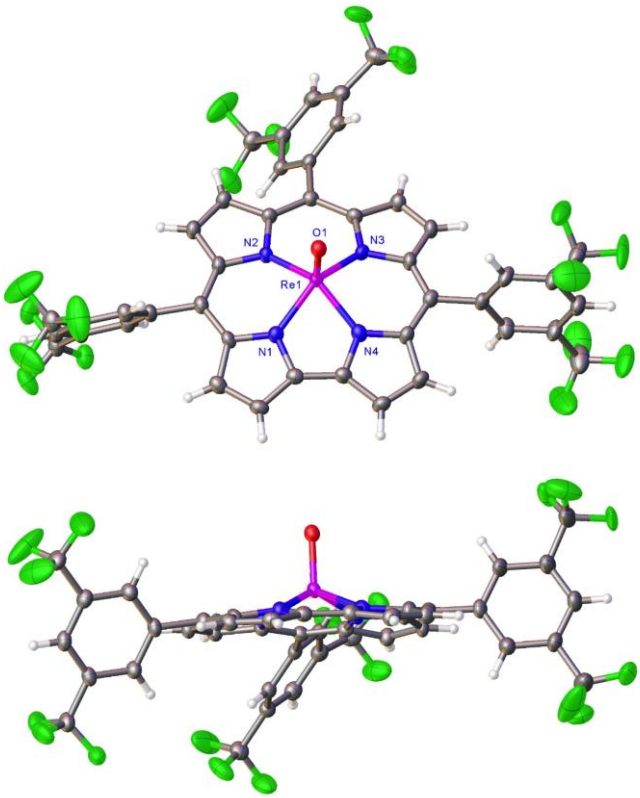

Figure 1. Two views of the thermal ellipsoid plot for Re[T3,5-CF_3PC](O) at 50% probability. Selected distances (Å): Re1-N1 1.992(3), Re1-N2 2.006(3), Re1-N3 2.015(3), Re1-N4 1.996(3), and Re1-O1 1.574(3) Å.

Table 1. Crystal and refinement data for Re[T3,5-CF_3PC](O).

Empirical formula	$C_{43}H_{17}F_{18}N_4ORe$
Formula weight	1133.80
Temperature	100(2) K
Wavelength	1.54184 Å
Crystal system	Triclinic
Space group	P□
Unit cell dimensions	a = 8.2583(2) Å ⟨= 73.4740(10)° b = 14.6249(3) Å ®= 89.726(2)° c = 17.9347(2) Å © = 85.316(2)°.
Volume	2069.30(7) $Å^3$
Z	2
Density (calculated)	1.820 Mg/m^3
Absorption coefficient	6.866 mm^{-1}
F(000)	1096
Crystal size	0.110 x 0.040 x 0.020 mm^3
Theta range for data collection	2.570 to 70.662°
Index ranges	$-10 \leq h \leq 10, -17 \leq k \leq 17, -21 \leq l \leq 20$
Reflections collected	88606
Independent reflections	7781 [R(int) = 0.0575]
Completeness to theta = 67.684°	99.5 %
Absorption correction	Analytical
Max. and min. transmission	0.875 and 0.661
Refinement method	Full-matrix least-squares on F^2
Data / restraints / parameters	7781 / 7 / 617
Goodness-of-fit on F^2	1.054
Final R indices [I > 2sigma(I)]	R1 = 0.0354, wR2 = 0.0943
R indices (all data)	R1 = 0.0378, wR2 = 0.0957
Extinction coefficient	n/a
Largest diff. peak and hole	1.157 and -1.549 $e.Å^{-3}$

All the complexes proved emissive in deoxygenated toluene at room temperature (Figure 1). The emission was efficiently quenched by molecular oxygen and is thus ascribed to phosphorescence. The absorption and excitation spectra (Figures S14-S19) proved virtually identical, indicating that the emission originates solely from the metal complexes, while also confirming the purity of the compounds. Although the emission spectra of the T3,5-CF_3PC and TPFPC complexes are generally similar to those of the previously studied TPC and T*p*CF_3PC complexes (Figure 2 and Table 2), the emission maxima were found to shift hypsochromically with increasing electron-withdrawing character of the *meso*-aryl substituents; this effect is observed for all three metal series examined.

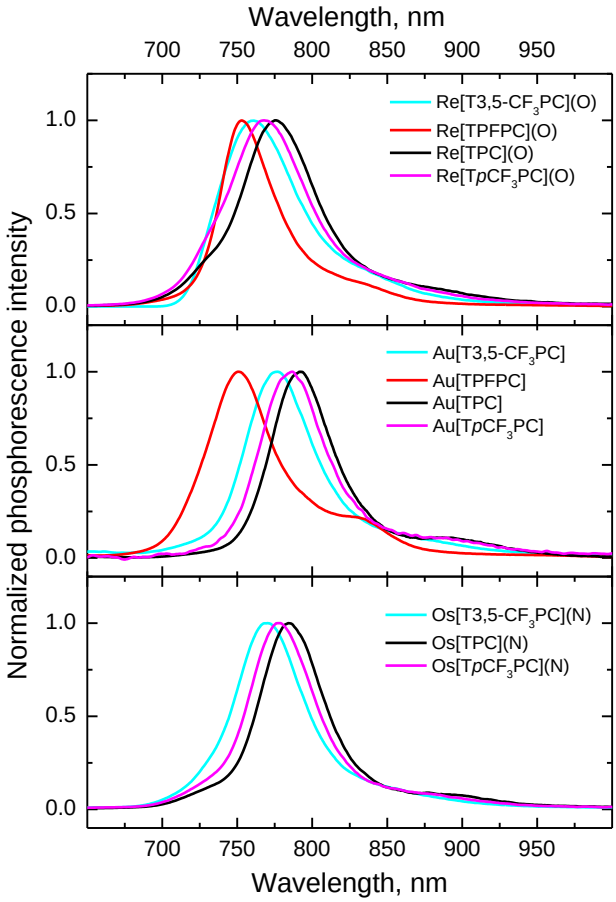

Figure 2. Emission spectra of the complexes in anoxic toluene at 23 °C. Excitation was performed into the maximum of the Soret band of the complexes.

Table 2. Photophysical and electrochemical properties of ReO, OsN and Au triarylcorroles in anoxic toluene (23 °C).

Complex	**λ_{max} abs, nm**	**$\lambda_{max\text{-}phos}$ (nm)**	**Φ_{phos} (%)**	**τ_{phos} (µs)**	**$E_{1/2ox1}$ (V)**	**$E_{1/2red1}$ (V)**	**$E_{1/2red2}$ (V)**
Re[TPC](O)	440, 554, 586	776 (770)[a]	1.2	60	0.98	-1.26	-
Re[T*p*CF_3PC](O)	440, 553, 586	768 (777)[a]	1.4 (1.5)[a]	74	1.10	-1.16	-
Re[T3,5-CF_3PC](O)	440, 553, 586	760	1.6	75	1.21	-1.11	-1.64
Re[TPFPC](O)	437, 552, 586	753	2.2	99	1.31	-1.04	-1.68
Os[TPC](N)	444, 554, 595	784	0.64 (0.54)[b]	125 (128)[c]	0.91	-1.28	-
Os[T*p*CF_3PC](N)	444, 554, 593	778	0.7 (0.54)[b]	139 (150)[c]	1.02	-1.19	-
Os[T3,5-CF_3PC](N)	443, 553, 588	770	0.81	155	1.12	-1.10	-1.62
Au[TPC]	421, 494, 532, 561, 575	792	0.23 (0.18)[d]	94 (86)[d]	0.80	-1.38	-
Au[T*p*CF_3PC]	423, 494, 532, 562 (sh), 575	786	0.26 (0.19)[d]	97 (98)[d]	0.94	-1.29	-
Au[T3,5-CF_3PC]	423, 495, 531, 567	777	0.33	99	1.07	-1.24	-1.68
Au[TPFPC]	422, 494, 530, 565	751	0.68	170			

[a] Ref 32; excitation in the Q-band.

[b] Ref 27; the Φ_{phos} values have been recalculated based on the corrected value (21%) for the standard (Pt[TPTBP]).[37]

[c] Ref 27; Frequency domain measurement.

[d] Ref 26.

As shown in Table 2, fluorination results in an increase in both luminescence quantum yields and decay times in the order TPC < T*p*CF_3PC < T3,5-CF_3PC < TPFPC, which is also the order of the redox potentials. Figure 3 presents a graphical representation of the quantum yields for the different complexes. The ReO complexes are by far the strongest emitters, followed by the OsN, and last by the Au (Figure 3, upper panel). Notably, compared with their TPC analogues, the luminescence of Au[TPFPC] is enhanced much more strongly that that of Re[TPFPC](O) (Figure 3, lower panel). Thus, whereas the phosphorescence quantum yield triples on going from Au[TPC] to Au[TPFPC], the enhancement is less than double for their ReO counterparts. As a result of the fluorination-mediated enhancement, Au[TPFPC] emits as efficiently as Os[TPC](N). The trend in the luminescence decay times parallels that observed for the luminescence quantum yields (Table 2). The decay time of Au[TPFPC] is thus much longer (170 μs) than that for the other Au triarylcorroles (94-99 μs).

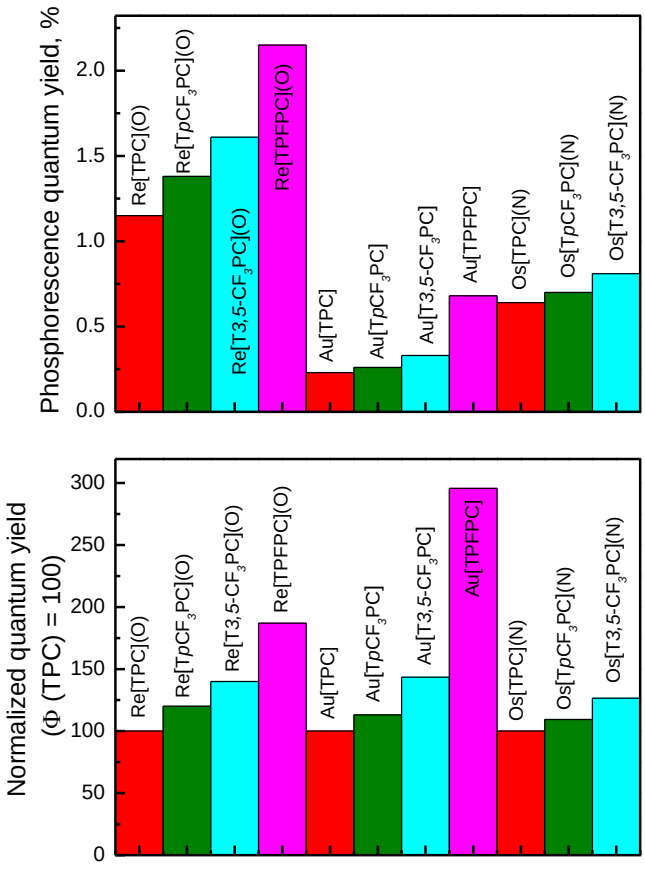

Figure 3. Phosphorescence quantum yields of the ReO, OsN, and Au corroles. The lower plot depicts the enhancement of the quantum yield upon fluorination: the values are normalized for the quantum yields of TPC complex of each metal, i.e., the Φ_{phos} of Re[TPC](O), Os[TPC](N), and Au[TPC] are each set as 100%.

The fact that the order of phosphorescence quantum yields parallels the order of redox potentials for each of three series of 5d metallocorroles (Table 2) suggests that the mechanism of enhanced luminescence is largely electronic in origin. However, the *ortho* fluorines in the TPFPC complexes may confer some degree of conformational rigidity, leading to increased triplet lifetimes. Fluorination also has a major impact on solute-solvent interactions, which in turn may also affect the luminescence properties. At this point, these potential influences remain to be disentangled and the striking impact of fluorination has been presented only as an empirical observation.

CONCLUSION

Introduction of fluorinated substituents onto the *meso*-phenyl groups results in enhancement of the luminescence properties of all three series of 5d metallocorroles: ReO, OsN, and Au. Substitution of phenyl groups by pentafluorophenyl groups leads to the highest increase in the luminescence quantum yields and decay times. This enhancement is particularly strong in case of the Au corroles, where the phosphorescence quantum yield triples on going from Au[TPC] to Au[TPFPC]. An intriguing question concerns whether peripheral fluorination might have a similar positive effect on the luminescence properties of other porphyrin-type complexes, such as true porphyrins, carbaporphyrins, hydroporphyrins, and dipyrrin derivatives. Time will tell.

EXPERIMENTAL SECTION

(a) Materials. Materials. Unless otherwise mentioned, all chemicals were obtained from Merck. Silica gel 60 (0.04-0.063 mm particle size, 230-400 mesh) was employed for flash chromatography. Silica gel 60 preparative thin-layer chromatographic plates (20 cm x 20 cm, 0.5 mm thick, Merck) were used for final purification of all complexes. Free-base corroles were synthesized according to previously reported procedures.[38,39]

(b) Instrumental methods. UV−visible spectra were recorded on an HP 8453 spectrophotometer. ^{1}H NMR spectra were recorded on a 400 MHz Bruker Avance III HD spectrometer equipped with a 5 mm BB/1H SmartProbe in $CDCl_3$ and referenced to residual $CHCl_3$ at 7.26 ppm. ^{19}F NMR spectra were acquired on the same spectrometer and referenced to hexafluorobenzene (C_6F_6, -164.9 ppm). High-resolution electrospray-ionization (HR-ESI) mass spectra were recorded from methanolic solution on an LTQ Orbitrap XL spectrometer**.**

Cyclic voltammetry was performed at 298 K using Gamry potentiostat with a three-electrode system, comprising a glassy carbon working electrode, a platinum wire counterelectrode, and a saturated calomel reference electrode (SCE), in CH_2Cl_2 (anhydrous) containing 0.1 M TBAP as supporting electrolyte. The electrolyte solution was purged with argon for several minutes, and electrochemical measurements were conducted under an argon blanket. All potentials are referenced to the SCE.

The luminescence of the compounds was studied on a Fluorolog 3 fluorescence spectrometer from Horiba (Japan) equipped with a NIR-sensitive photomultiplier R2658 from Hamamatsu (Japan). Prior to measurements, toluene solutions of the complexes in sealable quartz cells (StarnaGmbH, Pfungstadt, Germany) were deoxygenated by bubbling high-purity nitrogen (99.99999%, Linde gas, Austria) for at least 15 min. Emission spectra were acquired upon excitation at the maximum of the Soret band. An OG 590 filter (Schott) was positioned in front of the emission channel to eliminate second-order grating artefacts. Excitation spectra were recorded on more diluted solutions (Soret absorbance ≤ 0.1) by monitoring in the maximum of the emission band. The luminescence quantum yields were determined relative to platinum(II) tetraphenyltetrabenzoporphyrin (Pt[TPTBP], Φ = 21%). The ReO corroles were excited at 440 nm, whereas an excitation wavelength of 422 nm was used for OsN and Au corroles.

Luminescence decay times in solution were determined on the same spectrometer with the DeltaHub module (Horiba Scientific) controlling a SpectraLED-456 lamp (λ = 456 nm) and using DAS-6 analysis software for data analysis.

(c) Synthetic methods. All metalation procedures were adopted from our earlier work without modification.[5,10,18] Analytical details for new compounds are as follows.

Au[T3,5-CF$_3$PC]. Yield 24.1 mg (28.0%). UV-vis (CH_2Cl_2) λ_{max} [nm, ε x 10^{-4} ($M^{-1}cm^{-1}$)]: 421 (14.81)), 496 (0.060), 529 (1.20), 567 (3.26).^{1}H NMR (400 MHz, $CDCl_3$, 25 °C): (400 MHz, $CDCl_3$) δ 9.27 (d, 2H, *J* = 4.5 Hz, *β*-H), 8.95 (d, 2H, *J* = 4.9 Hz, *β*-H), 8.80 (d, 2H, *J* = 4.5 Hz, *β*-H), 8.74 (d, 6H, *J* = 5.7 Hz, *β*-H overlapping with 5,15-*o*-Ph), 8.66 (s, 2H, 10-*o*-Ph), 8.34 (s, 3H, 5,10,15-*p*-Ph); ^{19}F NMR -65 (s, 18F, 5,10,15(3,5-CF3). MS (ESI): [M + H]$^+$ = 1129.0907 (expt), 1129.0904 (calcd for $C_{43}H_{17}F_{18}N_4Au$).

Re[T3,5-CF$_3$PC](O). Yield 26.8 mg (22.4%). UV-vis (CH_2Cl_2) λ_{max} [nm, ε x 10^{-4} ($M^{-1}cm^{-1}$)]: 437 (10.99), 553 (1.85), 584 (2.10). ^{1}H NMR (400 MHz, $CDCl_3$, 25 °C) δ 9.79 (d, 2H, J = 4.5 Hz, *β*-H), 9.32 (d, 2H, J = 4.5 Hz, *β*-H), 9.28 (d, 2H, J = 4.9 Hz, *β*-H), 9.10 (d, 4H, J = 4.9 Hz, *β*-H overlapping with 5,15-*o*1-Ph), 9.04 (s, 1H, 10-*o*1-Ph), 8.55 (s, 2H, 5,15-*o*2-

Ph), 8.39 (s, 4H, 10-*o*2-Ph overlapping with 5,10,15-*p*-Ph). MS (ESI): $[M + H]^+$ = 1135.0748 (expt), 1135.0747 (calcd for $C_{43}H_{17}F_{18}N_4ORe$).

Re[TPFPC](O). Yield 34 mg (50.89%). UV-vis (CH_2Cl_2) λ_{max} [nm, ε x 10^{-4} ($M^{-1}cm^{-1}$)]: 326 (1.52), 434 (8.71), 550 (1.18), 583 (1.31). ^{1}H NMR (400 MHz, $CDCl_3$, 25 °C) δ 9.75 (d, J = 4.5 Hz, 2H, β-H), 9.32 (d, J = 4.6 Hz, 2H, β-H), 9.25 (d, J = 5.0 Hz, 2H, β-H), 9.14 (d, J = 4.9 Hz, 2H, β-H); ^{19}F NMR -136.03 (dddd, J = 43.4, 23.8, 8.9., 3.7 Hz, 3F, 5,10,15-*o*1-PF), -137.29-137.93 (m, 3F, 5,10,15-*o*2-PF), -151.99 (dt, J = 27.7, 21.1 Hz, 3F, 5,10,15-*p*-PF), -160.89 (tdd, J = 21.5, 12.5, 8.5 Hz, 3F, 5,10,15-*m*1-PF), -161.17 (dddd, J = 44.9, 23.7, 20.9, 8.6Hz, 3F, 5,10,15-*m*2-PF. MS (ESI): M^+ = 996.0014 (expt), 996.0012 (calcd for $C_{37}H_8F_{15}N_4ORe$).

Os[T3,5-CF$_3$PC](N). Yield 36.9 mg (35.1%). UV-vis (CH_2Cl_2) λ_{max} [nm, ε x 10^{-4} ($M^{-1}cm^{-1}$)]: 440 (11.52), 553 (1.51), 585 (2.22). ^{1}H NMR (400 MHz, $CDCl_3$) δ 9.70 (d, 2H, J = 4.5 Hz, β-H), 9.27 (d, 2H, J = 5.0 Hz, β-H), 9.21 (d, 2H, J = 4.5 Hz, β-H), 9.08 (s, 2H, 5,15-*o*1-Ph), 9.05 (d, 2H, J = 5.0 Hz β-H), 9.01 (s, 1H, 10-*o*1-Ph), 8.58 (s, 2H, 5,15-*o*2-Ph), 8.46 (s, 1H, 10-*o*2-Ph), 8.39 (s, 3H, 5,10,15-*p*-Ph). MS (ESI): $[M + H]^+$ = 1138.0887 (expt), 1138.0887 (calcd for $C_{43}H_{17}F_{18}N_5Os$).

X-ray structure determinations. X-ray data for Re[T3,5-CF$_3$PC](O) were collected at the National Crystallography Service at the University of Southampton. The crystal was coated in protective perfluoroether oil before being mounted on a MiTeGen loop and transferred to the goniometer head of a Rigaku 007HF diffractometer equipped with Varimax confocal mirrors, an AFC11 goniometer, and a HyPix 6000 detector. The sample was held at a temperature of 100(2) K with an Oxford Cryosystems CryostreamPlus device. Crystallographic data were measured using profile data from ω scans using Cu Kα radiation. The total number of runs and images was based on strategy calculation from the Rigaku's CrysAlisPro program. The structure was solved with intrinsic phasing methods (SHELXT[40]) and refined by full matrix least squares on F^2 (SHELXL-2018[41]) using the ShelXle GUI. Hydrogen atoms were included at their geometrically estimated positions. One CF_3 group was found to be disordered, and the two sites refined were with complementary occupancies. The C-F and F-F bonds were restrained to be equal across the two sites, and corresponding pairs of atoms (e.g. F17 in the two sites) were constrained to have equal anisotropic thermal displacement parameters. The two C(pyrrole)-C(CF_3) bond lengths were restrained to have equal length.

Acknowledgements. This work was supported in part by the Research Council of Norway (grant no. 324139 to AG).

ASSOCIATED CONTENT

Supporting Information. ^{1}H and ^{19}F NMR spectra, electrospray ionization mass spectra, optical spectra and additional photophysical data (11 pages).

Data availability statement. The data underlying this study are available in the published article and its Supporting Information.

Accession codes. The crystal structure reported in this paper has been deposited at the Cambridge Crystallographic Data Centre and assigned the deposition number CCDC 2247280.

Author Information

Correspondence authors:

Abraham B. Alemayehu: abraham.alemayehu@uit.no

Sergey M. Borisov: sergey.borisov@tugraz.at

Abhik Ghosh: abhik.ghosh@uit.no

Other authors:

Krister Engedal Johannesen: krister_98@hotmail.com

Martin Amund Langaas Johansen: martin.amund@gmail.com

Rune F. Einrem: rune_einrem93@hotmail.com

Laura M^{c}Cormick M^{c}Pherson: lauraj.mcco@gmail.com

Notes: The authors declare no competing financial interests.

References

([1]) Alemayehu, A. B.; Thomas, K. E.; Einrem, R. F.; Ghosh, A. The Story of 5d Metallocorroles: From Metal–Ligand Misfits to New Building Blocks for Cancer Phototherapeutics. *Acc. Chem. Res.* **2021**, *54*, 3095-3107.

([2]) Ghosh, A. Electronic Structure of Corrole Derivatives: Insights from Molecular Structures, Spectroscopy, Electrochemistry, and Quantum Chemical Calculations. *Chem. Rev.* **2017**, *117*, 3798-3881.

([3]) Nardis, S.; Mandoj, F.; Stefanelli, M.; Paolesse, R. Metal complexes of corrole. *Coord. Chem. Rev*., 2019, **388**, 360-405.

([4]) Buckley, H. L.; Arnold, J. Recent Developments in Out-of-Plane Metallocorrole Chemistry Across the Periodic Table. *Dalton Trans.* **2015,** *44*, 30-36.

([5]) Einrem, R. F.; Gagnon, K. J.; Alemayehu, A. B.; Ghosh, A. Metal-Ligand Misfits: Facile Access to Rhenium-Oxo Corroles by Oxidative Metalation. *Chem. Eur. J.* **2016,** *22*, 517-520.

([6]) Alemayehu, A. B.; Teat, S. J.; Borisov, S. M.; Ghosh, A. Rhenium-Imido Corroles. *Inorg. Chem*. **2020**, *59*, 6382–6389.

([7]) Alemayehu, A. B.; Einrem, R. F.; McCormick-McPherson, L. J.; Settineri, N. S.; Ghosh, A. Synthesis and molecular structure of perhalogenated rhenium-oxo corroles. *Sci. Rep*. **2020**, *10*, 19727.

([8]) Alemayehu, A. B.; M^{c}Cormick-M^{c}Pherson, L. J.; Conradie, J.; Ghosh, A. Rhenium Corrole Dimers: Electrochemical Insights into the Nature of the Metal-Metal Quadruple Bond. *Inorg. Chem.* **2021**, *60*, 8315-8321.

([9]) Einrem, R. F.; Jonsson, E. T.; Teat, S. J.; Settineri, N. S.; Alemayehu, A. B.; Ghosh, A. Regioselective formylation of rhenium-oxo and gold corroles: substituent effects on optical spectra and redox potentials. *RSC Adv.* **2021**, *11*, 34086-34094.

([10]) Alemayehu, A. B.; Gagnon, K. J.; Terner, J.; Ghosh, A. Oxidative Metalation as a Route to Size-Mismatched Macrocyclic Complexes: Osmium Corroles. *Angew. Chem. Int. Ed*. **2014**, *53*, 14411-14414.

([11]) Reinholdt, A.; Alemayehu, A. B.; Gagnon, K. J.; Bendix, J.; Ghosh, A. Electrophilic Activation of Osmium-Nitrido Corroles: The OsN Triple Bond as a π-Acceptor Metallaligand in a Heterobimetallic Os^{VI}N–Pt^{II} Complex. *Inorg. Chem*. **2020**, *59*, 5276–5280.

([12]) Alemayehu, A. B.; McCormick, L J.; Vazquez-Lima, H.; Ghosh, A. Relativistic Effects on a Metal–Metal Bond: Osmium Corrole Dimers. *Inorg. Chem*. **2019**, *58*, 2798–2806.

([13]) J. H. Palmer, M. W. Day, A. D. Wilson, L. M. Henling, Z. Gross and H. B. Gray, *J. Am. Chem. Soc.* 2008, **130**, 7786-7787.

([14]) Alemayehu, A. B.; Vazquez-Lima, H.; Beavers, C. M.; Gagnon, K. J.; Bendix, J.; Ghosh, A. Platinum Corroles. *Chem. Comm*. **2014**, *50*, 11093-11096.

([15]) Alemayehu, A. B.; McCormick, L. J.; Gagnon, K. J.; Borisov, S. M.; Ghosh, A. Stable Platinum(IV) Corroles: Synthesis, Molecular Structure, and Room-Temperature Near-IR Phosphorescence. *ACS Omega* **2018**, *3*, 9360-9368.

([16]) Alemayehu, A. B.; Ghosh, A. Gold Corroles. *J. Porphyrins Phthalocyanines* **2011**, *15*, 106-110.

([17]) Rabinovitch, E.; Goldberg, I.; Gross, Z. Gold(I) and Gold(III) Corroles. *Chem. Eur. J.* **2011**, *17*, 12294–12301.

([18])Thomas, K. E.; Alemayehu, A. B.; Conradie, J.; Beavers, C.; Ghosh, A. Synthesis and Molecular Structure of Gold Triarylcorroles. *Inorg. Chem.* **2011**, *50*, 12844–12851.

([19]) Thomas, K. E.; Beavers, C. M.; Ghosh, A. Molecular Structure of a Gold *β*-Octakis(trifluoromethyl)-*meso*-triarylcorrole: An 85° Difference in Saddling Dihedral Relative to Copper. *Mol. Phys*. **2012**, *110*, 2439-2444.

([20])Thomas, K. E.; Vazquez-Lima, H.; Fang, Y.; Song, Y.; Gagnon, K. J.; Beavers, C. M.; Kadish, K. M.; Ghosh, A. Ligand Noninnocence in Coinage Metal Corroles: A Silver Knife-Edge. *Chem. - Eur. J.* **2015,** *21*, 16839-16847.

([21]) Capar, J.; Zonneveld, J.; Berg, S.; Isaksson, J.; Gagnon, K. J.; Thomas, K. E.; Ghosh, A. Demetalation of Copper Undecaarylcorroles: Molecular Structures of a Free-Base Undecaarylisocorrole and a Gold undecaarylcorrole. *J. Inorg. Biochem*. **2016**, *162*, 146-153.

([22]) Sinha, W.; Sommer, M.G.; van der Meer, M.; Plebst, S.; Sarkar, B.; Kar, S. Structural, electrochemical and spectroelectrochemical study on the geometric and electronic structures of $[(\text{corrolato})\text{Au}^{\text{III}}]^{n}$ (n = 0, + 1, − 1) complexes. *Dalton Trans.* **2016**, *45*, 2914-2923.

([23]) Thomas, K. E.; Gagnon, K. J.; McCormick, L. J.; Ghosh, A. Molecular structure of gold 2,3,7,8,12,13,17,18-octabromo-5,10,15-tris(4′-pentafluorosulfanylphenyl)corrole: Potential insights into the insolubility of gold octabromocorroles. *J. Porphyrins Phthalocyanines* **2018**, *22*, 596-601.

([24]) Palmer, J. H.; Durrell, A. C.; Gross, Z.; Winkler, J. R.; Gray, H. B. Near-IR Phosphorescence of Iridium(III) Corroles at Ambient Temperature. *J. Am. Chem. Soc.* **2010**, *132*, 9230–9231.

([25]) Sinha, W.; Ravotto, L.; Ceroni, P.; Kar, S. NIR-emissive iridium (III) corrole complexes as efficient singlet oxygen sensitizers. *Dalton Trans.* **2015**, *44*, 17767-17773.
([26]) Alemayehu, A. B.; Jae Day, N. U.; Mani, T.; Rudine, A. B.; Thomas, K. E.; Gederaas, O. A.; Vinogradov, S. A.; Wamser, C. C.; Ghosh, A. Gold Tris(carboxyphenyl)corroles as Multifunctional Materials: Room Temperature Near-IR Phosphorescence and Applications to Photodynamic Therapy and Dye-Sensitized Solar Cells. *ACS Appl. Mater. Interfaces* **2016**, *8*, 18935-18942.
([27]) Borisov, S. M.; Alemayehu, A.; Ghosh, A. Osmium-Nitrido Corroles as NIR Indicators for Oxygen Sensors and Triplet Sensitizers for Organic Upconversion and Singlet Oxygen Generation. *J. Mater. Chem. C* **2016**, *4*, 5822-5828.
([28]) Sudhakar, K.; Mizrahi, A.; Kosa, M.; Fridman, N.; Tumanskii, B.; Saphier, M.; Gross, Z.. Effect of selective CF_3 substitution on the physical and chemical properties of gold corroles. *Angew. Chem. Int. Ed*. **2017**, *56*, 9837-9841.
([29]) Lemon, C. M.; Powers, D. C.; Brothers, P. J.; Nocera, D .G. Gold Corroles as Near-IR Phosphors for Oxygen Sensing. *Inorg. Chem.* **2017**, *56*, 10991-10997.
([30]) Teo, R. D., Hwang, J. Y., Termini, J., Gross, Z.; Gray, H. B. Fighting Cancer with Corroles. *Chem. Rev*. **2017**, *117*, 2711-2729.
([31]) Alemayehu, A. B.; McCormick, L. J.; Gagnon, K. J.; Borisov, S. M.; Ghosh, A. Stable Platinum(IV) Corroles: Synthesis, Molecular Structure, and Room-Temperature Near-IR Phosphorescence. *ACS Omega* **2018**, *3*, 9360-9368.
([32]) Borisov, S. M.; Einrem, R. F.; Alemayehu, A. B.; Ghosh, A. Ambient-temperature near-IR phosphorescence and potential applications of rhenium-oxo corroles. *Photochem. Photobiol. Sci.* **2019**, *18*, 1166-1170.
([33]) Thomassen, I. K.; McCormick-McPherson, L. J.; Borisov, S. M.; Ghosh, A. Iridium Corroles Exhibit Weak Near-Infrared Phosphorescence but Efficiently Sensitize Singlet Oxygen Formation. *Sci. Rep.* **2020**, *10*, Art. No. 7551.
([34]) Lemon, C. M. Corrole photochemistry. *Pure Appl. Chem*. **2019**, *92*, 1901-1919.
([35]) Higashino, T.; Kurumisawa, Y.; Alemayehu, A. B.; Einrem, R. F.; Sahu, D.; Packwood, D.; Kato, K.; Yamakata, A.; Ghosh, A.; Imahori, H. Heavy Metal Effects on the Photovoltaic Properties of Metallocorroles in Dye-Sensitized Solar Cells. *ACS Appl. Energy Mater*. **2020**, *3*, 12460-12467.

([36]) Einrem, R. F.; Alemayehu, A. B.; Borisov, S. M.; Ghosh, A.; Gederaas, O. A. Amphiphilic Rhenium-Oxo Corroles as a New Class of Sensitizers for Photodynamic Therapy. *ACS omega* **2020**, *5*, 10596-10601.

([37]) Zach, P. W.; Freunberger, S. A.; Klimant, I.; Borisov, S. M. *ACS Appl. Mater. Interfaces* **2017**, *9*, 38008–38023.

([38]) Gryko, D. T.; Koszarna, B. Refined methods for the synthesis of *meso*-substituted A_3- and *trans*-A_2B-corroles. *Org. Biomol. Chem.* **2003**, 1, 350-357.

([39]) Koszarna, B.; Gryko, D. T. Efficient Synthesis of *meso*-Substituted Corroles in a H_2O−MeOH Mixture. *J. Org. Chem.* **2005**, *71*, 3707-3717.

([40]) Sheldrick, G. M. SHELXT - Integrated Space-Group and Crystal-Structure Determination. *Acta Cryst.* **2015**, *A71*, 3-8.

([41]) Sheldrick, G. M. Crystal Structure Refinement with SHELXL. *Acta Cryst.* **2015**, *C71*, 3-8.

TOC graphic

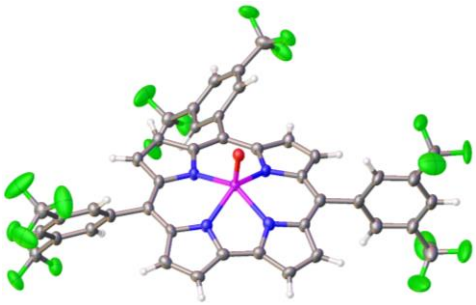

Synopsis: Fluorinated *meso*-aryl substituents have been found to lead to enhanced phosphorescence quantum yields and longer triplet decay times for rhenium-oxo, oxmium-nitrido, and gold corroles. The highest phosphorescence quantum yield, 2.2%, has been been found for rhenium-oxo tris(pentafluorophenyl)corrole.